Tomas Bata University in Zlín

Doctoral Thesis

Study the crystallization, electroconductivity and mechanical properties in selected engineering polymers and blends

Studium krystalizace, elektrické vodivosti a mechanických vlastností vybraných inženýrských polymerů a směsí

Author:	Ing. Ahmed Nasr
Degree programme:	P2808 Chemistry and Materials Technology
Degree course:	2808v006 Technology of Macromolecular Compounds
Supervisor:	prof. Ing. Petr Svoboda, Ph.D.

ZLIN 2023

Published by **Tomas Bata University in Zlín** in the Edition **Doctoral Thesis Summary.**
The publication was issued in the year 2023.

Key words in Czech: *Elektrická vodivost, krystalizace, tepelná degradace, optická mikroskopie, DSC, SAXS.*

Key words: *Electrical conductivity, Crystallization, Thermal degradation, Optical microscopy, DSC, SAXS.*

Full text of the doctoral thesis is available in the Library of TBU in Zlín.

ABSTRACT

This doctoral thesis investigated the multifaceted interplay between crystallization dynamics, electroconductivity, and mechanical attributes within selected engineering polymers and their blends. The overarching objective was to unravel the intricate relationships governing these fundamental properties and their implications for advanced material applications.

Firstly, the influence of thermal degradation on the crystallization of Poly(butylene terephthalate) (PBT) was meticulously examined. The research revealed a substantial shift in the crystallization temperature, indicative of profound modification. This shift occurred through distinct phases, involving initial rise, steep decrease, and subsequent degradation-induced changes. The corresponding trends in crystallinity and crystallization kinetics were observed, with particular attention to the influence of differing lamellar thicknesses. These findings underscored the intricate nature of PBT's crystallization behavior under thermal degradation, contributing to a broader understanding of polymer degradation and its implications for crystallization processes.

Furthermore, the research delved into the intricate terrain of Poly(butylene terephthalate) crystallization kinetics, particularly in response to various fusion temperatures. The empirical results demonstrated a pivotal correlation between fusion temperature and the resultant heat flow curve, revealing a nuanced interplay between crystallinity and heat flow profile. The Ozawa and Avrami models were adeptly employed to elucidate crystallization kinetics, affirming the role of fusion temperature in nucleation and crystal growth mechanisms. These findings hold promise for optimizing processing parameters and enhancing material attributes across diverse applications.

Moreover, the intricate interplay between fusion temperature, duration, and nonisothermal crystallization kinetics in polyamide 6 (PA6) was explored. Employing advanced analytical techniques, the study unveiled insights into nucleation centers, crystallization temperature shifts, and kinetics. The models utilized effectively shed light on the complex relationship between fusion temperature and crystallization processes, furthering our comprehension of polymer material processing.

Lastly, the work explored the integration of carbon fibers within an elastic polymer matrix, yielding EOC/CF composites. The study meticulously analyzed the resulting mechanical attributes and morphology alongside implications for electroconductivity. The study demonstrated a marked enhancement in tensile modulus and stress through various analytical methodologies while maintaining elasticity. Moreover, the investigation delved into electrical properties, revealing a critical percolation threshold in the composites. These results suggest the potential for advanced composites, particularly for applications in electronics engineering.

This doctoral thesis comprehensively explores the intricate relationships among crystallization, electroconductivity, and mechanical attributes within engineering polymers and blends. The findings have far-reaching implications for material design and applications, paving the way for innovative advancements in diverse fields.

Key words: *Electrical conductivity, Crystallization, Thermal degradation, Optical microscopy, DSC, SAXS.*

ABSTRAKT

Tato disertační práce se zabývala mnohostrannými interakcemi mezi dynamikou krystalizace, elektrickou vodivostí a mechanickými vlastnostmi vybraných technických polymerů a jejich kompozitů a směsí. Hlavním cílem bylo odhalit složité vztahy, jimiž se tyto základní vlastnosti řídí, a jejich důsledky pro aplikace pokročilých materiálů.

Nejprve byl pečlivě zkoumán vliv tepelné degradace na krystalizaci poly(butylentereftalátu) (PBT). Výzkum odhalil podstatný posun v teplotě krystalizace, což svědčí o hluboké modifikaci. K tomuto posunu došlo v různých fázích, které zahrnovaly počáteční nárůst, prudký pokles a následné změny vyvolané degradací. Byly sledovány odpovídající trendy v krystalinitě a kinetice krystalizace, přičemž zvláštní pozornost byla věnována vlivu na rozdílnou tloušťku lamel. Tato zjištění zdůraznila složitou povahu krystalizačního chování PBT při tepelné degradaci a přispěla k širšímu pochopení degradace polymerů a jejích důsledků pro krystalizační procesy.

Výzkum dále pronikl do složité oblasti kinetiky krystalizace poly(butylentereftalátu), zejména v závislosti na různých teplotách tavení. Empirické výsledky prokázaly klíčovou korelaci mezi teplotou tavení a výslednou křivkou tepelného toku a odhalily jemnou souhru mezi krystalinitou a profilem tepelného toku. K objasnění kinetiky krystalizace byly vhodně použity Ozawův a Avramiho model, které potvrdily roli teploty tavení v mechanismech nukleace a růstu krystalů. Tato zjištění jsou příslibem pro optimalizaci parametrů zpracování a zlepšení vlastností materiálu v různých aplikacích.

Kromě toho byla zkoumána složitá souhra mezi teplotou tavení, dobou trvání a kinetikou neizotermické krystalizace v polyamidu 6 (PA6). S využitím pokročilých analytických technik studie odhalila poznatky o nukleačních centrech, teplotních posunech a kinetice krystalizace. Použité modely účinně osvětlují složitý vztah mezi teplotou tavení a krystalizačními procesy a prohlubují naše porozumění zpracování polymerních materiálů.

Nakonec práce zkoumala integraci uhlíkových vláken do elastické polymerní matrice, čímž vznikly kompozity EOC/CF. Studie pečlivě analyzovala výsledné mechanické vlastnosti a morfologii spolu s důsledky pro elektrickou vodivost. Studie prokázala výrazné zvýšení modulu pružnosti v tahu a napětí pomocí

různých analytických metodik při zachování elasticity. Kromě toho se zkoumaly elektrické vlastnosti a odhalil se kritický práh perkolace v kompozitech. Tyto výsledky naznačují potenciál pokročilých kompozitů, zejména pro aplikace v elektronice.

Tato disertační práce komplexně zkoumá složité vztahy mezi krystalizací, elektrickou vodivostí a mechanickými vlastnostmi v rámci technických polymerů a směsí. Zjištění mají dalekosáhlé důsledky pro konstrukci a aplikace materiálů a otevírají cestu k inovativnímu pokroku v různých oblastech.

Klíčová slova: *Elektrická vodivost, krystalizace, tepelná degradace, optická mikroskopie, DSC, SAXS.*

CONTENTS

ACKNOWLEDGEMENTS

All praise to almighty Allah, the most merciful and compassionate, the creator of the universe, who enabled me to complete this research work successfully.

With profound privilege, I extend my heartfelt acknowledgments to my esteemed research supervisor, Prof. Petr Svoboda. His invaluable guidance and support have been worthy in shaping the trajectory of this research work.

I am profoundly grateful to the Department of Polymer Engineering, housed within the Faculty of Technology at Tomas Bata University in Zlin. Their support, both in terms of infrastructure and financial support, has provided the bedrock upon which this research has thrived.

In addition, I offer my humble gratitude to my departed parents, whose early-life encouragement has paved the way for my achievements. Their influence has been the cornerstone of my existence, and I recognize that their blessings have been a guiding force throughout my entire life.

Quran [96:1]

LIST OF PAPERS

1. **Influence of Thermal Degradation on the Crystallization of Poly(butylene terephthalate)**

   Ahmed Nasr * and Petr Svoboda

   Submitted to the journal of Express Polymer Letters, August 2023.

2. **Effect of fusion temperature on the crystallization kinetics of poly(butylene terephthalate)**

   Ahmed Nasr * and Petr Svoboda

   Published in journal of CrystEngComm, 2023. 25(34):4848-4855.
   DOI: 10.1039/D3CE00669G

3. **Influence of Fusion Temperature on Nonisothermal Crystallization Kinetics of Polyamide 6**

   Ahmed Nasr * and Petr Svoboda

   Published in journal of Polymers, 2023;15(8):1952.

   DOI: 10.3390/polym15081952

4. **Elastic Electrically Conductive Composites Based on Vapor-Grown Carbon Fibers for Use in Sensors**

   Ahmed Nasr *, Ondřej Mrhálek and Petr Svoboda

   Published in journal of Polymers, 2023;15(9):2005.

   DOI: 10.3390/polym15092005

AIM OF WORK

The primary objective of this research is to comprehensively investigate and analyze the intricate interplay between crystallization kinetics, electric conductivity, and mechanical properties within selected engineering polymers and their composites and blends. This work aims to unravel the underlying mechanisms governing these fundamental properties and their interdependencies, providing valuable insights into the design, optimization, and application of advanced materials with enhanced functionalities.

By studying the influence of factors such as fusion temperature, thermal degradation, and filler incorporation on crystallization behaviour, this research seeks to uncover the underlying principles that govern the crystalline structure and kinetics of polymers. Furthermore, by assessing the electric conductivity of polymer composites, a deeper understanding of their electrical behaviour will be achieved, allowing for potential applications in fields like electronics engineering and sensor technology.

Another pivotal objective of this work is to analyze the mechanical properties of engineered polymers and their composites. Investigating the tensile modulus, stress-strain behaviour, and viscoelastic properties contributes to comprehending how these materials respond to mechanical stresses and strains. This knowledge can lead to developing materials with tailored mechanical properties suitable for various industrial and engineering applications.

Overall, this thesis aims to bridge the gaps between these interconnected properties and establish a comprehensive understanding of how they influence each other. This understanding, in turn, can inform the design and fabrication of innovative materials with improved properties, enabling advancements in fields ranging from materials science and polymer engineering to electronics and beyond.

1. THEORITICAL BACKGROUND

1.1. Introduction

Polymers exhibit diverse properties, including their crystallization ability, influenced by temperature and molecular weight distribution, impacting their mechanical strength [1, 2]. In terms of elasticity, polymers can display both elastomeric and rigid characteristics, making them versatile for various applications. Additionally, the electrical conductivity of polymers can be modified by incorporating conductive fillers, enabling their use in electrically conductive materials when factors like filler content and morphology are carefully controlled [3].

In polymer science and engineering, crystallization is crucial in determining polymers' physical and mechanical properties. The crystallization process involves transforming a disordered polymer melt into a crystalline structure, influenced by various factors such as thermal degradation, fusion temperature, fusion time, and polymer morphology [4]. Polymer crystallization is a complex process that involves multiple stages, including nucleation, growth, and final morphology development. Several factors, such as degradation, temperature, cooling rate, and molecular weight, influence these stages' kinetics. Fusion temperature, the temperature at which a polymer is melted, significantly impacts the crystallization process [5].

In general, reduced fusion temperatures result in an accelerated crystallization rate, increased crystalline structure, and diminished crystal dimensions. Specific engineering polymers, such as polyamide 6 (PA6) and Polybutylene Terephthalate (PBT), possess distinct characteristics that render them apt for various industrial uses. The influence of fusion temperature, thermal degradation, fusion time, and morphology on the crystallization process of these polymers has been extensively studied [6, 7]. Differential scanning calorimetry (DSC) and polarized optical microscopy (OM) are commonly used techniques to analyze the crystallization kinetics of these polymers.

Incorporating conductive fillers, such as carbon fibres, in polymer matrices can lead to materials with elastic and electrically conductive properties. The electrical conductivity of polymer blends depends on factors such as filler content, morphology, and the nature of the polymer matrix [8]. The percolation threshold, the minimum filler content required to achieve electrical conductivity, is an essential parameter in designing electrically conductive polymers [9]. Investigating the electrically conductive properties of EOC/CF blends can provide

valuable insights into their potential applications in electronics, sensors, and actuators.

This thesis focuses on selected engineering polymers and blends, specifically PA6, PBT, EOC and EOC/PBT blends. The study will provide valuable insights into the crystallization kinetics, elastic electrically conductive properties, and morphology of these materials, thus contributing to optimizing their design for specific applications. The findings of this research will benefit various industries, including automotive, aerospace, electronics, and construction, seeking to develop high-performance materials with tailored properties.

1.2. Crystallization Kinetics

Polymers are widely used materials with a broad range of applications due to their unique properties. One of the key properties of polymers is their ability to crystallize. Crystallization is the process of polymers forming an ordered, solid structure from a disordered liquid state. The kinetics of crystallization are essential to consider when processing polymer materials. There are two main types of crystallization kinetics: isothermal and nonisothermal crystallization [10].

1.2.1 Isothermal crystallization

Isothermal crystallization refers to the process by which a polymer is carried outat a constant temperature and allowed to crystallize. The kinetics of isothermal crystallization can be described using several models, including the Avrami and Ozawa models [11].

The Avrami model assumes that the crystallization rate is proportional to the amount of uncrystallized material remaining. This model assumes that the nucleation and growth of crystalline structures occur simultaneously and uniformly throughout the polymer melt [12].

The Ozawa model is dependent on the Avrami model, but it accounts for the effect of the degree of undercooling on the crystallization rate. The degree of undercooling refers to the difference between the crystallization temperature and the polymer's melting temperature. The Ozawa model can also be applied to the nonisothermal crystallization kinetics of polymers.

1.2.2 Nonisothermal crystallization

Nonisothermal crystallization refers to the process by which a polymer is heated or cooled at a specific rate and allowed to crystallize. Nonisothermal crystallization kinetics can be described using several models, including the Kissinger and Hoffman-Lauritzen models.

The Ziabicki model assumes that the rate of crystallization is corresponding to the degree of undercooling and the number of active nuclei. The degree of undercooling is the difference between the crystallization temperature and the equilibrium melting temperature of the polymer, and the number of active nuclei is a measure of the degree of crystallization. The Ziabicki model also accounts for the effect of crystal growth on the crystallization rate. This model has been used to describe the nonisothermal crystallization of several polymer materials, including polyethylene, polypropylene, and polycarbonate.

On the other hand, the Nakamura model assumes that the crystallization rate is proportional to the degree of undercooling and the nucleation rate. The rate of nucleation is a measure of the number of nucleation sites in the polymer melt. The Nakamura model also accounts for the effect of crystal growth on the rate of crystallization. This model has been used to describe the nonisothermal crystallization of several polymer materials, including polyethylene, polypropylene, and polyamide.

1.3. Electric Conductivity in Polymers

Introducing conductive additives, like carbon fibres, into polymer matrices can yield flexible and electrical conductivity materials. The electrical conductance of polymer combinations is influenced by elements such as the quantity of additives, the material's structure, and the inherent properties of the polymer matrix. The percolation threshold, which denotes the minimum amount of additives needed for electrical conductivity, is a critical parameter when formulating electrically conductive polymer mixtures. An exploration into the electrical conductive characteristics of EOC/CF blends has the potential to offer valuable insights into their prospective applications in fields like electronics, sensors, and actuators.

1.4. Morphology and its Influence on Properties

The morphology of polymers and blends is critical in determining their mechanical, thermal, and electrical properties. Factors such as crystallinity, phase separation, and interface adhesion can influence the performance of the materials. In the case of PA6, PBT, PHB, and EOC/CF blends, the morphology is closely

related to the crystallization kinetics and elastic electrically conductive properties. Studying the relationship between these materials' morphology, crystallization kinetics, and electrical conductivity can contribute to their efficient design and application.

1.5. Polymer Materials:

1.5.1. Polyamide 6 (PA6)

Polyamide 6 (PA6) is a semi-crystalline thermoplastic material renowned for its remarkable combination of high strength, toughness, and stiffness, rendering it a highly appealing choice for many applications [1, 2]. During processing PA6, the fusion temperature plays a pivotal role in governing the polymer's crystallization characteristics [3, 4]. The crystallization patterns of polyamide 6 are subject to the influence of several variables, including temperature, cooling rate, and molecular weight [5]. Notably, most polyamides, called nylons, exhibit a linear structure characterized by recurring amide units. These amide groups facilitate hydrogen bonding within the polymer chain, a phenomenon of paramount importance in shaping the material's physical and chemical attributes [2, 6]. Establishing hydrogen bonds within PA6 yields a robust, inflexible, and crystalline framework, contributing significantly to the material's elevated levels of strength, stiffness, and thermal resilience. Furthermore, this distinctive configuration of chemical bonds confers impressive resistance to chemical agents and low moisture absorption to polyamides, rendering them exceptionally well-suited for various textiles, automotive manufacturing, and electronics applications.

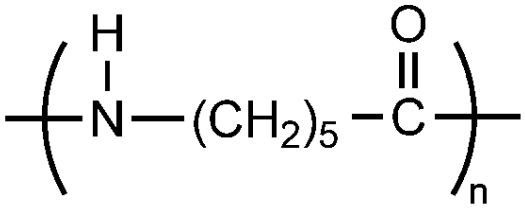

Figure 1. PA6 formula.

1.5.2. Polybutylene terephthalate (PBT)

Polybutylene terephthalate (PBT) is a world-wide semi-crystalline thermoplastic. It belongs to the group of polyesters together with, for example, polyethylene and polycarbonate, so it contains at least one ester bond. PBT typically has a crystallinity of around 35-40%. The glass transition temperature is in the range of 30-50°C and the melting point is usually between 222-232°C. It is fiber-forming, chemically resistant, has high strength and rigidity and low moisture content [13, 14].

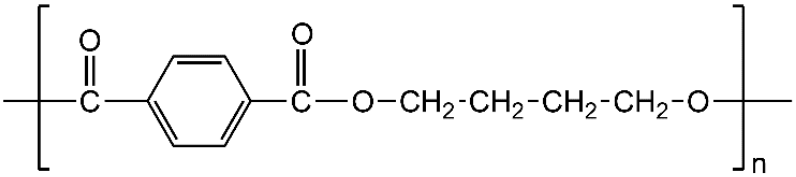

Figure 2. The chemical formula of PBT.

1.5.3. Ethylene-octane copolymer (EOC)

Another polymer used was ethylene-octane copolymer. In our case, a polymer called EOC39 was used, where the number 39 represents the mass percentage of the octane monomer. EOC39 has good flow characteristics, a melt flow index of 0,50 g/10 min (at 190 °C and load 2,16 kg) and a density of 0,868 g/cm3. The polymer is resistant to peroxides silanes. It has a melting point of 55 °C and a glass transition temperature of -52 °C. The properties of EOC39 are enhanced in mixtures with polypropylene and polyethylene [15-17].

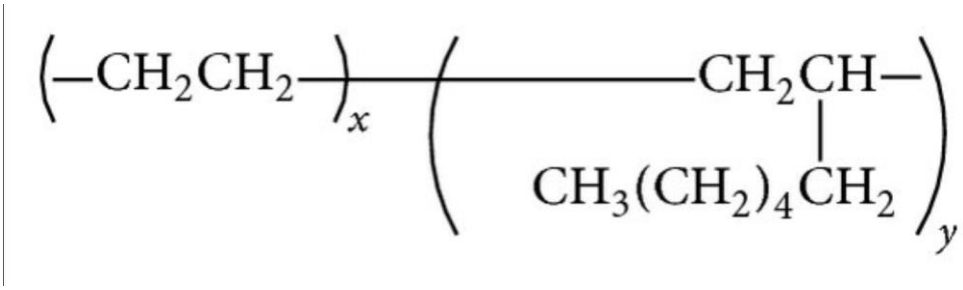

Figure 3. The structural formula of Ethylene-octene copolymer [18].

1.5.4. EOC/PBT Blend

PBT/EOC mixtures were prepared using the Haake Minilab extruder under the following conditions: 250 °C, 50 rpm and 9 minutes. An overview of all prepared mixtures and pure PBT is given in the table 1 and figure 4 below.

Table 1: Overview of prepared mixtures

Mixture	hm.% PBT	hm.% EOC
EOC/PBT	30	70
EOC/PBT	32. 5	67. 5
EOC/PBT	35	65
EOC/PBT	37. 5	62. 5
EOC/PBT	40	60
PBT	100	-

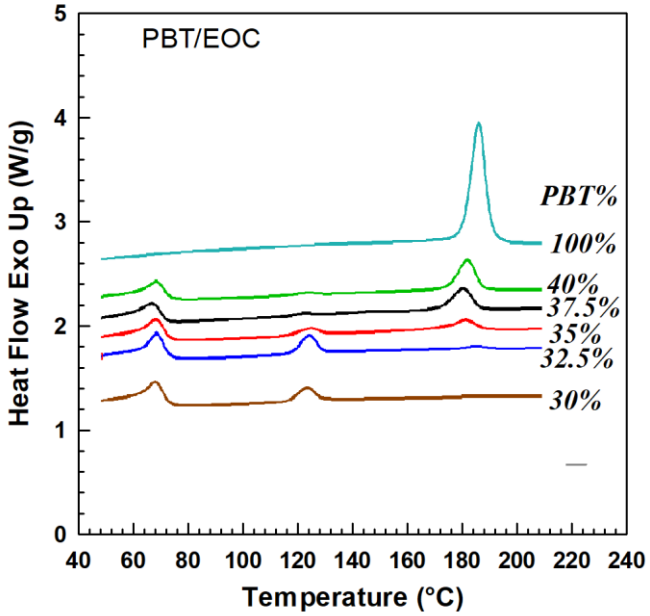

Figure 4. DSC curves of PBT/EOC blend and pure PBT.

1.6. Experimental Methods

1.6.1. Differential Scanning Calorimetry (DSC)

Differential scanning calorimetry (DSC) measurements were performed on the polymer samples to study their crystallization kinetics and thermal properties. The samples were heated and cooled at different rates, and the resulting DSC curves were analyzed to obtain crystallization and melting temperatures [19, 20].

The measurement is carried out in an inert atmosphere and two pans, one empty, the reference and the other containing the sample to be examined. Each pan has its heating device, which must change the temperature at the same rate [21].

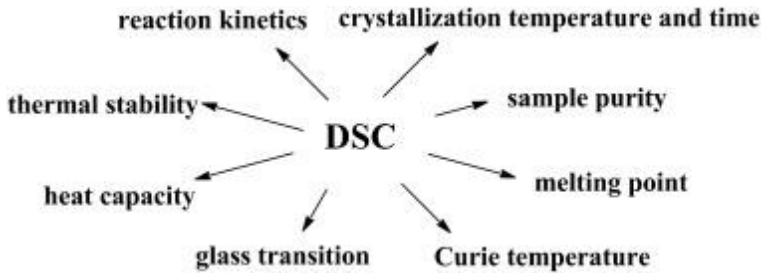

Figure 5. Applications of DSC [20].

1.6.2. Electrical Conductivity Measurements

A strain gauge is employed to assess the sample's electrical resistance. This strain gauge is a sensor with an electrical resistance that varies in response to applied force. The calibration procedure entails utilizing different weights. During calibration, the sensor's zero offset and linearity are scrutinized by comparing its output when subjected to reference weights. Adjustments to the sensor are made as necessary [22]. The measurement of electrical resistance is executed using a multimeter configured in ohms, and the obtained values are subsequently compared with the manufacturer's calibration certificate to ascertain their close correspondence.. The dependence of the electrical conductivity on the carbon fibre content and blend morphology was investigated to understand the percolation behaviour and the role of filler dispersion and distribution [23, 24].

1.6.3. Scanning Electron Microscopy (SEM)

Scanning electron microscopy (SEM) was employed to examine the morphology of the selected polymers and blends. The samples were cryogenically fractured, sputter-coated with a thin layer of conductive material, and then observed under high vacuum conditions to obtain high-resolution images of the fracture surfaces [25-27].

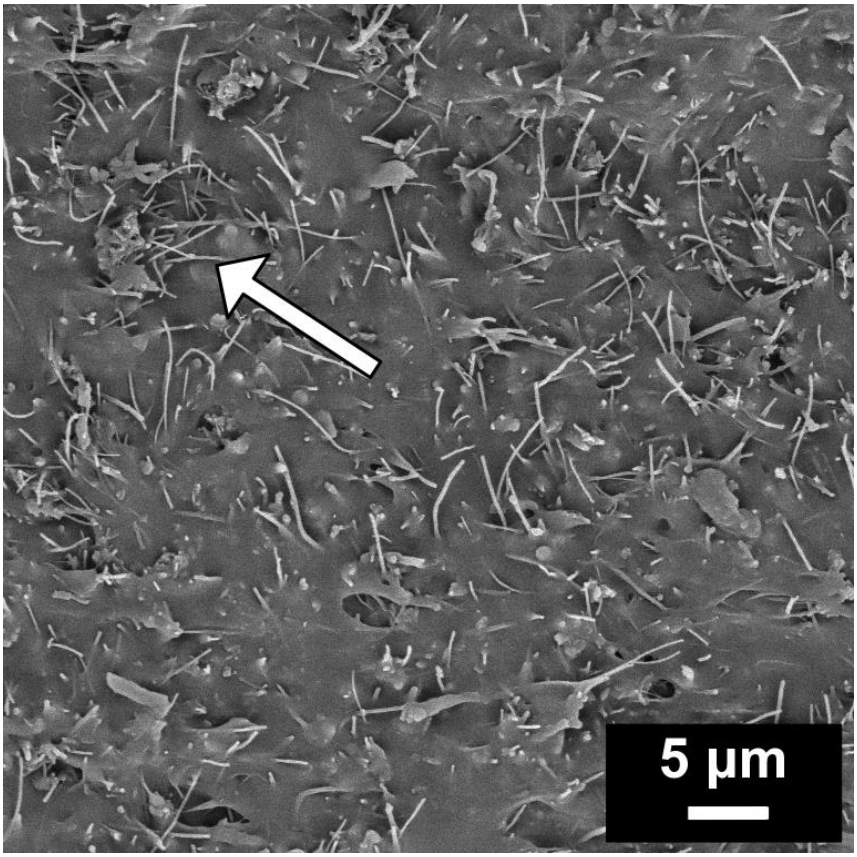

Figure 6. SEM image of EOC/CF composite with 30 wt.% of CF [25].

1.6.4. Small Angle X-ray Scattering (SAXS)

Small-angle X-ray scattering (SAXS) is a non-destructive analytical technique employed to probe nanostructures present in both liquid and solid substances. In a SAXS experiment, a focused X-ray beam is directed at a nanostructured specimen, which can encompass substances like proteins, macromolecules, or nanoparticle dispersions. The scattering pattern generated during this process varies depending on the size of the particles within the sample, yielding valuable insights into their dimensions and size distribution. What sets SAXS apart is its ability to offer representative structural information covering a substantial sample area. This feature distinguishes it from microscopic methods, which may provide detailed data but are often limited in their capacity to capture the overall structural characteristics of a sample. Consequently, SAXS is an excellent complementary method, particularly when assessing the specific surface area of materials, enhancing our understanding of nanoscale structures and their properties in diverse scientific applications. [28, 29].

1.6.5. Twin Screw Extruder

A twin screw extruder, often referred to as a twin-screw extruder, is a machinery utilized within the plastics sector to manipulate and blend plastic substances. This device comprises a closed barrel housing two screws interning and rotating on splined shafts. The screws are precisely meshed and turn unison, facilitating thorough material mixing and shaping. Twin-screw extruders have extensive application in processing powder blends, requiring meticulous blending and reactive extrusion processes [30-32].

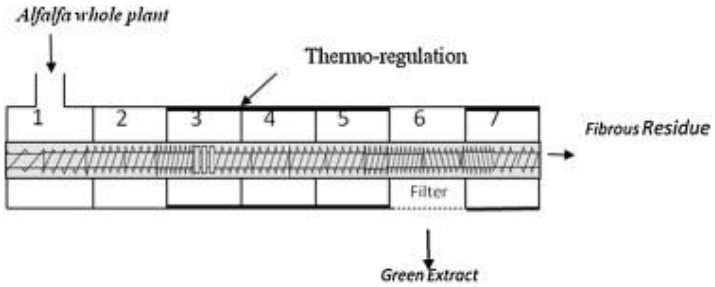

Figure 7. Schematic representation of the twin-screw extruder barrel [33].

1.6.6. Mechanical Testing

Mechanical properties of the selected polymers and blends, such as tensile strength, elongation at break, and modulus, were determined using a universal testing machine. The specimens were prepared according to the relevant standards, and the tests were conducted at a constant strain rate [34-36].

REFERENCES

[1] Valerga AP, Fernandez-Vidal SR, Girot F, Gamez AJ. On the Relationship between Mechanical Properties and Crystallisation of Chemically Post-Processed Additive Manufactured Polylactic Acid Pieces. Polymers (Basel). 2020;12(4). https://doi.org/10.3390/polym12040941.

[2] Ma X-l, Wen L-h, Wang S-y, Xiao J-y, Li W-h, Hou X. Inherent relationship between process parameters, crystallization and mechanical properties of continuous carbon fiber reinforced PEEK composites. Defence Technology. 2023;24:269-284. https://doi.org/https://doi.org/10.1016/j.dt.2022.04.010.

[3] Kim N, Lienemann S, Petsagkourakis I, Alemu Mengistie D, Kee S, Ederth T, Gueskine V, Leclère P, Lazzaroni R, Crispin X, Tybrandt K. Elastic conducting polymer composites in thermoelectric modules. Nature Communications. 2020;11(1):1424. https://doi.org/10.1038/s41467-020-15135-w.

[4] McKeen L. 3 - Introduction to the Physical, Mechanical, and Thermal Properties of Plastics and Elastomers. In: McKeen L, editor. The Effect of Sterilization on Plastics and Elastomers (Third Edition). Boston: William Andrew Publishing; 2012. p. 57-84.

[5] Cheng SZD, Jin S. Chapter 5 - Crystallization and melting of metastable crystalline polymers. In: Cheng SZD, editor. Handbook of Thermal Analysis and Calorimetry: Elsevier Science B.V.; 2002. p. 167-195.
[6] Groeninckx G, Vanneste M, Everaert V. Crystallization, Morphological Structure, and Melting of Polymer Blends. In: Utracki LA, editor. Polymer Blends Handbook. Dordrecht: Springer Netherlands; 2003. p. 203-294.
[7] Zhao D, Yan D, Fu X, Zhang N, Yang G. Rheological and Crystallization Properties of ABS/PA6-Compatibilized Blends via In Situ Reactive Extrusion. Acs Omega. 2020;5(25):15257-15267. https://doi.org/10.1021/acsomega.0c01298.
[8] Sumita M, Sakata K, Asai S, Miyasaka K, Nakagawa H. Dispersion of fillers and the electrical conductivity of polymer blends filled with carbon black. Polymer Bulletin. 1991;25(2):265-271. https://doi.org/10.1007/BF00310802.
[9] Rahaman M, Aldalbahi A, Govindasami P, Khanam NP, Bhandari S, Feng P, Altalhi T. A New Insight in Determining the Percolation Threshold of Electrical Conductivity for Extrinsically Conducting Polymer Composites through Different Sigmoidal Models. Polymers2017.
[10] Lemanowicz M, Mielańczyk A, Walica T, Kotek M, Gierczycki A. Application of Polymers as a Tool in Crystallization -A Review. Polymers. 2021;13:2695. https://doi.org/10.3390/polym13162695.
[11] Papageorgiou G, Achilias D, Bikiaris D, Karayannidis G. Isothermal and non-isothermal crystallization kinetics of branched and partially crosslinked PET : DSC study. Journal of Thermal Analysis and Calorimetry. 2006;84:85-89. https://doi.org/10.1007/s10973-005-7366-4.
[12] Avrami M. Kinetics of Phase Change. I General Theory. The Journal of Chemical Physics. 1939;7:1103. https://doi.org/10.1063/1.1750380.
[13] Huang JW, Wen YL, Kang CC, Yeh MY, Wen SB. Morphology, melting behavior, and non-isothermal crystallization of poly(butylene terephthalate)/poly(ethylene-co-methacrylic acid) blends. Thermochimica Acta. 2007;465(1-2):48-58. https://doi.org/10.1016/j.tca.2007.09.004.
[14] Papageorgiou GZ, Achilias DS, Bikiaris DN. Crystallization Kinetics of Biodegradable Poly(butylene succinate) under Isothermal and Non-Isothermal Conditions. 2007;208(12):1250-1264. https://doi.org/https://doi.org/10.1002/macp.200700084.
[15] Svoboda P. Influence of Branching Density in Ethylene-Octene Copolymers on Electron Beam Crosslinkability. Polymers2015. p. 2522-2534.
[16] Zykova A, Pantyukhov P, Popov A. Mechanical properties of ethylene-octene copolymer (EOC) - lignocellulosic fillers biocomposites in dependence to filler content. AIP Conference Proceedings. 2016;1736(1):020123. https://doi.org/10.1063/1.4949698.
[17] Rajeshbabu R, Gohs U, Naskar K, Thakur V, Wagenknecht U, Heinrich G. Preparation of polypropylene (PP)/ethylene octene copolymer (EOC) thermoplastic vulcanizates (TPVs) by high energy electron reactive processing. Radiation Physics and Chemistry. 2011;80(12):1398-1405. https://doi.org/https://doi.org/10.1016/j.radphyschem.2011.07.001.
[18] Tesarikova A, Merinska D, Kalous J, Svoboda P. Ethylene-Octene Copolymers/Organoclay Nanocomposites: Preparation and Properties. Journal of Nanomaterials. 2016;2016:1-13. https://doi.org/10.1155/2016/6014064.
[19] Kong Y, Hay JN. The measurement of the crystallinity of polymers by DSC. Polymer. 2002;43(14):3873-3878. https://doi.org/https://doi.org/10.1016/S0032-3861(02)00235-5.
[20] Drzeżdżon J, Jacewicz D, Sielicka A, Chmurzyński L. Characterization of polymers based on differential scanning calorimetry based techniques. TrAC Trends in Analytical Chemistry. 2019;110:51-56. https://doi.org/https://doi.org/10.1016/j.trac.2018.10.037.

[21] Al-Qatami O, Mazzanti G. The effect of the sample pan position on the determination of the specific heat capacity for lipid materials using heat flux DSC. Thermochimica Acta. 2022;710:179148. https://doi.org/https://doi.org/10.1016/j.tca.2022.179148.
[22] Chen Z, Ding Y, Pacheco-torgal F, Zhang Y. 4 - Self-sensing concrete with nanomaterials. In: Pacheco-Torgal F, Diamanti MV, Nazari A, Granqvist CG, editors. Nanotechnology in Eco-Efficient Construction: Woodhead Publishing; 2013. p. 53-74.
[23] Mironov VS, Kim JK, Park M, Lim S, Cho WK. Comparison of electrical conductivity data obtained by four-electrode and four-point probe methods for graphite-based polymer composites. Polymer Testing. 2007;26:547-555. https://doi.org/10.1016/j.polymertesting.2007.02.003.
[24] Topcu A, Daricik F, Aydin K, Celik S. Electrical Properties of the Carbon Nano tube (CNT) Reinforced Composite Plates for the PEM Fuel Cell Bipolar Plate Application2021.
[25] Nasr A, Mrhálek O, Svoboda P. Elastic Electrically Conductive Composites Based on Vapor-Grown Carbon Fibers for Use in Sensors. Polymers2023.
[26] Chen D, Li J, Yuan Y, Gao C, Cui Y, Li S, Liu X, Wang H, Peng C, Wu Z. A Review of the Polymer for Cryogenic Application: Methods, Mechanisms and Perspectives. Polymers (Basel). 2021;13(3). https://doi.org/10.3390/polym13030320.
[27] An Q, Hong C, Wen H. Fracture Patterns of Rocks Observed under Cryogenic Conditions Using Cryo-Scanning Electron Microscopy. Processes2023.
[28] Oliver RC, Rolband LA, Hutchinson-Lundy AM, Afonin KA, Krueger JK. Small-Angle Scattering as a Structural Probe for Nucleic Acid Nanoparticles (NANPs) in a Dynamic Solution Environment. Nanomaterials (Basel). 2019;9(5). https://doi.org/10.3390/nano9050681.
[29] Bogan M, Boutet S, Barty A, Benner H, Frank M, Lomb L, Shoeman R, Starodub D, Seibert M, Hau-Riege S, Woods B, DeCorwin-Martin P, Bajt S, Schulz J, Rohner U, Iwan B, Timneanu N, Marchesini S, Schlichting I, Chapman H. Single-shot femtosecond x-ray diffraction from randomly oriented ellipsoidal nanoparticles. PHYSICAL REVIEW SPECIAL TOPICS-ACCELERATORS AND BEAMS. 2010;13. https://doi.org/10.1103/PhysRevSTAB.13.094701.
[30] Lewandowski A, Wilczyński K. Modeling of Twin Screw Extrusion of Polymeric Materials. Polymers2022.
[31] Uitterhaegen E, Evon P. Twin-screw extrusion technology for vegetable oil extraction: A review. Journal of Food Engineering. 2017;212:190-200. https://doi.org/https://doi.org/10.1016/j.jfoodeng.2017.06.006.
[32] Mikulionok IO. Screw extruder mixing and dispersing units. Chemical and Petroleum Engineering. 2013;49(1):103-109. https://doi.org/10.1007/s10556-013-9711-y.
[33] Colas D, Doumeng C, Pontalier PY, Rigal L. Twin-screw extrusion technology, an original solution for the extraction of proteins from alfalfa (Medicago sativa). Food and Bioproducts Processing. 2013;91(2):175-182. https://doi.org/https://doi.org/10.1016/j.fbp.2013.01.002.
[34] Huerta E, Corona Hdez J, Oliva A, Aviles F, González-Hernández J. Universal testing machine for mechanical properties of thin materials. Revista mexicana de física. 2010;56:317-322.
[35] Johns J, Rao V. Mechanical properties of MA compatibilised NR/CS blends. Fibers and Polymers. 2009;10(6):761-767. https://doi.org/10.1007/s12221-009-0761-x.
[36] Bartczak Z, Galeski A. Mechanical Properties of Polymer Blends. In: Utracki LA, Wilkie CA, editors. Polymer Blends Handbook. Dordrecht: Springer Netherlands; 2014. p. 1203-1297.

PAPERS SUMMARIES

This section summarises the significant results from Papers I to IV.

Paper I focus on the influence of thermal degradation on the crystallization of poly(butylene terephthalate). The results demonstrate a significant shift in PBT's crystallization temperature (T_c), indicating a significant modification. Throughout the experiment, T_c transitions from an initial value of 193°C to a final value of 133°C, signifying a noteworthy decrease of 60°C. This shift unfolds through three distinct phases: an initial rise in T_c, an intermediate stage marked by a steep decrease, and a subsequent degradation period characterized by a more moderate decline. The trends in crystallinity and crystallization kinetics mirror this pattern, with an increase followed by a sharp decrease during the intermediate degradation phase and a moderate decrease in the late-stage period. Furthermore, the investigation identifies the existence of two distinct melting peaks within the DSC data, implying the presence of differing lamellar thicknesses. These peaks experience a reduction in melting point (T_m). The higher melting point, T_{m1}, shifts during degradation from 225 to 187°C, constituting a decrease of 38°C. Conversely, the lower melting point, T_{m2}, undergoes a degradation-induced change from 213 to 172°C, reflecting a decrease of 41°C. Using a small angle X-ray scattering (SAXS) analysis provides additional support for the changes caused by degradation, revealing a decrease in the long period (L). Our investigation effectively underscores the impact of the stages of degradation on non-isothermal crystallization, accentuating the gradual decrease in T_c, peak height, crystallinity, and crystallization kinetics during the late-stage degradation phase. The research underscores the intricate nature of PBT's crystallization behaviour under thermal degradation, reflecting the interplay of lamellar thickness and molecular weight. The comprehensive analysis, coupled with comparisons to relevant research, contributes to a broader understanding of polymer degradation and its implications for the crystallization process. Further exploration into the intricate mechanisms behind these changes has the potential to offer valuable insights into improving polymer properties for specific applications. This, in turn, can foster advancements in the realms of polymer engineering and materials science.

Paper II focuses on the profound influence of fusion temperature on the intricate crystallization kinetics of poly(butylene terephthalate). The empirical results underscored a pivotal correlation between fusion temperature and the resultant heat flow curve, exemplified by a conspicuous shift towards lower thermal regimes. Elevation of the fusion temperature engendered a corresponding reduction in crystallinity, coupled with a discernible shift in the position of the heat flow profile. A significant shift in both peak position and crystallinity manifested within the fusion temperature range of 232-240°C. Subsequently, a nuanced transformation emerged within the range of 240-246°C. Remarkably, the range of 246-260°C exhibited a consistent absence of modification in peak position or crystallinity. The Ozawa model unveiled a compelling insight into the reciprocal interplay between cooling rate and relative crystallinity. This, in turn, underscored the temperature-dependent intricacies of nucleation and crystal growth mechanisms. Meanwhile, the Avrami model, renowned for its aptitude in scrutinizing isothermal crystallization kinetics, emerged as a highly fitting model for analysis. Isothermal experiments, mirroring the trends observed in the nonisothermal counterparts, duly ratified the profound imprint of fusion temperature on crystallization kinetics. Lower fusion temperatures were associated with accelerated crystallization kinetics, whereas a gradual diminishment was witnessed within the fusion temperature range of 232-242°C. Notably, this decrement stabilized within the temperature range of 242-250°C. These findings afford invaluable insights into the intricate terrain of PBT's crystallization kinetics. They provide a convincing foundation for optimizing processing parameters and enhancing material attributes across diverse applications. This research further beckons for future exploration, encouraging an in-depth scrutiny of the intricate nexus between crystallization kinetics and the resulting material properties of PBT. Such endeavours hold the potential to catalyze advancements in industrial applications and bolster the performance of this versatile material.

Paper III delved into a comprehensive exploration of the profound impact of fusion temperature and duration on the intricate nonisothermal crystallization kinetics of polyamide 6 (PA6). Employing differential scanning calorimetry (DSC) in conjunction with polarized optical microscopy (OM), the study unveiled a wealth of insights. Specifically, an augmentation of the fusion temperature was associated with narrower and diminished exothermic traces. This, in turn, results in the creation of diminutive nucleation centres, coupled with a discernible shift in crystallization temperature and a decrease in crystallization kinetics. Furthermore, an interesting correlation materialized between fusion temperature and the crystallization half-time. Evidently, higher temperatures result in longer times needed to reach a given level of crystallinity due to increased molecular mobility and crystal growth. The study harnessed the Ziabicki, Ozawa, and Nakamura models to illuminate the intricacies of crystallization kinetics. These models collectively underscored the profound influence of varying fusion temperatures, significantly impacting both nucleation and the progression of the crystalline phase. The implications of these findings extend to the domain of polymer material processing and its ensuing properties. This inquiry augments our comprehension of the underlying mechanisms at play and sheds light on strategies for enhancing the attributes of polymer materials through judicious control of fusion conditions.

Paper IV meticulously scrutinized the transformative influence of carbon fibres integrated within an elastic polymer matrix on the mechanical attributes and morphology of ethylene octene copolymer/carbon fibres (EOC/CF) composites. A comprehensive of numerous analytical methodologies underpinned this exploration. SEM images definitively affirmed the successful dispersion of carbon fibres within the EOC matrix. Furthermore, the stress-strain profiles eloquently conveyed that the introduction of CF engendered a marked enhancement in both tensile modulus and stress while preserving the composites' inherent elasticity. The mechanical underpinning of these composites was subjected through theoretical models, such as the Guth-Gold and Guth-Smallwood models. These models provided quantitative estimates for the tensile modulus, accounting for different filler geometries. The viscoelastic behaviour of the composites was comprehensively evaluated via the Burgers model. Dynamic mechanical analysis, in turn, furnished a revelation: the storage modulus increased with frequency, and the *tan* δ curves notably signaled the prevalence of elastic behaviour. Additionally, this investigation encompassed an inquiry into the electrical properties of the composites. Evidently, the EOC/CF composites exhibited a critical percolation threshold at a weight fraction of 10% CF. This investigation points to unique combinations of thermoplastic elastomers and carbon fibres, which have implications for developing advanced composites with improved properties and can be used in electronics engineering, especially pressure/strain sensors.

PAPER I

Influence of Thermal Degradation on the Crystallization of Poly(butylene terephthalate)

Ahmed Nasr * and Petr Svoboda

Department of Polymer Engineering, Faculty of Technology, Tomas Bata University in Zlin, Vavreckova 5669, 760 01 Zlin, Czech Republic

ABSTRACT

Our work reveals a notable shift in the crystallization temperature (T_c) of PBT at which crystallization occurs due to exposure to prolonged thermal degradation at 270°C in an environment of nitrogen gas. The initial Tc of 193°C undergoes a marked decrease, settling at 133°C, which signifies a considerable 60°C shift towards lower temperature ranges. This transition is discernible across three distinct degradation stages: an initial phase of increase, an intermediate phase characterized by a sharp decline, and a subsequent late stage of the degradation phase characterized by a more moderate decrease in T_c. Both crystallinity and crystallization kinetics consistently mirror this pattern, demonstrating an initial rise, a rapid subsequent drop, and a gradual decline in the late-stage period. Evident from the presence of two melting peaks, the research implies differing lamellar thicknesses. As the degradation progresses, the melting points of these peaks, denoted as T_{m1} and T_{m2}, decline at 38°C and 41°C, respectively. Validation of the degradation-induced changes is provided by a small angle X-ray scattering (SAXS), which corroborates the observed decrease in the long period (L). A contextualization of the results against prior studies underscores analogous trends in the alteration of crystallization behaviour consequent to degradation.

KEYWORDS

PBT; DSC; SAXS; thermal degradation; crystallization kinetics

1. INTRODUCTION

The behaviour of polymers under various conditions of temperature and environmental exposure is paramount in materials science and engineering [1]. Polymer degradation, driven by thermal, mechanical or chemical factors, can change their macroscopic and molecular properties, influencing their overall performance and applicability [2]. Poly(butylene terephthalate) (PBT) is a high-performance thermoplastic polymer that has garnered significant attention within the domain of materials science and engineering due to its exceptional combination of mechanical, thermal, and electrical properties [3]. This semi-crystalline polymer is derived from the condensation polymerization of terephthalic acid or dimethyl terephthalate with 1,4-butanediol. The resultant polymer exhibits a range of attributes that render it suitable for diverse industrial applications [4]. The alteration of PBT's crystallization behaviour under thermal degradation has emerged as a significant area of investigation, given its implications for material integrity and longevity [5].

The crystalline nature of polymers strongly influences their mechanical, thermal, and optical properties, rendering a comprehensive understanding of the crystallization process essential for informed material design and utilization [6]. Crystallization is a dynamic phenomenon involving transforming polymer chains from a disordered state to an ordered crystalline structure. This transformation is governed by a delicate interplay of many factors like temperature, molecular weight, processing conditions, and, notably, structural defects and degradation [7].

In recent years, researchers have increasingly turned their attention to the impact of thermal degradation on the crystallization kinetics and behaviour of polymers [8-11]. The structural changes induced by degradation can introduce defects, alter molecular weight distributions, and perturb chain mobility, all of which can influence crystallization dynamics. The scientific exploration of such changes advances our fundamental understanding of polymer behaviour and offers valuable insights for practical applications, ranging from polymer processing and engineering to developing degradation-resistant materials. To our knowledge, no previous research has investigated the influence of thermal degradation on PBT's crystallization, which was carried out under a very long-time experiment.

This paper delves into the specific poly(butylene terephthalate) case and its crystallization behaviour under prolonged thermal degradation. By employing differential scanning calorimetry (DSC) and small angle X-ray scattering (SAXS)

techniques, the study examines the shifts in crystallization temperature (Tc), crystallinity, and crystallization kinetics as PBT undergoes various stages of thermal degradation. The investigation considers the complexities introduced by lamellar thickness variations and melting point shifts, shedding light on the intricate relationships between degradation-induced structural changes and crystallization tendencies.

Through a systematic analysis of the effects of thermal degradation on PBT's crystallization behaviour, this study contributes to a deeper comprehension of polymer degradation mechanisms and their repercussions. The insights garnered have the potential to inform the design of polymers with enhanced durability and performance in the face of degradative conditions. Furthermore, by establishing parallels with prior research, this work aims to contextualize its findings within the broader landscape of polymer science, enriching the collective knowledge that underpins advancements in polymer engineering and material design.

2. EXPERIMENTAL METHOD

The PBT variant used in this study, ARNITE T08-200, was supplied by DSM Company, headquartered in Genk, Belgium. An illustration representing the molecular configuration of this PBT type is presented in Figure 1. For the small angle X-ray scattering (SAXS) analysis, we used the Anton Paar SAXSpace instrument. Samples were placed in the holder, and the distance between the sample and the detector was $268.5\,mm$. $CuK\alpha$ was used with $U = 40\,kV,\ I = 50\,mA$, exposition time $t = 15\,min$. An imaging plate was used as a detector.

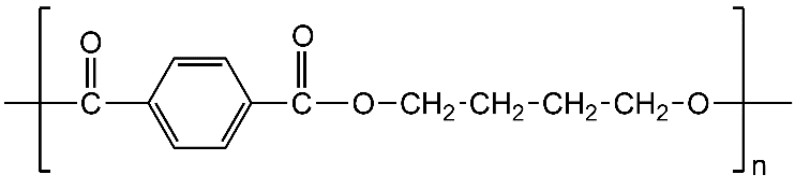

Figure 1. Chemical structure of PBT.

The degradation, crystallization and melting behaviour studies were performed in Mettler Toledo DSC 1 machine under the Nitrogen with a flow rate set at 200 ml/min. This DSC machine has some limits, e.g., the maximum number of steps being 40. Initially we did not know how long the experiment would last and how significant changes in crystallization and melting would happen. So initially, we chose the 50 min degradation steps. The 150 h degradation-crystallization

experiment took 14 long experiments (each composed of 40 steps lasting about 15 h). The first-day experimental plan was slightly different from the following plans. Step #1: heating from 25°C to 270°C at heating rate 20°C/min, step #2: isothermal annealing 1 min at 270°C, step #3: cooling from 270°C to 60°C at cooling rate being 20°C/min, step #4: heating from 60°C to 270°C at heating rate 20°C/min, step #5: isothermal annealing 50 min at 270°C, step #6: cooling from 270°C to 60°C at cooling rate 20°C/min, step #7: heating from 60°C to 270°C at heating rate 20°C/min, step #8: isothermal annealing 50 min at 270°C, step #9: cooling from 270°C to 60°C at cooling rate 20°C/min, … continued similarly till step 40. Heating steps were: 1, 4, 7, 10, 13, 16, 19, 22, 25, 28, 31, 34, 37 and 40, all were done at 20°C/min heating rate. Cooling steps were: 3, 6, 9, 12, 15, 18, 21, 24, 27, 30, 33, 36 and 39, all were done at 20°C/min cooling rate. The program was slightly modified the following days, and all the isothermal annealing steps at 270°C lasted 50 min. The crystallinity percentage of PBT was calculated at a heat of fusion of 142 J/g for 100% crystalline PBT [12].

3. RESULTS AND DISCUSSION

At the beginning of the degradation experiment, we observed an interesting increase in the position of crystallization temperature T_c from 182 to 189°C, peak height increased from about 2.1 to 3.1 W/g; it changed from broad to narrower – see Figure 2. After integration, the relative crystallinity curves were obtained, called "S-curve", and then the slope in the inflection point was evaluated, which relates to the maximum in crystallization kinetics. The slope (or the crystallization kinetics) has significantly increased from 0.035 to 0.044 (Table 1). The kinetics were also evaluated with the help of a modified Avrami equation (for non-isothermal crystallization). Our results in the initial period of degradation agree well with other researchers [13, 14].

Avrami model [15] provides a mathematical framework to analyze the fraction of crystalline material as a function of time, which is described in equation (1):

$$ln[-ln(1-X_t)] = ln\,k + n\,ln\,t \qquad (1)$$

Where *n* is Avrami exponent, k Avrami rate constant, and X_t is the crystallinity of polymer at time *t*.

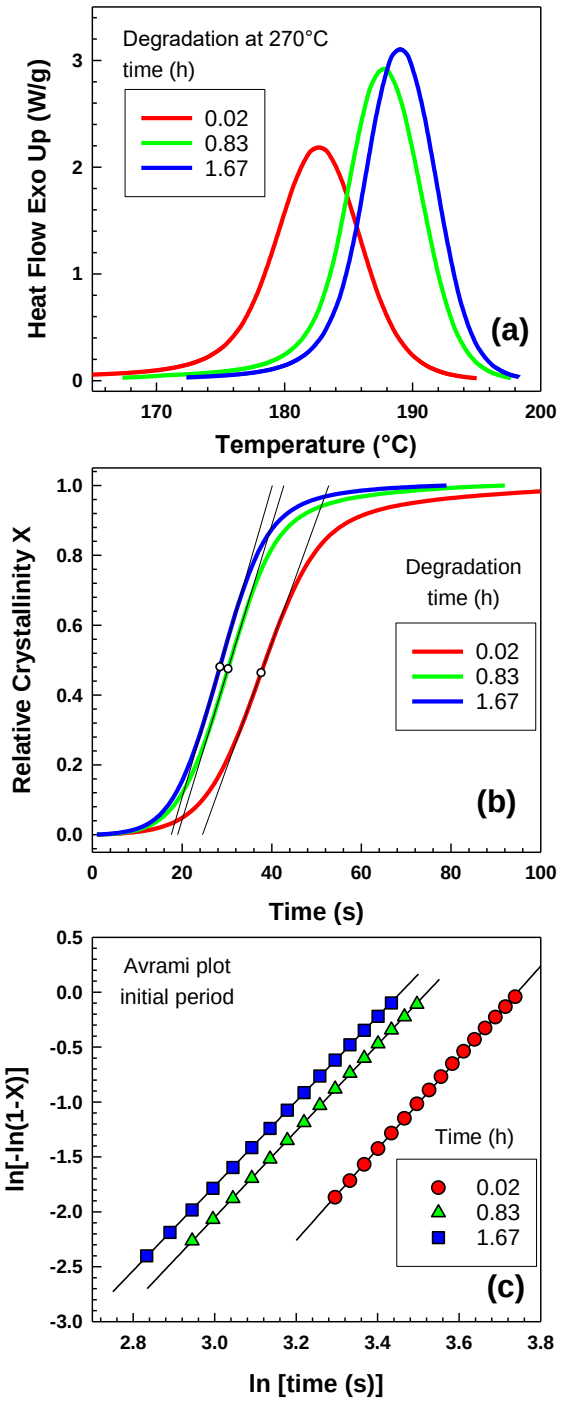

Figure 2. Non-isothermal crystallization – initial period.

Degradation causes increased T_c [13]. Rangari and Vasanthan showed that PLA sample had T_c before degradation at 89°C, and after 10 days of degradation the T_c was 96°C. Hoffman and Miller explained an increase in crystallization kinetics with decreasing molecular weight by reptation model. Shorter molecules are easier to pull out towards the growing front of crystal lamella [14].

Table 1. Positions of crystallization peak T_c and relative crystallinity X from the cooling experiment at 20°C/min as a function of degradation time at 270°C.

Time (h)	T_c (°C)	X
0.02	185.2	42.11
0.83	190.8	47.60
1.67	192.3	48.58
5.83	190.4	51.40
10.00	184.9	50.71
12.50	180.3	49.65
16.67	177.4	50.03
20.83	172.7	50.24
23.33	167.4	50.12
27.50	161.1	48.62
31.67	156.5	47.61
38.33	151.4	48.35
60.00	145.3	40.68
77.50	143.0	30.93
99.17	138.6	24.05
150.83	132.9	14.75

Unlike the initial crystallization period, the intermediate period shows a decrease in the crystallization peak position T_c – see Figure 3. In the time range 5-38h, the T_c has changed from 187 to 149°C (a significant 38°C decrease), and the peak height decreased initially from 3.2 to 2.3 W/g (time 5-20h), and then it remained approximately constant (time 20-38h). Our data agree well with other researchers.

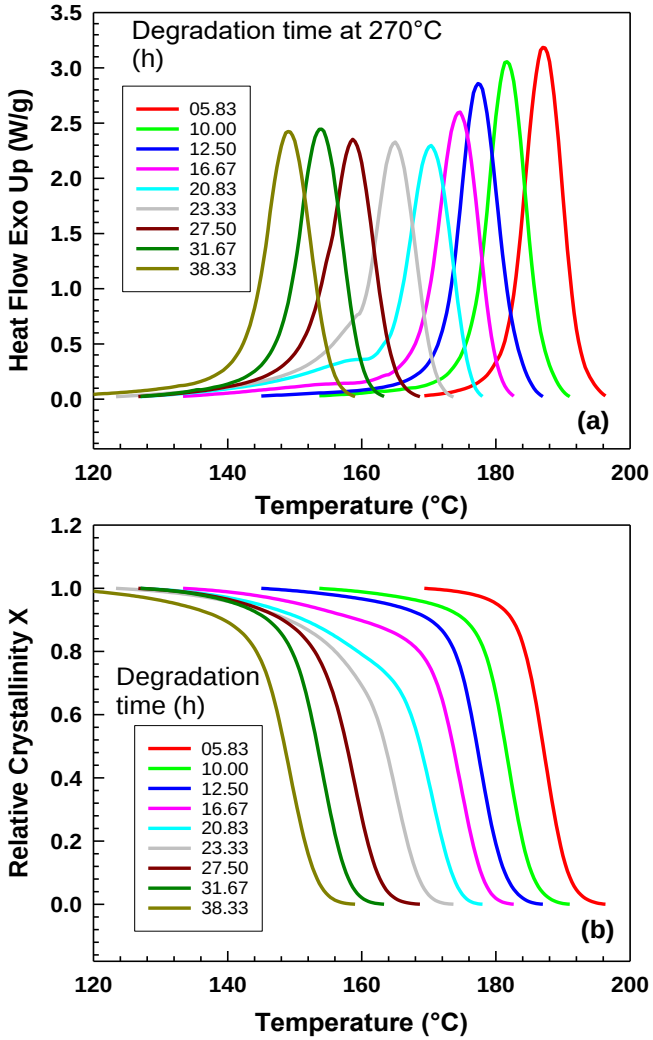

Figure 3. Non-isothermal crystallization – intermediate period.

Rabello and White [16] observed decreased T_c for photodegraded polypropylene; initially, the T_c was 115°C, and after 24 weeks of photodegradation, it was 108°C. Muthuraj et al. [17] studied poly(butylene succinate) (PBS) and observed a decrease in T_c after degradation - 30 days of continuous conditioning at 50°C and 90% relative humidity (RH). Initially, the PBS sample had T_c 92°C and after degradation, it was 77°C. Avela et al. [18] observed a lower T_c for polypropylene with lower molecular weight. Wang et al. [19] observed a decreased T_c for poly(trimethylene terephthalate) samples with lower molecular weight. Xu and Shi [20] studied the crystallization kinetics of silsesquioxane-based hybrid star poly(epsilon-caprolactone) and found a lower position of crystallization peak T_p for polymer with lower molecular weight.

Figure 4 illustrates the late degradation stage's influence on non-isothermal crystallization. The time frame for degradation was 38-150h. The prolonged degradation at 270°C is taking a toll on the polymer sample. We have observed a further decrease in T_c (from 149 to 132°C), but this time, there is also a tremendous decrease in peak height (from 2.4 to 0.26 W/g) reflected in a significantly decreased crystallinity. Also, the crystallization kinetics expressed as the slope in the inflection point decreases from 0.035 to 0.013 (as shown in Table 2).

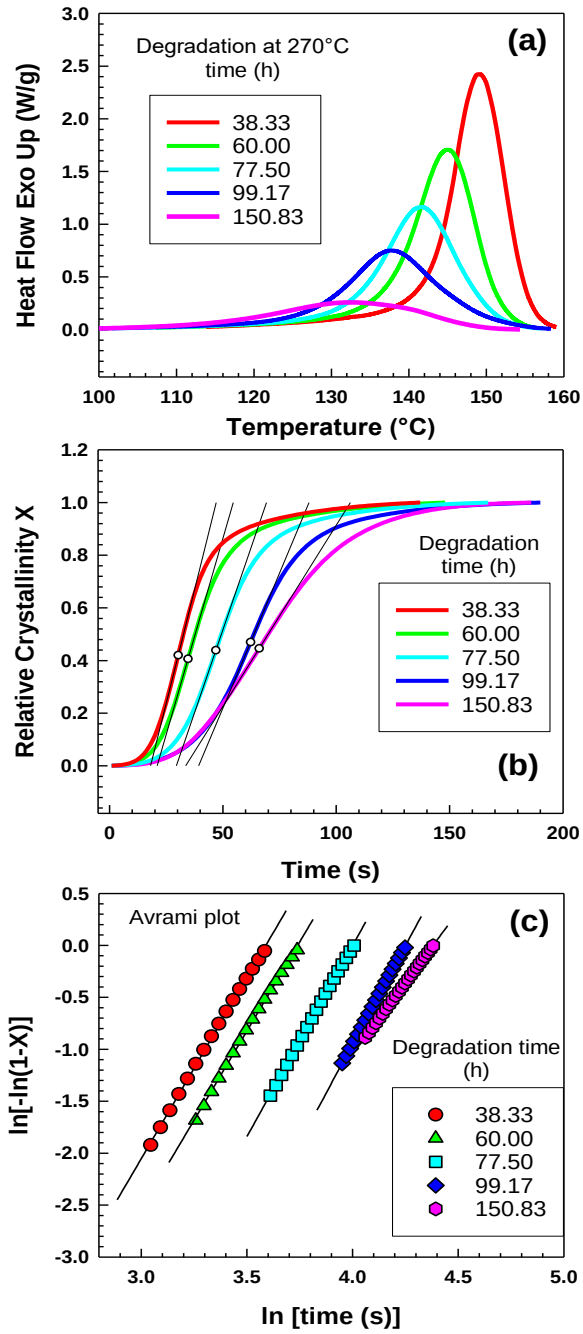

Figure 4. Non-isothermal crystallization – late stage.

Table 2. Crystallization kinetics parameters as a function of degradation time at 270°C: half time of crystallization $\tau_{1/2}$, reciprocal half-time of crystallization $\tau_{1/2}^{-1}$, Nakamura parameter $K = k^{1/n}$, the slope at the inflection point.

Time (h)	$\tau_{1/2}$ (s)	$\tau_{1/2}^{-1}$ (s^{-1})	$K = k^{1/n}$	Slope (s^{-1})
0.02	38.63	0.02589	0.02330	0.03545
0.83	30.84	0.03243	0.02907	0.04219
1.67	28.86	0.03465	0.03105	0.04437
5.83	28.86	0.03464	0.03091	0.04379
10.00	29.74	0.03362	0.02973	0.04131
12.50	30.43	0.03286	0.02906	0.03968
16.67	28.14	0.03553	0.03032	0.03943
20.83	28.78	0.03474	0.02853	0.03902
23.33	31.43	0.03182	0.02668	0.03771
27.50	33.64	0.02973	0.02576	0.03751
31.67	30.88	0.03238	0.02835	0.03621
38.33	32.56	0.03071	0.02683	0.03459
60.00	37.73	0.02650	0.02324	0.02978
77.50	49.32	0.02027	0.01812	0.02515
99.17	63.62	0.01572	0.01418	0.02054
150.83	69.91	0.01430	0.01250	0.01377

Our results correspond well with Rabello and White [16], who also observed a decreased crystallization kinetics for photodegraded polypropylene and Fraise et al. [21], who observed a decreased crystallization kinetics for photo and thermo-aged poly(ethylene oxide). Ergoz et al. [22] found a tremendous decrease in the crystallization kinetics of linear polyethylene when Mw decreased from 20000 to 5000 g/mol.

Figure 5 and Table 1 illustrate the change in position of crystallization peak T_c and crystallinity X as a function of degradation time. The change in T_c position can be divided into three time ranges. The T_c increases sharply in the initial period (0.02-1.67h). The T_c decreases sharply during the intermediate time range (3.3-31.7h). Finally, in the late stage of degradation (45-150h), the decrease of T_c is relatively moderate. The crystallinity curve can also be divided into three stages. Initially (0.02-3.33h), the crystallinity increases. Then, in the intermediate degradation time (3.33-38.33h) the crystallinity remains almost constant. In the late stage of degradation (38-150h) the crystallinity gradually decreases.

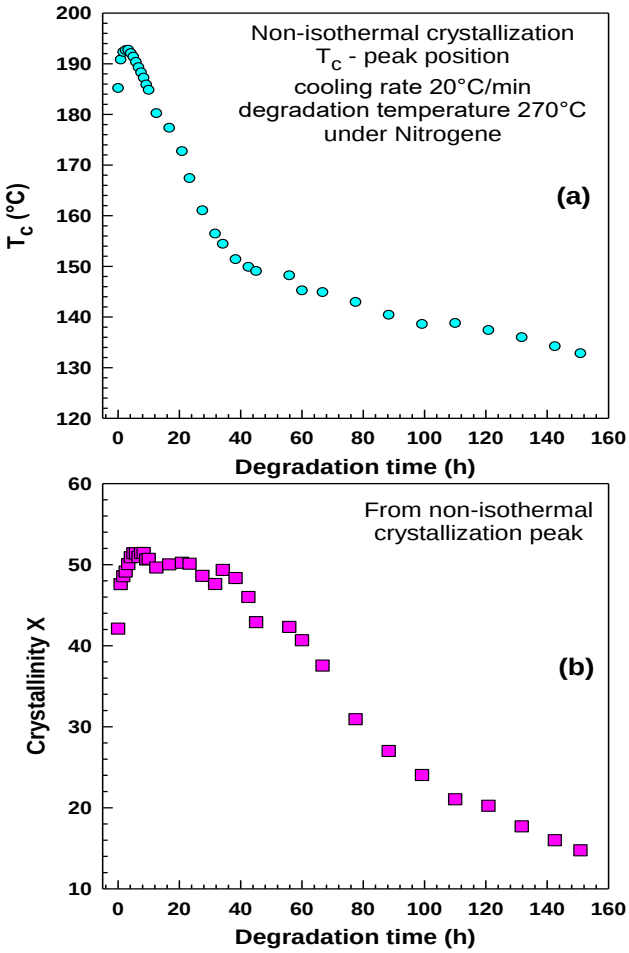

Figure 5. (a) Crystallization peak position Tc and (b) crystallinity X as a function of degradation time at 270°C.

Our initial increase in T_c corresponds well with Rangari and Vasanthan [13], who studied crystallization after and enzymatic degradation of poly(L-lactic acid) (PLLA) films. In their case, the T_c has increased from 89°C to 96°C after 10 days of degradation, and crystallinity has increased from 19.7 to 23.2 % [13].

Initially, we observed an increase in crystallinity. Tsuji et al. [23] studied the hydrolytic degradation of poly(L-lactic acid) and found an increase in crystallinity during the degradation.

Figure 6 and Table 2 illustrate the influence of thermal degradation on (a) the slope at the inflection point, (b) the Nakamura K parameter and (c) the reciprocal of crystallization half-time [$t_{1/2}^{-1}$]. The crystallization kinetics is highly influenced by the degradation time.

As can be seen, a parallel trend emerges, consistent with the alterations observed in crystallinity and peak position (see Figure 5).

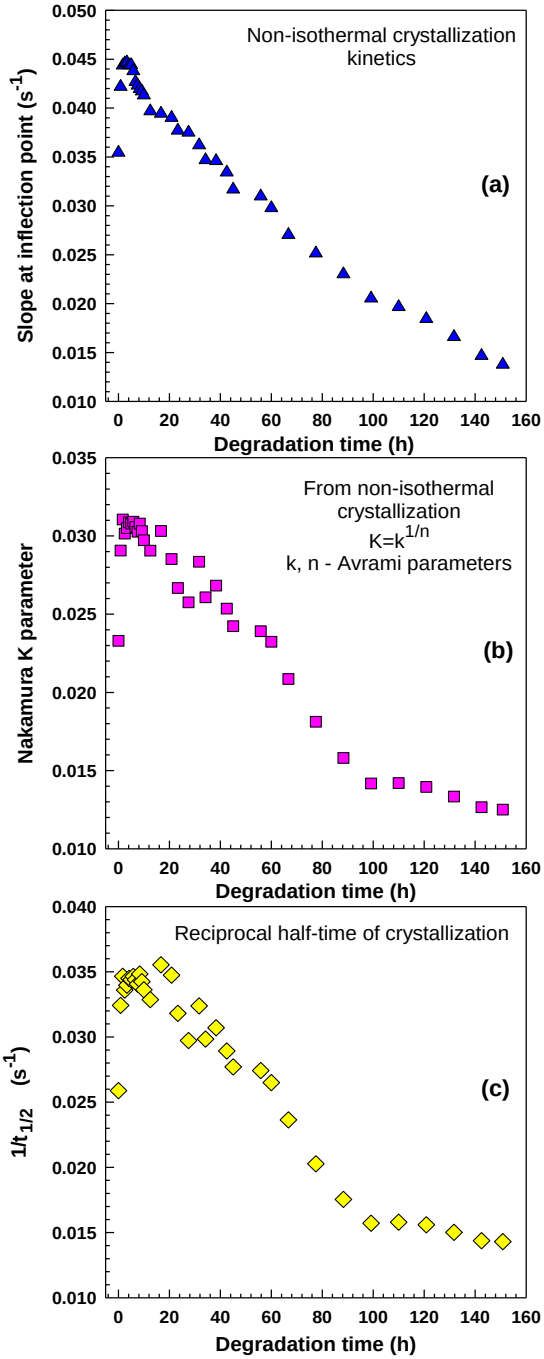

Figure 6. Crystallization kinetics expressed by: (a) slope at the inflection point of the S-curve, (b) Nakamura K, (c) reciprocal crystallization half-time $\tau_{1/2}^{-1}$.

Initially introduced in 1973, the Nakamura model [24] is a firmly established paradigm for characterizing non-isothermal polymer crystallization. Rooted in this model is a comprehensive consideration of both temperature and the degree of crystallization within the polymer, further encompassing the crystallization kinetics delineated by the Avrami equation.

$$K(T) = k(T)^{\frac{1}{n}} \qquad (2)$$

Where *n* and *k* are Avrami parameters, required to calculate the Nakamura K constant.

Rabello and White [16] observed similar behaviour for photodegraded polypropylene. After 3 weeks of photodegradation, they observed increased crystallization kinetics followed by steady decrease till the end of the experiment (24 weeks).

Fraisse et al. [21] reported a decrease in crystallization kinetics for poly(ethylene oxide) sample exposed to thermo-ageing using photo DSC at 55°C. The half time of crystallization for photo-oxidation of PEO at 15°C has increased from 105s to 345s. For the thermo-oxidation experiment at 75°C, the time of crystallization increased from 101s to 266s after thermo-oxidation for 1200s, i.e., the crystallization kinetics became relatively slower.

Overall, the thermal degradation exerts a significant influence on the crystallization kinetics of PBT. Its inherent crystallization behaviour is notably altered as it undergoes thermal degradation, characterized by chain scission, crosslinking, and molecular weight reduction. The variations in molecular weight distribution, chain mobility, and polymer conformation introduced by degradation intricately impact the nucleation and growth processes central to crystallization kinetics. These alterations in polymer structure can lead to changes in crystallization temperature, crystallinity, and growth rates, necessitating a comprehensive analysis to unravel the underlying mechanisms. Next we will illustrate the effects of thermal degradation on the melting temperatures of PBT and clarify the appearance of double melting points that is associated with lamella thickness.

Several authors have reported a change in melting point T_m towards lower values during degradation [16, 23, 25, 26]. Figure 7 shows the change in melting temperature by the thermal degradation at 270°C. Increasing the degradation time, the peak shifts to lower temperatures and then two melting points appear (T_{m1} and T_{m2}).

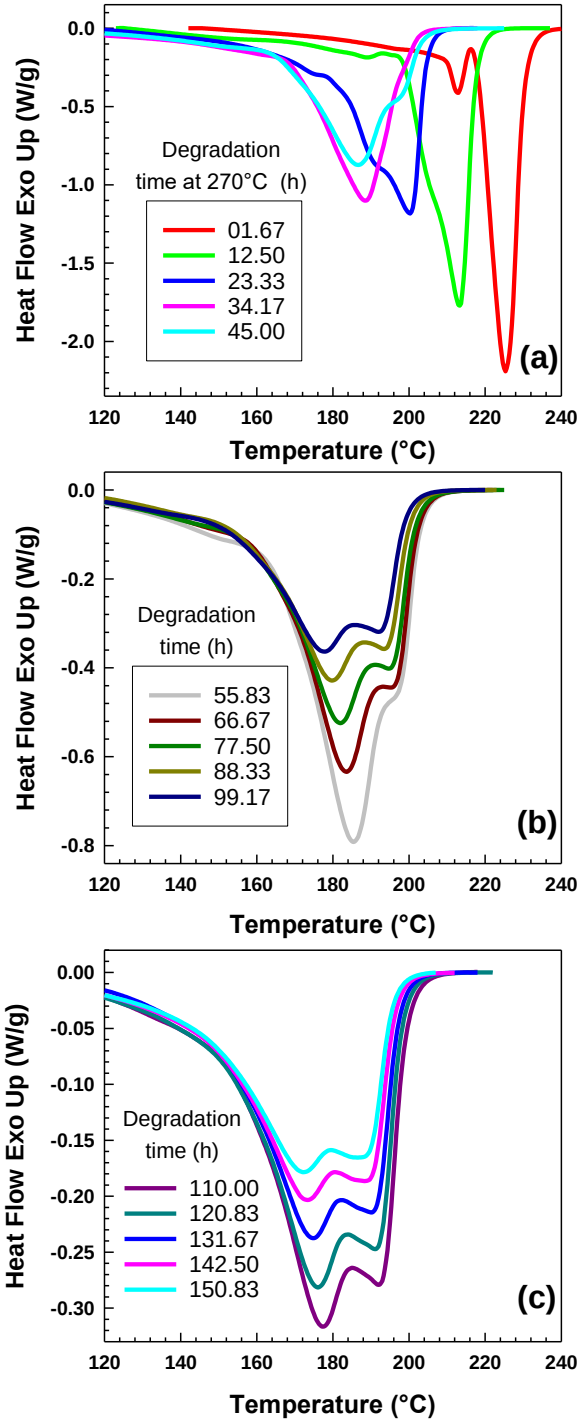

Figure 7. Change in melting behaviour by the thermal degradation at 270°C.

Figure 8 and Table 3 confirm this effect of thermal degradation on PBT's melting temperature and crystallinity. Initially (0-20h), the change in T_m for PBT is enormous, then from 20 to 150h the change is relatively moderate. The presence of two melting peaks is clear.

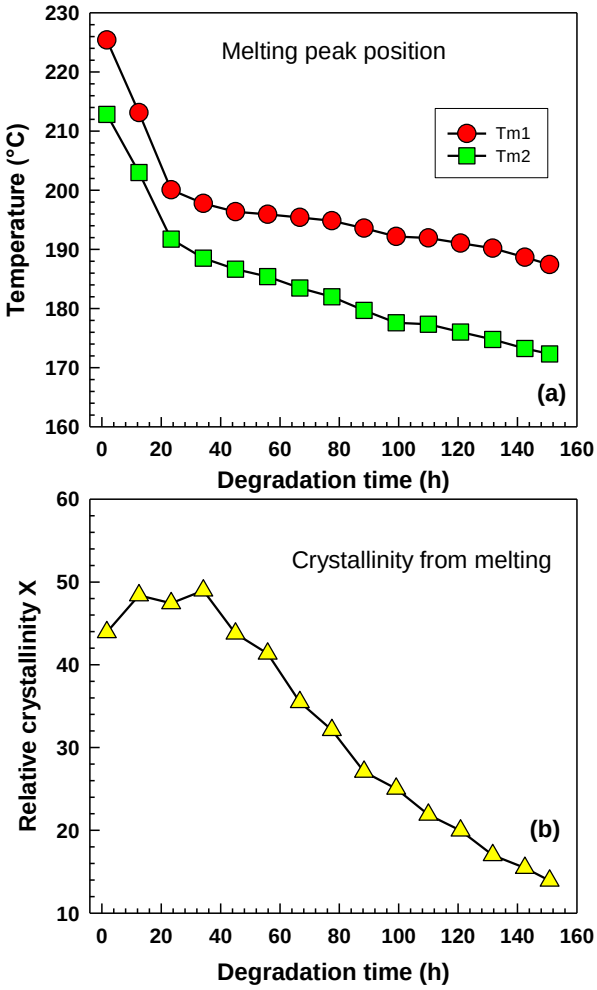

Figure 8. (a) Positions of higher and lower melting peaks, (b) change in crystallinity derived from melting peaks.

Table 3. Positions of melting peaks T_{m1} and T_{m2} and relative crystallinity X from heating experiment at 20°C/min as a function of degradation time at 270°C.

Time (h)	T_{m1} (°C)	T_{m2} (°C)	X
1.67	225.4	212.8	43.93
12.50	213.1	203.0	48.39
23.33	200.1	191.8	47.43
34.17	197.8	188.5	48.96
45.00	196.4	186.7	43.76
55.83	195.9	185.4	41.35
66.67	195.4	183.5	35.48
77.50	194.8	182.0	32.11
88.33	193.6	179.7	27.07
99.17	192.2	177.6	25.02
110.00	191.9	177.3	21.89
120.83	191.1	176.0	19.98
131.67	190.2	174.8	17.01
142.50	188.7	173.3	15.46
150.83	187.4	172.3	13.92

The presence of two melting peaks (in the DSC experiment) suggests that the situation is more complicated, i.e. the presence of thicker and thinner lamellae and the thickness of both decreases during the degradation [27]. Many researchers have described the long period and lamellar thickness calculation from SAXS data [28-33].

Crystalline structure analysis was undertaken using SAXS and determining the long period involved using equation (3) [33].

$$L = \frac{2\pi}{q_{max}} \qquad (3)$$

L is the long period related to the scattering peak position, and q is the scattering vector.

A clear reduction in the long period is observed due to irradiation. The initial sample exhibited a long period of $L = 12.31\ nm$, whereas the sample subjected to irradiation at a degradation time of 30h demonstrated a long period of $L = 10.91\ nm$ (see Table 4).

Table 4. SAXS results: peak position q_{max} (nm^{-1}) and long period L (nm) as a function of degradation time at 270°C.

Time (h)	q_{max} (nm^{-1})	L (nm)
0.83	0.5179	12.13
23.33	0.5605	11.21
30.00	0.5761	10.91

The effect of thermal degradation on the lamellar thickness can be noted clearly, which can be described by the Gibbs-Thomson equation. The equation calculates the change in melting point with lamella thickness. It assumes that the crystal sizes *a* and *b* with thickness *l*, we can calculate the melting temperature (T_m) by [32]:

$$T_m(l) = T_m^0\left(1 - \frac{2}{\Delta h}\left(\frac{\sigma}{a} + \frac{\sigma}{b} + \frac{\sigma_e}{l}\right)\right) \qquad (4)$$

Where Δh is the fusion temperature, σ is the surface free energy, and σ_e is the end surface free energy. Equation 4 can be modified into:

$$T_m(l) = T_m^0 - \frac{C}{l}, \qquad where\ C = \frac{2\sigma_e T_m^0}{\Delta h} \qquad (5)$$

In the case of a particular material, it becomes feasible to assess the reduction in lamellar thickness by gauging the decline in melting point:

$$\frac{l_2}{l_1} = \frac{T_m^0 - T_{m1}(l)}{T_m^0 - T_{m2}(l)} \qquad (6)$$

We have observed a decrease in melting point during the degradation. Based on the Gibbs-Thomson equation, we can assume that the lamellar thickness decreases during degradation. Initially, there is mainly one peak (even though the second peak is also present). The situation during the initial part of degradation could be graphically represented by Figure 10. In the later part of degradation, the presence of two peaks is evident and suggests the presence of lamellae with two different thicknesses (see Figure 11).

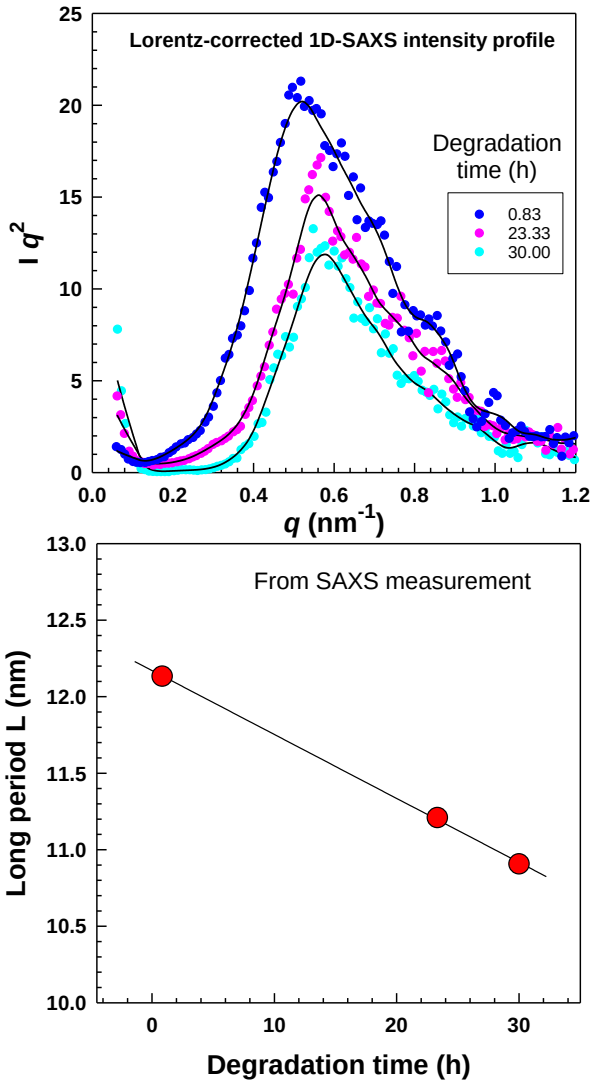

Figure 9. (a) Lorentz-corrected 1D-SAXS intensity profiles. (b) Change in long period L during the degradation.

The T_{m1} and T_{m2} are still moving towards the lower temperatures, so we can assume a moderate decrease in both lamellar thicknesses. The results from SAXS (see Figure 9 and Table 4) confirmed a decrease in long period L that comprises the lamellae's thickness plus the amorphous layer's thickness. The data from SAXS indicate a decrease in lamellar thickness during the degradation [34].

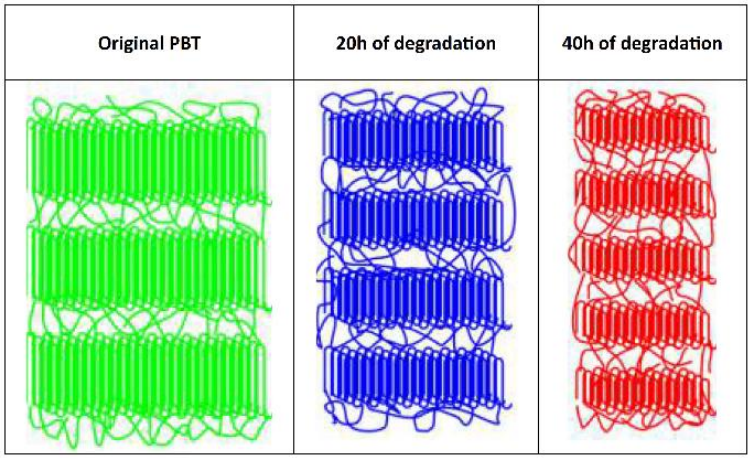

Figure 10. Decrease in lamellar thickness during the degradation (from SAXS).

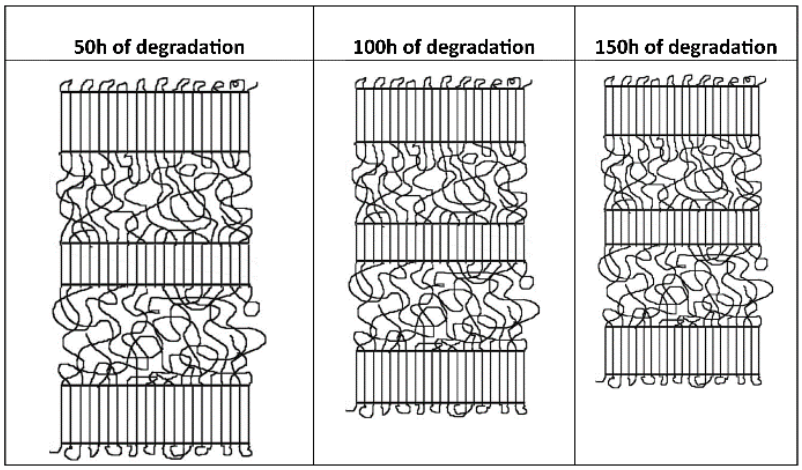

Figure 11. Two lamellar thicknesses are possibly decreasing during the degradation (from DSC).

4. CONCLUSION

The results reveal a substantial shift in T_c, indicating a significant alteration in the crystallization temperature of PBT. Throughout the experiment, the T_c shifts from an initial value of 193°C to a final value of 133°C, marking a notable 60°C decrease. This shift progresses through three distinct periods: an initial increase in T_c, an intermediate stage characterized by a steep decrease, and a late-stage degradation period with a more moderate decline. Crystallinity and crystallization kinetics exhibit a similar trend, with an increase followed by a steep decrease during the intermediate degradation period and a subsequent moderate decrease in the late-stage period. Additionally, the study identifies the presence of two melting peaks in the DSC data, suggesting the presence of two distinct lamellar thicknesses. These peaks experience a decrease in melting point (T_m), where the higher melting point T_{m1} changed during degradation from 225 to 187°C (a 38°C decrease) while the lower melting point T_{m2} changed during degradation from 213 to 172°C (a 41°C decrease). Small angle X-ray scattering (SAXS) analysis further supports the degradation-induced changes, revealing a decrease in the long period (*L*). Our work effectively illustrates the influence of the degradation stages on non-isothermal crystallization, highlighting the gradual decrease in T_c, peak height, crystallinity, and crystallization kinetics during the late-stage degradation. Our research emphasizes the complex nature of the crystallization behaviour of PBT under thermal degradation, reflecting the interplay of factors such as lamellar thickness and molecular weight. The study's comprehensive analysis and comparison with related research contribute to the broader understanding of polymer degradation and its impact on the crystallization process. Further investigations into these changes' intricate mechanisms could offer valuable insights into tailoring polymer properties for specific applications, fostering advancements in polymer engineering and materials science.

ACKNOWLEDGMENTS

The authors thank Tomas Bata University in Zlin for supporting this research through the Internal Grant Agency, ref. No: IGA/FT/2023/008.

REFERENCES

[1] Wang M, Guo L, Sun H. Manufacture of Biomaterials. In: Narayan R, editor. Encyclopedia of Biomedical Engineering. Oxford: Elsevier; 2019. p. 116-134.
[2] Parra DF, Fusaro J, Gaboardi F, Rosa DS. Influence of poly (ethylene glycol) on the thermal, mechanical, morphological, physical–chemical and biodegradation properties of poly (3-

hydroxybutyrate). Polymer Degradation and Stability. 2006;91(9):1954-1959. https://doi.org/https://doi.org/10.1016/j.polymdegradstab.2006.02.008.
[3] Huang J, Wang J, Qiu Y, Wu D. Mechanical properties of thermoplastic polyester elastomer controlled by blending with poly(butylene terephthalate). Polymer Testing. 2016;55:152-159. https://doi.org/https://doi.org/10.1016/j.polymertesting.2016.08.020.
[4] Díaz A, Katsarava R, Puiggalí J. Synthesis, Properties and Applications of Biodegradable Polymers Derived from Diols and Dicarboxylic Acids: From Polyesters to Poly(ester amide)s. 2014;15(5):7064-7123.
[5] Bikiaris DN, Karayannidis GP. Effect of carboxylic end groups on thermooxidative stability of PET and PBT. Polymer Degradation and Stability. 1999;63(2):213-218. https://doi.org/https://doi.org/10.1016/S0141-3910(98)00094-9.
[6] Murmu U, Adhikari J, Naskar A, Dey D, Roy A, Ghosh A, Ghosh M. Mechanical Properties of Crystalline and Semicrystalline Polymer Systems. 2022.
[7] Payal RS, Sommer JU. Crystallization of Polymers under the Influence of an External Force Field. Polymers (Basel). 2021;13(13). https://doi.org/10.3390/polym13132078.
[8] Samperi F, Puglisi C, Alicata R, Montaudo G. Thermal degradation of poly(butylene terephthalate) at the processing temperature. Polymer Degradation and Stability. 2004;83(1):11-17. https://doi.org/10.1016/S0141-3910(03)00167-8.
[9] Mcneill IC, Bounekhel M. Thermal-Degradation Studies of Terephthalate Polyesters .1. Poly(Alkylene Terephthalates). Polymer Degradation and Stability. 1991;34(1-3):187-204. https://doi.org/Doi 10.1016/0141-3910(91)90119-C.
[10] Lum RM. Thermal-Decomposition of Poly(Butylene Terephthalate). Journal of Polymer Science Part a-Polymer Chemistry. 1979;17(1):203-213. https://doi.org/10.1002/pol.1979.170170120.
[11] Passalacqua V, Pilati F, Zamboni V, Fortunato B, Manaresi P. Thermal-Degradation of Poly(Butylene Terephthalate). Polymer. 1976;17(12):1044-1048. https://doi.org/Doi 10.1016/0032-3861(76)90004-5.
[12] Hage E, Hale W, Keskkula H, Paul DR. Impact modification of poly(butylene terephthalate) by ABS materials. Polymer. 1997;38(13):3237-3250. https://doi.org/https://doi.org/10.1016/S0032-3861(96)00879-8.
[13] Rangari D, Vasanthan N. Study of Strain-Induced Crystallization and Enzymatic Degradation of Drawn Poly(L-lactic acid) (PLLA) Films. Macromolecules. 2012;45(18):7397-7403. https://doi.org/10.1021/ma301482j.
[14] Hoffman JD, Miller RL. TEST OF THE REPTATION CONCEPT - CRYSTAL-GROWTH RATE AS A FUNCTION OF MOLECULAR-WEIGHT IN POLYETHYLENE CRYSTALLIZED FROM THE MELT. Macromolecules. 1988;21(10):3038-3051. https://doi.org/10.1021/ma00188a024.
[15] Avrami M. Kinetics of Phase Change. I General Theory. The Journal of Chemical Physics. 1939;7:1103. https://doi.org/10.1063/1.1750380.
[16] Rabello MS, White JR. Crystallization and melting behaviour of photodegraded polypropylene .2. Re-crystallization of degraded molecules. Polymer. 1997;38(26):6389-6399. https://doi.org/10.1016/S0032-3861(97)00214-0.
[17] Muthuraj R, Misra M, Mohanty AK. Hydrolytic degradation of biodegradable polyesters under simulated environmental conditions. Journal of Applied Polymer Science. 2015;132(27). https://doi.org/10.1002/app.42189.
[18] Avella M, Dellerba R, Martuscelli E. Fiber reinforced polypropylene: Influence of IPP molecular weight on morphology, crystallization, and thermal and mechanical properties. Polymer Composites. 1996;17(2):288-299. https://doi.org/10.1002/Pc.10613.

[19] Wang XS, Yan DY, Tian GH, Li XG. Effect of molecular weight on crystallization and melting of poly(trimethylene terephthalate). 1: Isothermal and dynamic crystallization. Polymer Engineering and Science. 2001;41(10):1655-1664. https://doi.org/10.1002/Pen.10863.
[20] Xu JW, Shi WF. Synthesis and crystallization kinetics of silsesquioxane-based hybrid star poly(epsilon-caprolactone). Polymer. 2006;47(14):5161-5173. https://doi.org/10.1016/j.polymer.2006.04.062.
[21] Fraisse F, Nedelec JM, Grolier JPE, Baba M. Isothermal crystallization kinetics of in situ photo and thermo aged poly(ethylene oxide) using photoDSC. Physical Chemistry Chemical Physics. 2007;9(17):2137-2141. https://doi.org/10.1039/B618701c.
[22] Ergoz E, Fatou JG, Mandelkern L. Molecular-Weight Dependence of Crystallization Kinetics of Linear Polyethylene .1. Experimental Results. Macromolecules. 1972;5(2):147-157. https://doi.org/10.1021/Ma60026a011.
[23] Tsuji H, Shimizu K, Sato Y. Hydrolytic degradation of poly(L-lactic acid): Combined effects of UV treatment and crystallization. Journal of Applied Polymer Science. 2012;125(3):2394-2406. https://doi.org/10.1002/app.36498.
[24] Nakamura K, Katayama K, Amano T. Some Aspects of Nonisothermal Crystallization of Polymers .2. Consideration of Isokinetic Condition. Journal of Applied Polymer Science. 1973;17(4):1031-1041. https://doi.org/10.1002/app.1973.070170404.
[25] Rodriguez EJ, Marcos B, Huneault MA. Hydrolysis of polylactide in aqueous media. Journal of Applied Polymer Science. 2016;133(44). https://doi.org/10.1002/app.44152.
[26] Saha SK, Tsuji H. Effects of rapid crystallization on hydrolytic degradation and mechanical properties of poly(L-lactide-co-epsilon-caprolactone). Reactive & Functional Polymers. 2006;66(11):1362-1372. https://doi.org/10.1016/j.reactfunctpolym.2006.03.020.
[27] Ren YM, Zou H, Wang SJ, Liu JY, Gao DL, Wu CJ, Zhang SJ. Effect of annealing on microstructure and tensile properties of polypropylene cast film. Colloid and Polymer Science. 2018;296(1):41-51. https://doi.org/10.1007/s00396-017-4220-8.
[28] Housmans JW, Gahleitner M, Peters GWM, Meijer HEH. Structure-property relations in molded, nucleated isotactic polypropylene. Polymer. 2009;50(10):2304-2319. https://doi.org/10.1016/j.polymer.2009.02.050.
[29] Janicek M, Cermak R, Obadal M, Piel C, Ponizil P. Ethylene Copolymers with Crystallizable Side Chains. Macromolecules. 2011;44(17):6759-6766. https://doi.org/10.1021/ma201017m.
[30] Mamun A, Rahman SMM, Aiken C. Influences of the chemical defects on the crystal thickness and their melting of isothermally crystallized isotactic polypropylene. Journal of Polymer Research. 2017;24(9). https://doi.org/10.1007/s10965-017-1304-6.
[31] Picu RC, Osta AR. Elastic constants of lamellar and interlamellar regions in and mesomorphic isotactic polypropylene by AFM indentation. Journal of Applied Polymer Science. 2016;133(27). https://doi.org/10.1002/app.43649.
[32] Svoboda P, Trivedi K, Stoklasa K, Svobodova D, Ougizawa T. Study of crystallization behaviour of electron beam irradiated polypropylene and high-density polyethylene. Royal Society Open Science. 2021;8(3). https://doi.org/10.1098/rsos.202250.
[33] Liu X, Dai K, Hao X, Zheng G, Liu C, Schubert DW, Shen C. Crystalline Structure of Injection Molded β-Isotactic Polypropylene: Analysis of the Oriented Shear Zone. Industrial & Engineering Chemistry Research. 2013;52(34):11996-12002. https://doi.org/10.1021/ie401162c.
[34] Mani MR, Chellaswamy R, Marathe YN, Pillai VK. New Understanding on Regulating the Crystallization and Morphology of the beta-Polymorph of Isotactic Polypropylene Based on Carboxylate-Alumoxane Nucleating Agents. Macromolecules. 2016;49(6):2197-2205. https://doi.org/10.1021/acs.macromol.5b02466.

PAPER II

Effect of Fusion Temperature on the Crystallization Kinetics of Poly(butylene terephthalate)

Ahmed Nasr * and Petr Svoboda

Department of Polymer Engineering, Faculty of Technology, Tomas Bata University in Zlin, Vavreckova 5669, 760 01 Zlin, Czech Republic

ABSTRACT

A tremendous effect of fusion temperature on the crystallization kinetics of poly(butylene terephthalate) (PBT) was discovered. The crystallization peak shifted 22°C towards lower temperatures, and kinetics changed about ten times. The nonisothermal crystallization experiments revealed that an increase in fusion temperature led to a noticeable shift in the heat flow curve towards lower temperatures, indicating a significant change in the number of nucleation centres. This shift was observed within the temperature range of 232°C to 246°C, beyond which the heat flow curve stabilized. The analysis of relative crystallinity showed a decrease in crystallinity with increasing fusion temperature up to 246°C, accompanied by a shift of the S-curve towards lower temperatures. Detailed analysis revealed that the peak position of the heat flow curve decreased significantly from 232 to 240°C and then continued to decrease slightly until 246°C, then in the range 246-260°C, it remained constant. The influence of cooling rate on relative crystallinity was also investigated, revealing that faster cooling rates shifted the relative crystallinity curve towards lower temperatures. The Ozawa model was linear and demonstrated the significant effect of cooling rate (for 15, 20 and 25 °C/min) on nonisothermal crystallization kinetics. The Avrami model is perfectly implemented to evaluate the isothermal crystallization kinetics. The isothermal crystallization experiments confirmed the trends observed in the nonisothermal experiments, with the fastest crystallization occurring at lower fusion temperatures. During the isothermal crystallization experiment, the kinetics was gradually decreasing in the fusion temperature range 232-242°C, and then in the range 242-250°C, it remained constant. Overall, the study provides insights into the crystallization behaviour of PBT under different fusion temperatures and cooling rates.

KEYWORDS

PBT; DSC; fusion temperature; isothermal; nonisothermal; crystallization kinetics; cooling function

1. INTRODUCTION

Poly(butylene terephthalate) (PBT) is an essential semi-crystalline thermoplastic polymer with a crucial role in various industrial fields, having established its reputation based on superb mechanical and thermal properties [35, 36]. It has outstanding dimensional stability that sets PBT apart, allowing it to maintain its structure under different conditions. Its high resistance to numerous chemicals, low friction coefficient, and impressive synergy between strength and flexibility mark PBT as a material of substantial value. These attributes have led to widespread application in many fields [37]. From the automotive industry, where it forms critical parts, to electronics, where it is used in essential components, and even in manufacturing diverse industrial equipment, the usability of PBT is extensive and undeniable [38].

A key determinant of PBT's features and its broad-based use across multiple industries is its behaviour during crystallization. Crystallization kinetics, a cornerstone of polymer science, sheds light on the pace at which crystals form within a material. These crystallization rates hold substantial sway over the polymer's mechanical and physical properties, such as its durability, resilience, and ability to withstand heat and chemical exposures [39-41]. When exploring the kinetics of crystallization, researchers usually focus on two distinct scenarios: isothermal and nonisothermal crystallization. In the case of isothermal crystallization, a polymer is quickly cooled down and annealed at a constant temperature, enabling the monitoring of phase changes over a certain period. That provides valuable insight into how the material crystallizes under stable conditions. On the other hand, nonisothermal crystallization requires cooling the polymer at different cooling rates. This method mimics more authentic processing conditions, providing a more practical understanding of how the material might conduct in real-world applications [42-45].

The fusion temperature and the cooling rate are two crucial parameters in shaping the crystallization kinetics of PBT. Fusion temperature has a remarkable influence on the crystallization kinetics and, thereby, the final properties of PBT. Likewise, the cooling rate, which refers to the speed at which the polymer cools from its fusion temperature, is significant in determining the crystallization process, crystallinity yield, and properties of the resultant material [46, 47]. The complexity of crystallization kinetics has led to the development of numerous mathematical models, including the Avrami, Ozawa, Nakamura, and Ziabicki models [15, 24, 48, 49]. The Avrami model is a time-tested approach that provides

insights into the growth and nucleation processes during crystallization. The Ozawa model, introduced in 1971, offers a model for nonisothermal crystallization kinetics at various cooling rates.

Ziabicki et al., 1995. studied the memory effect phenomenon. According to his model, the impact of fusion temperature and time of fusion on the crystallization kinetics of polypropylene is apparent. The work discovered that raising the fusion temperature decelerated the overall crystallization process. However, it also led to an enhanced final degree of crystallinity. This outcome was attributed to the molecular arrangement and the alterations in the form of the polymer crystals brought on by the increased fusion temperature. This effect is highly relevant to the study of PBT, given its extensive use in processes such as injection molding and extrusion, where the thermal history varies considerably. As far as we know, such an investigation has yet to be carried out specifically for PBT.

This research article aims to provide an in-depth analysis of how the fusion temperature affects the crystallization kinetics of PBT, with a particular focus on the implications of the Ziabicki memory effect. By conducting thorough experimental studies and employing sophisticated mathematical models, we aim to elucidate how variations in fusion temperature and cooling rate influence the crystallization behaviour of PBT, thereby providing valuable insights that can aid in enhancing the processing and applications of this versatile polymer.

2. EXPERIMENTAL SECTION

ARNITE T08-200, a type of PBT, was provided by DSM Company, based in Genk, Belgium. A depiction of the PBT molecular structure can be found in Figure 1, with fundamental attributes of the substance summarized in Table 1. The experiments used PBT granules, which needed to be dried to remove moisture, a process conducted at 85°C for 12 hours. The dried granules were analyzed directly by differential scanning calorimetry (DSC). A different set of samples were used for each experiment.

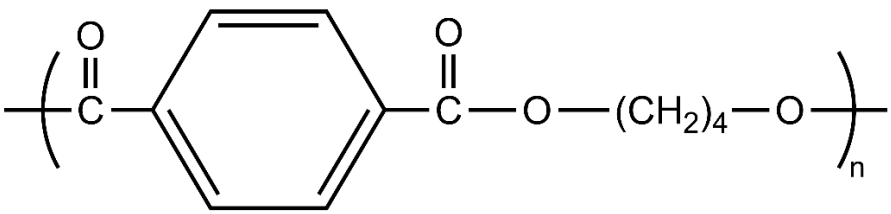

Figure 1. Molecular structure of PBT.

The thermal behaviour of PBT was analyzed using Mettler Toledo's differential scanning calorimeter (DSC-1) from Greifensee in Switzerland. Approximately 10 mg of the sample was used for the analysis, with a nitrogen flow rate of 30 mL per minute to prevent significant thermal degradation. For nonisothermal crystallization, the samples were heated to various melting points ranging from 232 °C to 260 °C for 300 seconds before being cooled to 25 °C. The experiment was also conducted at various cooling rates, precisely 15, 20, and 25°C/min. Similarly, the samples were melted at different fusion temperatures ranging from 232 to 250°C for a fusion time of 300 seconds for the isothermal crystallization at 212°C. The crystallinity percentage of PBT was calculated at the heat of fusion of 142 j/g for 100% of crystalline PBT [50, 51].

Table 1. Properties of PBT material.

Property	PBT DSM Arnite T08-200
Melt temperature (10 °C/min)	225 °C (ISO 11357-1/-3)
Tensile modulus	2550 MPa (ISO 527-1/-2)
Charpy notched impact strength	6 kJ/m^2 at 23 °C (ISO 179/1eA)
Density	1300 kg/m^3 (ISO 1183)

3. THEORETICAL BACKGROUND

3.1. Avrami Model

The Avrami model [15], a mathematical representation frequently employed in analyzing the kinetics of isothermal crystallization of polymers, suggests that the speed of crystallization in any polymer system is directly linked to the quantity of amorphous substance present at any moment. This model incorporates several factors in its Equation: the portion of crystalline material that is generated at a specified time, the temperature of crystallization, the rate constant contingent upon the polymer and the crystallization conditions, and the Avrami exponent that characterizes the process of crystallization. The mathematical representation of the Avrami model can be seen in Equation (1):

$$1 - X_t = exp(-kt^n) \qquad (1)$$

Where *k* represents the Avrami rate constant, *n* represents the Avrami exponent. The growth rate mechanisms and the nucleation process of the spherulites influence the values of both *k* and *n*.

The parameters for isothermal crystallization, derived from the differential scanning calorimetry (DSC), are employed to determine the crystallinity X_t. That is done by taking the area of heat flow peak (exothermic peak) during the crystallization period t, and then dividing this by the entire peak area:

$$X_t = \frac{\int_0^t \left(\frac{dH}{dt}\right) dt}{\int_0^\infty \left(\frac{dH}{dt}\right) dt} \qquad (2)$$

In Equation (2), the numerator signifies the heat produced at a specific time (*t)*, while the denominator denotes the cumulative heat produced until the crystallization process is fully accomplished.

These parameters (*k* and *n*) can be assessed using the linear regression as outlined in Equation (1), and then a double logarithmic transformation was implemented to give the below Equation:

$$ln[-ln(1-X_t)] = ln\,k + n\,ln\,t \qquad (3)$$

From the linear regression line, the values of *n* and *k* can be derived from the obtained intercept and slope, as demonstrated by Equation (3).

3.2. Ozawa Model

Ozawa model [48] takes into consideration the impacts of the distribution of crystal size on the nonisothermal crystallization kinetics, as depicted in Equation (4):

$$X = 1 - e^{\left(\frac{K}{\Phi^m}\right)} \qquad (4)$$

In Equation (4), *X* symbolizes crystallinity, *m* is the Ozawa parameter illustrating the nucleation and growth of crystals, *K* is Ozawa's rate constant, and ϕ represents the cooling rate. Equation (5) is obtained by applying double logarithms to Equation (4):

$$log\,[-ln\,(1-X)\,] = log\,K - m\,log\,\Phi \qquad (5)$$

3.3. Nakamura Model

The Nakamura model [24] is widely recognized for describing the crystallization kinetics in polymers. This model takes into account both the temperature and the degree of crystallization within the polymer, along with the crystallization kinetics as described by the Avrami Equation. The speed of crystallization is decided by the rate constant, which depends on the temperature, and the Avrami exponent that illustrates the three-dimensional growth of the crystal. The crystallization rate can be articulated using Equation (6) as follows:

$$X_t = \ 1 - \ exp\left[-\left(\int_0^t K(T)\,dt\right)^n\right] \quad (6)$$

In this context, Nakamura's rate constant *K* is correlated with Avrami's constant *k* from Equation (1), and it can be computed using Equation (6), as shown below:

$$K(T) \ = \ k(T)^{\frac{1}{n}} \quad (7)$$

Furthermore, the Nakamura model considers the influence of temperature on the crystallization kinetics by applying the nonisothermal model. This model represents how responsive the crystallization rate is to temperature variations.

3.4. Muthukumar's Model

Muthukumar Model [52] highlights that the crystallization processes of polymers at the crystallization temperature depend on the initial melt state and exhibit memory effects. A theory involving an intermediate inhomogeneous melt state is proposed to explain these phenomena. Initially, he studied the transition from the melt phase to the crystalline state. The free energy of the melt phase is expressed as the following equation:

$$F^l = \ h^l - Ts^l \quad (8)$$

where h^l and s^l represent the enthalpy and entropy of the system which formed in the homogeneous liquid state. In a similar manner, the free energy of the crystalline state will be:

$$F^c = \ h^c - Ts^c \quad (9)$$

with the superscript indicating the crystalline state. At the equilibrium melting temperature T_m^0, where $F^l = F^c$:

$$T_m^0 = \frac{\Delta h}{\Delta s} \qquad (10)$$

where $\Delta h = h^l - h^c$ is the latent heat of fusion and $\Delta s = s^l - s^c$ is the entropy of fusion for the system.

The theory has a broad applicability in addressing various types of melt-memory effects, which are contingent upon whether the melt temperature (T_m) is higher or lower than the equilibrium melting temperature (T_m^0).

4. RESULTS AND DISCUSSION

4.1. Nonisothermal crystallization

The nonisothermal crystallization of PBT was done under different cooling rates [53, 54]. Our work aims to examine PBT under a range of fusion temperatures set between 232°C and 260°C, with a fusion duration of 300 seconds at various cooling rates (15, 20, and 25°C/min). As demonstrated in Figure 2, the heat flow within PBT is considerably influenced by the variation in fusion temperatures [55].

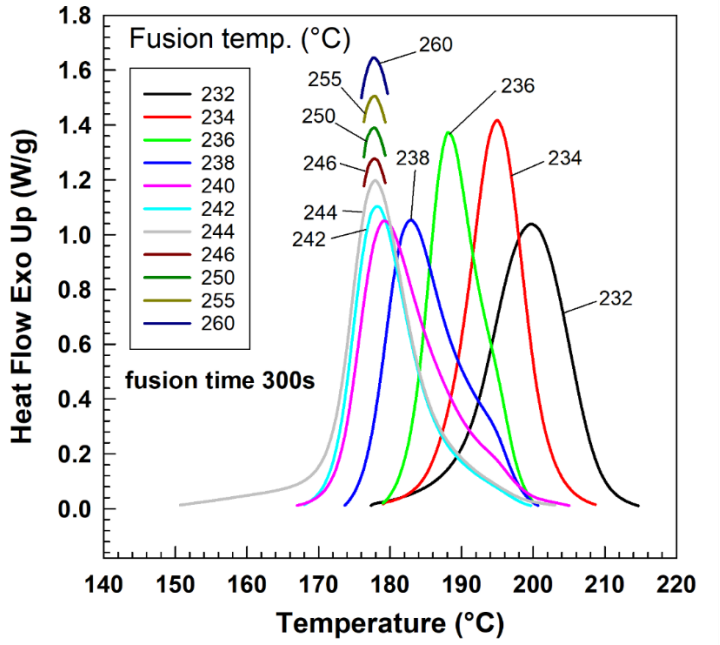

Figure 2. PBT Exothermic heat flow from DSC at different fusion temperatures, fusion time of 300 sec and cooling rate of 20 °C/min, nonisothermal crystallization experiment.

With the fusion temperature increase to approximately 242°C, there is a noticeable shift in the heat flow curve toward lower temperatures. However, the exothermic curve remains almost unchanged beyond 242°C up to the upper limit of 260°C. Most likely, some crystals remain unmelted at lower fusion temperatures, serving as nucleation points, or at least the polymer chains do not move very far from the positions in the original lamellae. Increasing the fusion temperature leads to more crystals that undergo melting, resulting in smaller nucleation centres. This scenario makes the crystallization process more challenging, necessitating high supercooling [56, 57]. As a result, the crystallization temperature undergoes a shift towards lower values. This shift is markedly evident within a temperature range of 232°C–242°C. As the fusion temperature rises beyond this range, the peak of the heat flow curve seems to stabilize at a similar temperature.

The S-curve, which illustrates relative crystallinity, can demonstrate the effect of applying various fusion temperatures on the crystallization kinetics [58]. Figure 3 presents the relative crystallinity curves of PBT corresponding to different fusion temperatures (232–244°C). A notable trend is observed; with an increase in fusion temperature, there is a subsequent decrease in crystallinity, as shown in Table 2. Furthermore, this decrease is accompanied by shifting the S-curve towards lower temperatures. This phenomenon can be elucidated by referring to the thermodynamics involved in the crystallization process. At elevated temperatures, an enhancement in molecular mobility and crystal growth is generally observed, extending the duration required to achieve a specific degree of crystallinity [46, 49].

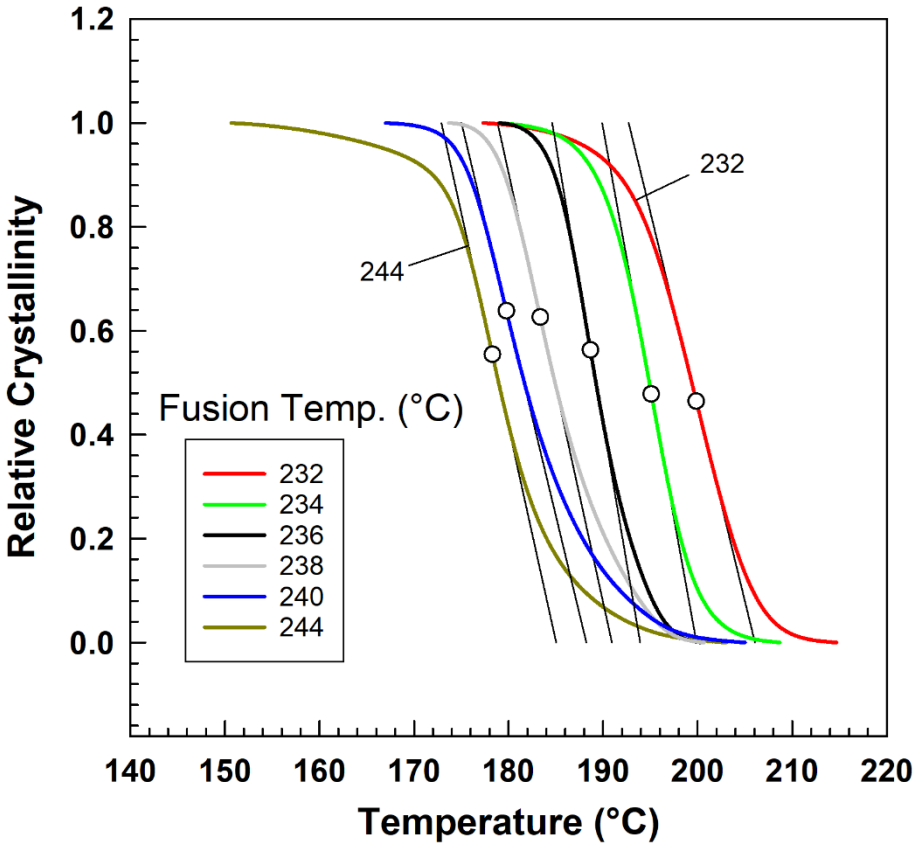

Figure 3. Relative crystallinity vs. temperature.

Figure 4 and Table 2 illustrate the position of the peak heat flow for PBT at different fusion temperatures, ranging from 232°C to 260°C. There is a significant decrease in the peak position as the fusion temperature increases to 240°C. Beyond this point, the decrease in the peak position continues, albeit at a slower rate, until the fusion temperature reaches 246°C. Any further increase in the fusion temperature does not affect the peak position, which remains constant [55]. It was widely accepted that when the melting temperature of a polymer is sufficiently low to allow the presence of self-nuclei within the melt, the polymer crystallization process is notably expedited. Additionally, this phenomenon leads to a significant alteration in the crystal structure during the subsequent cooling phase. Researchers commonly employ the DSC-based thermal procedure Fillon et. al., [59] developed to investigate the melt memory effect in polymers. The melting or fusion temperature can be classified into three distinct domains based on their decreasing order: Domain I, characterized by an isotropic melt state; Domain II, associated with self-nucleation; and Domain III, involving both self-nucleation and annealing processes.

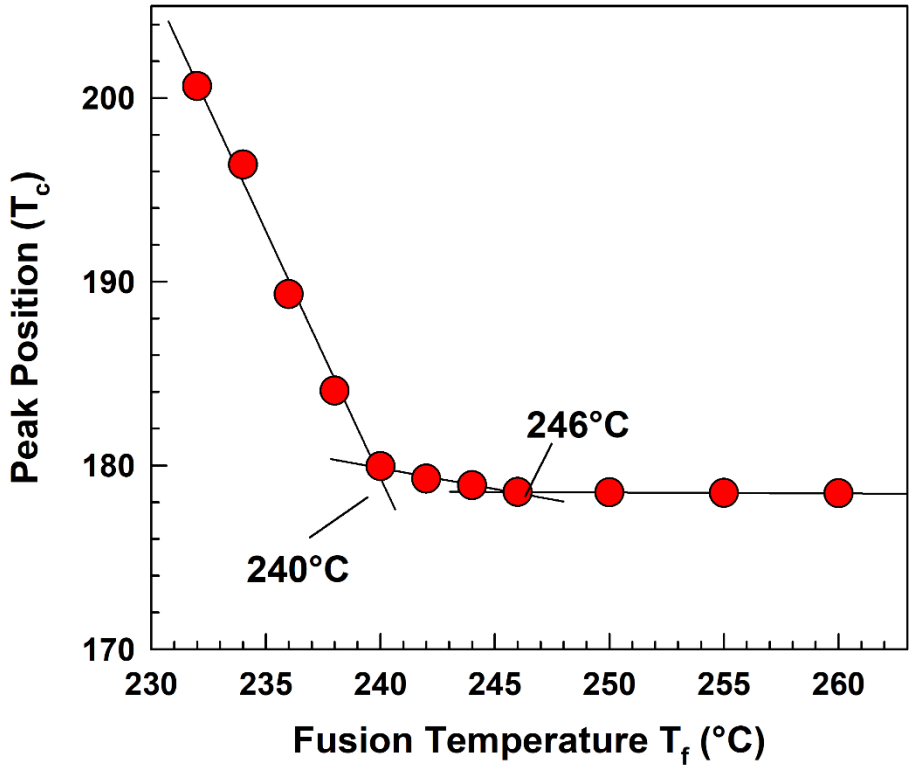

Figure 4. Influence of fusion temperature on the peak position of PBT.

Table 2. PBT crystallinity and peak position at various fusion temperatures.

Fusion Temp. (°C)	Crystallinity (X)	Peak Position (Tc)
232	33.02	200.64
234	32.88	196.36
236	32.53	189.32
238	32.33	184.06
240	30.54	179.95
242	28.49	179.27
244	26.95	178.92
246	25.85	178.55
250	25.59	178.53
255	25.23	178.50
260	25.17	178.48

The Ozawa model is a practical approach for studying the nonisothermal crystallization kinetics of polymers, applicable when crystallization happens at a steady cooling or heating rate [48]. In this model, the degree of crystallization is a function of both temperature and time, accounting for the cooling rate. The model's cooling function is depicted by the rate constant, K, which indicates the temperature-dependent rate of the crystallization process. The cooling rate impacts the resulting crystals' size and structure, with high cooling rates leading to smaller, numerous crystals and slower rates resulting in larger, more ordered crystals. While the model makes certain assumptions, such as continuous and simultaneous nucleation and growth, it remains a valuable tool in studying nonisothermal crystallization.

Figure 5 shows the influence of the cooling rate on the relative crystallinity [48, 60]. The relative crystallinity shifts towards lower temperatures because of the consequence of a faster cooling rate. This shift results from the significant temperature dependence of both nucleation and crystal growth mechanisms. With a slower cooling rate, molecules have improved diffusivity and fluidity due to reduced viscosity and increased crystallization time, resulting in higher crystallinity at higher temperatures than samples undergoing rapid cooling. When the cooling rate is held constant, the relative crystallinity changes in response to decreasing temperatures [61].

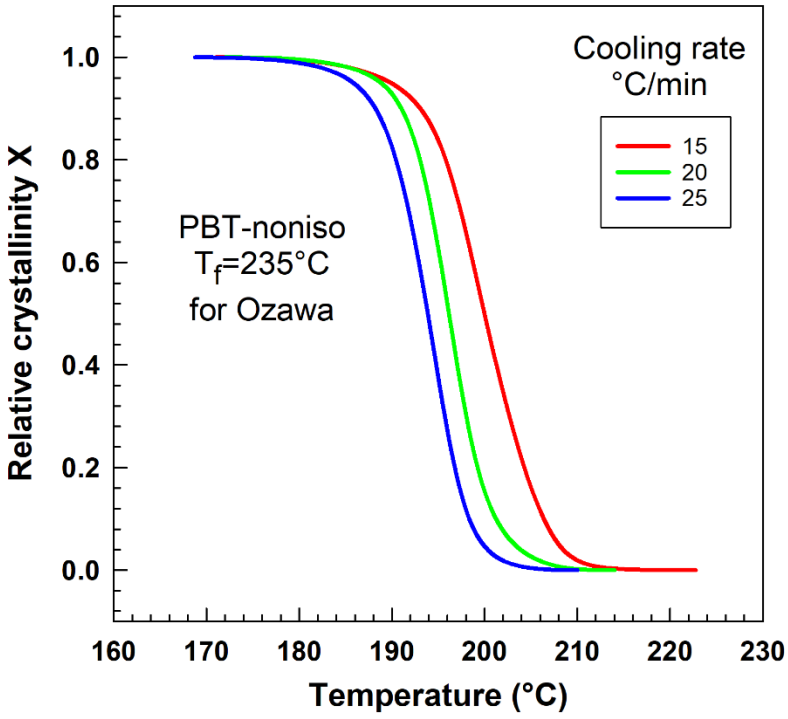

Figure 5. Influence of cooling rate on the relative crystallinity.

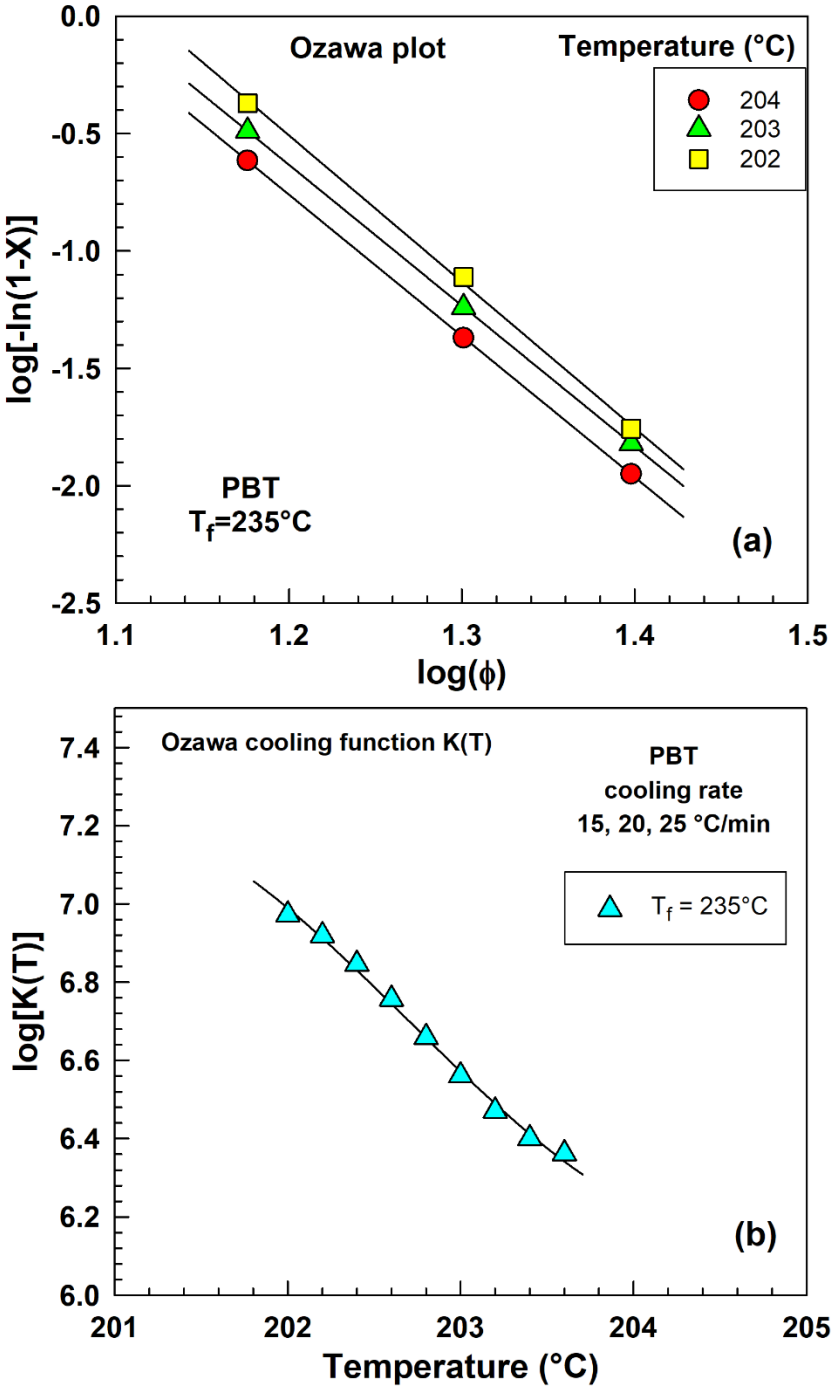

Figure 6. Ozawa cooling function (a) Cooling rate (b) fusion temperature.

Ozawa's plot in Figure 6 shows the significant effect of the cooling rate [48, 60, 62]. Figure 6a shows an excellent linear relationship between $\log[-\ln(1-X(t))]$ and $\log \phi$ during nonisothermal crystallization after melting at 235°C. The cooling function K(T) has been calculated using three different cooling rates. Figure 6b shows the cooling function versus the temperature. Overall, the Ozawa model appears suitable for characterizing the nonisothermal crystallization kinetics of PBT when the cooling rates are close to each other (15, 20, and 25°C/min).

4.2. Isothermal crystallization

The isothermal crystallization at 212°C rendered a similar conclusion to the nonisothermal one above. Initially, the heat flow curves are shown in Figure 7. The fastest crystallization happens at the lowest fusion temperatures (232°); also, the peak shows the highest heat flow value. As the fusion temperature increases, the peak is gradually lower and broader, and the crystallization takes longer until the fusion temperature reaches approximately 242°C. Then in the fusion temperature range of 242 – 250°C, the heat flow peaks look very similar [47, 49, 55].

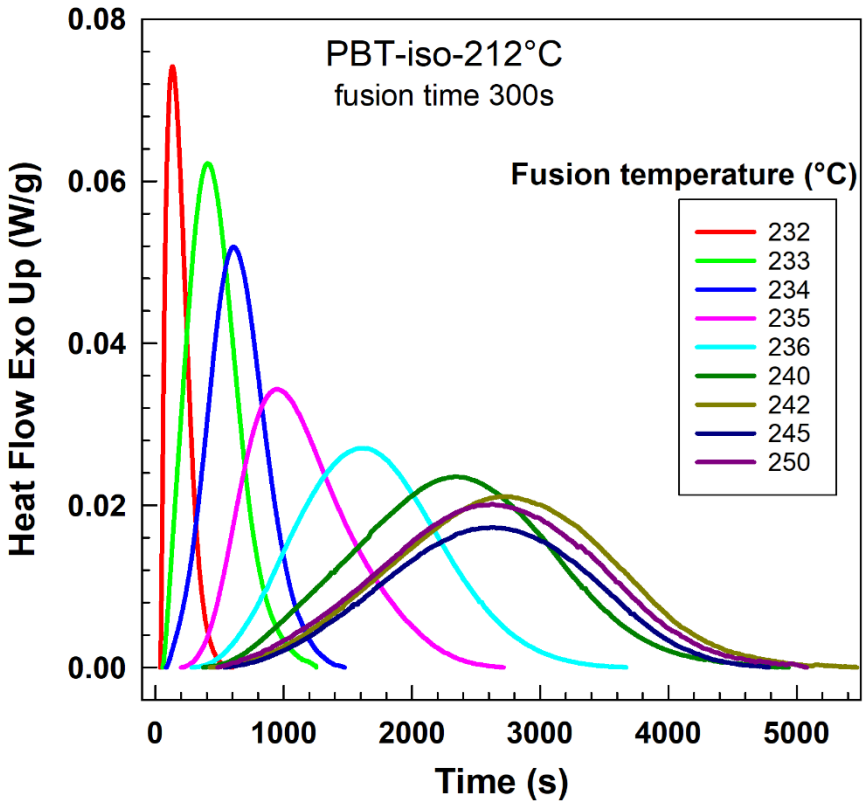

Figure 7. Isothermal crystallization at 212°C at various fusion temperatures.

For the crystallization kinetics study, it is convenient to integrate the heat flow curves and plot the relative crystallinity versus time plot, called the S-curve (see Figure 8) [46, 58]. We have analyzed the crystallization kinetics from three various points of view and listed the results in Table 3. At first, we listed the half-time of crystallization. The dependence of half time of crystallization $\tau_{1/2}$ as a function of fusion temperature is illustrated in Figure 10. The crystallization half-time is increasing (i.e., the crystallization is getting slower) up to about 241°C. Then it remains almost constant until 250°C. This result confirms the nonisothermal study shown in Figure 4 when there was a great change in crystallization peak position in the fusion temperature range 232-240°C, and then in the range 240-260°C; there was almost no change in peak position.

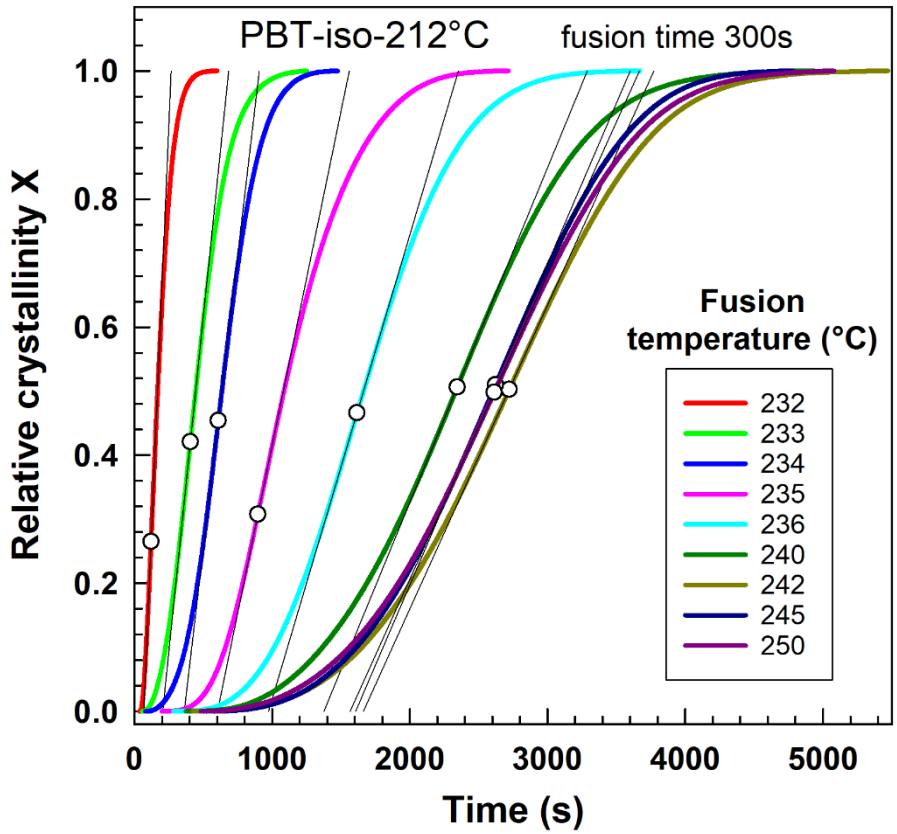

*Figure **8.** Relative crystallinity as a function of time during isothermal crystallization at 212°C after melting at various fusion temperatures by DSC.*

Table 3. Isothermal crystallization kinetics parameters at **212°C** from DSC.

Fusion temp.	**Half time of crystallization**	**One over half time of crystallization**	**Slope at inflection**	**Avrami**		**Nakamura**
T_f (°C)	$\tau_{1/2}$ (s)	$\tau_{1/2}^{-1}$ (s-1)	s-1	n	k	$K = k^{1/n}$
232	168	0.0059482	0.0050558	2.310	4.956E-06	0.0050482
233	444	0.0022508	0.0020843	2.629	7.582E-08	0.0019570
234	634	0.0015769	0.0015346	3.339	3.044E-10	0.0014119
235	1085	0.0009213	0.0010449	3.058	3.593E-10	0.0008155
236	1394	0.0007174	0.0007253	3.470	4.617E-12	0.0005408
240	2332	0.0004288	0.0005223	3.510	1.045E-12	0.0003862
241	2582	0.0003873	0.0004958	3.682	2.689E-13	0.0003855
242	2675	0.0003738	0.0004739	3.712	1.235E-13	0.0003334
243	2655	0.0003766	0.0004889	3.568	5.569E-13	0.0003677
244	2616	0.0003823	0.0004985	3.689	1.569E-13	0.0003381
245	2603	0.0003841	0.0005014	3.772	9.080E-14	0.0003485
250	2617	0.0003821	0.0004757	3.593	3.636E-13	0.0003450

Many researchers use the Avrami plot to evaluate isothermal crystallization (see Figure 9) [63-65]. One can evaluate the Avrami constants n and k from this plot. These two constants are listed in Table 3. Interconnected two parameters describe the S-curve, and the trend of rate constant k is unclear. Therefore, we have used Nakamura's rate constant $K = k^{1/n}$ that shows a better trend (even though it was originally developed for nonisothermal crystallization).

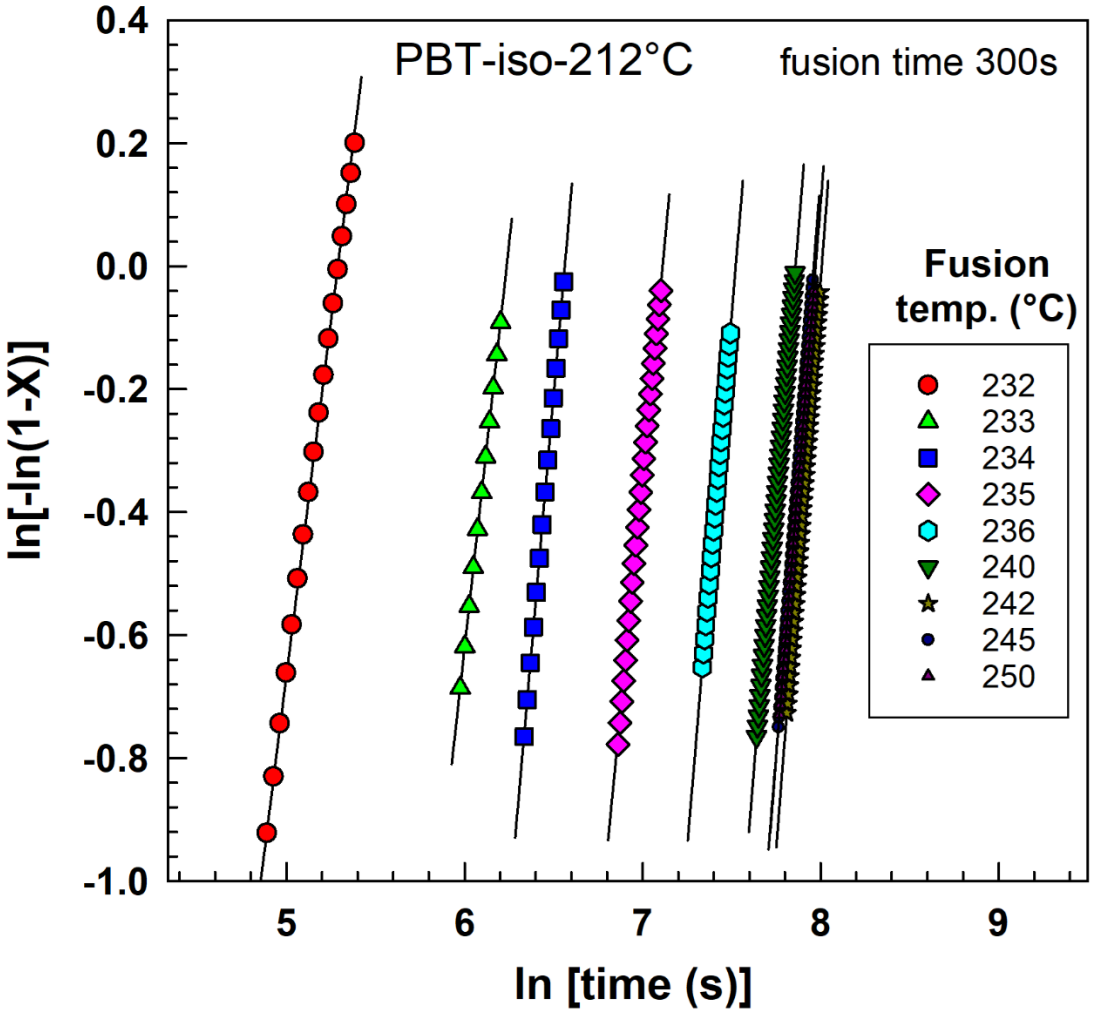

Figure 9. Avrami plot from isothermal crystallization at 212°C after melting at various fusion temperatures by DSC.

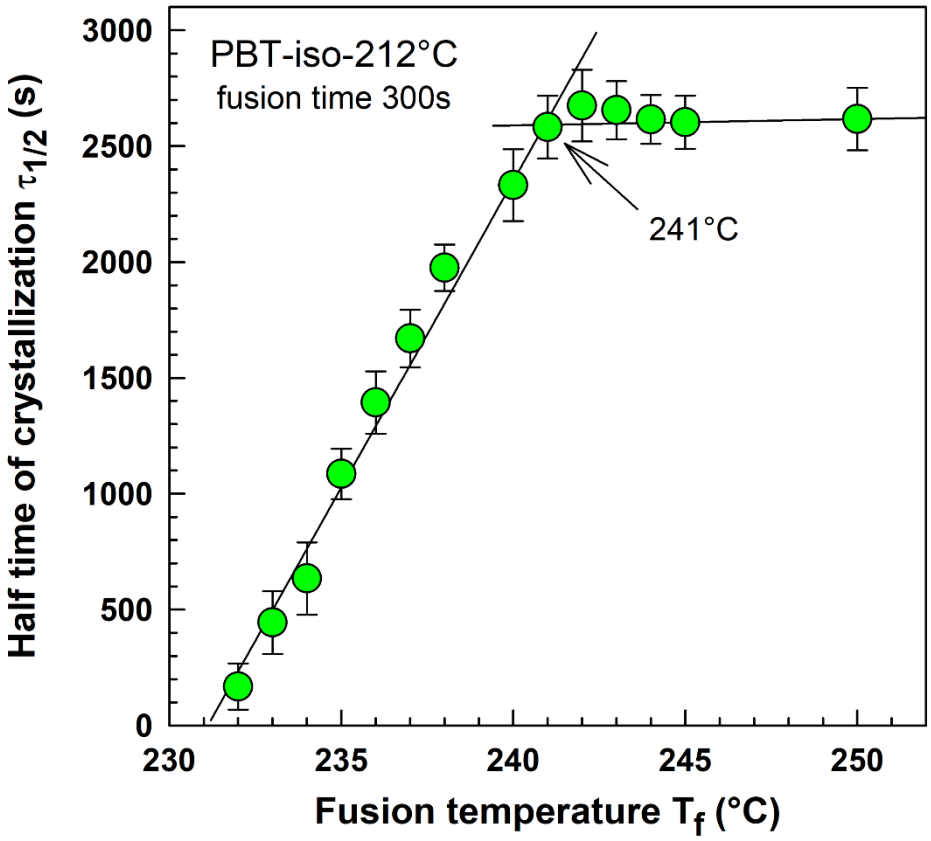

Figure 10. Half-time of crystallization $\tau_{1/2}$ as a function of fusion temperature T_f, from isothermal crystallization at 212°C.

In our work, we used the slope at the inflection point of the S-curve to evaluate crystallization kinetics. The slopes are listed in Table 3 and show a clear decreasing trend in the range 232-242°C, and then the kinetics stabilizes in the range 242-250°C fusion temperature range.

4.3. The equilibrium melting point (Hoffman–Weeks)

The Hoffman-Weeks theory [66] is a widely used model to determine a semi-crystalline polymer's equilibrium melting temperature (T_m^0) of a semi-crystalline polymer. This theory is based on the assumption that a crystalline polymer's measured melting temperature (T_m) depends on the temperature at which it was crystallized (T_c). As the crystallization temperature approaches the equilibrium melting temperature, the difference between T_m and T_c minimizes. One can derive the equilibrium melting temperature by extrapolating a plot of T_m versus T_c to the

line where T_m equals T_c. As shown in Figure 11, the melting temperature of PBT concerning the crystallization temperature was estimated based on the Hoffman–Weeks theory. The equilibrium melting point T_m^0 is determined at the intersection of the extrapolated line and the $T_m = T_c$ line. In our study, the equilibrium melting point T_m^0 was found to be at 243.9°C, which complies with other works [67-69]. The multiple-melting behaviour has been interpreted in the context of the melting–recrystallization–remelting phenomena [70].

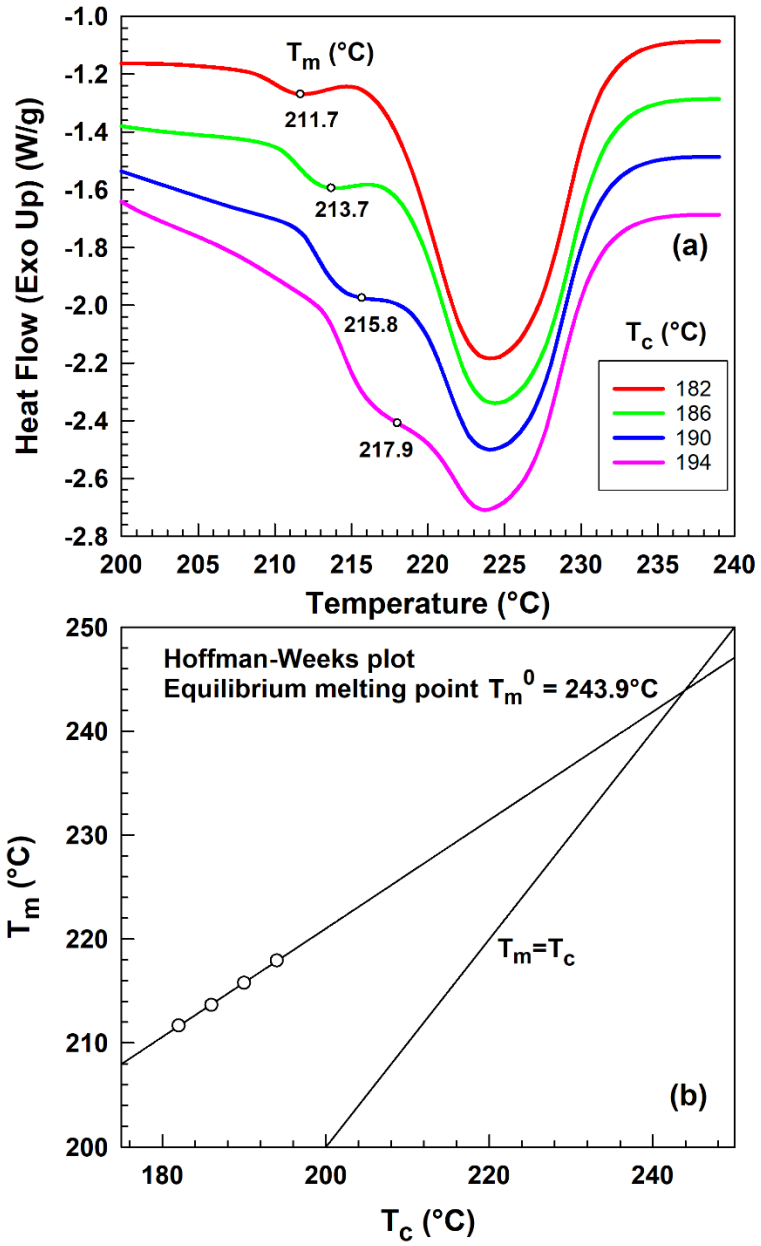

Figure 11. (a) Determination of melting temperature after 30 min of isothermal crystallization at various temperatures T_c, (b) Hoffman-Weeks plot for determination of equilibrium melting point T_m^0, melting point of peak I vs. crystallization temperature.

5. CONCLUSIONS

In conclusion, this study investigated the impact of fusion temperature on the crystallization behaviour of PBT. The results demonstrated that the fusion temperature significantly influenced the heat flow curve, with a noticeable shift towards lower temperatures. Increasing the fusion temperature led to a decrease in crystallinity and a change in the position of the heat flow peak. A major shift in peak position and crystallinity was observed for fusion temperatures in the range of 232-240°C. Then in the range of 240-246°C, a slight change was observed. In the range of 246-260°C, no change in peak position or crystallinity was observed. The Ozawa model revealed the influence of cooling rate on relative crystallinity, indicating the temperature dependence of nucleation and crystal growth mechanisms. The Avrami model is highly suitable for assessing the kinetics of isothermal crystallization. The isothermal experiments supported the trends observed in the nonisothermal ones, confirming the effect of fusion temperature on crystallization kinetics. At lower fusion temperatures, the crystallization kinetics was faster. The kinetics gradually decreased in the fusion temperature range of 232-242°C; then, it remained constant in the range of 242-250°C. These findings provide valuable insights into understanding and controlling the crystallization behaviour of PBT, which can inform the optimization of processing conditions and the improvement of its properties in various applications. Further research can explore the relationship between crystallization kinetics and the resulting material properties of PBT, enhancing its industrial applications and performance.

ACKNOWLEDGMENTS

The authors thank Tomas Bata University in Zlin for supporting this research through the Internal Grant Agency, ref. No: IGA/FT/2023/008.

REFERENCES

[1] Arai S, Tsunoda S, Kawamura R, Kuboyama K, Ougizawa T. Comparison of crystallization characteristics and mechanical properties of poly(butylene terephthalate) processed by laser sintering and injection molding. Materials & Design. 2017;113:214-222. https://doi.org/10.1016/j.matdes.2016.10.028.

[2] Xu JL, Kang CH, Niu L, Xu CC, Zhang JB, Ma JQ. The crystallization, thermal and mechanical properties of nano-Sb2O3 filled poly(butylene terephthalate). Journal of Vinyl & Additive Technology. 2020;26(3):268-281. https://doi.org/10.1002/vnl.21741.

[3] Liu B, Wu W. Influence of epoxidized ethylene propylene diene rubber on nonisothermal crystallization kinetics and mechanical properties of poly(butylene terephthalate)/polypropylene blend. Journal of Polymer Engineering. 2019;39(3):216-227. https://doi.org/10.1515/polyeng-2018-0283.

[4] Chen S, Fu X, Jing Z, Chen H. Non-isothermal crystallization kinetics and rheological behaviors of PBT/PET blends: effects of PET property and nano-silica content. Designed Monomers and Polymers. 2022;25(1):32-46. https://doi.org/10.1080/15685551.2022.2041784.

[5] de Almeida A, Nébouy M, Baeza GP. Bimodal Crystallization Kinetics of PBT/PTHF Segmented Block Copolymers: Impact of the Chain Rigidity. Macromolecules. 2019;52(3):1227-1240. https://doi.org/10.1021/acs.macromol.8b01689.

[6] Al-Mulla A, Mathew J, Yeh S-K, Gupta R. Nonisothermal crystallization kinetics of PBT nanocomposites. Composites Part A: Applied Science and Manufacturing. 2008;39(2):204-217. https://doi.org/10.1016/j.compositesa.2007.11.001.

[7] Chen X, Xu J, Lu H, Yang Y. Isothermal crystallization kinetics of poly(butylene terephthalate)/attapulgite nanocomposites. 2006;44(15):2112-2121. https://doi.org/10.1002/polb.20870.

[8] Wu DF, Zhou CX, Fan X, Mao DL, Zhang B. Nonisothermal crystallization kinetics of poly(butylene terephthalate)/montmorillonite nanocomposites. Journal of Applied Polymer Science. 2006;99(6):3257-3265. https://doi.org/10.1002/app.22782.

[9] Al-Mulla A, Mathew J, Shanks R. Isothermal crystallization studies of poly(butylene terephthalate) composites. Journal of Polymer Science Part B-Polymer Physics. 2007;45(11):1344-1353. https://doi.org/10.1002/polb.21160.

[10] Huang JW, Wen YL, Kang CC, Yeh MY, Wen SB. Morphology, melting behavior, and non-isothermal crystallization of poly(butylene terephthalate)/poly(ethylene-co-methacrylic acid) blends. Thermochimica Acta. 2007;465(1-2):48-58. https://doi.org/10.1016/j.tca.2007.09.004.

[11] Huang JW. Poly(butylene terephthalate)/Clay Nanocomposite Compatibilized with Poly(ethylene-co-glycidyl methacrylate). I. Isothermal Crystallization. Journal of Applied Polymer Science. 2008;110(4):2195-2204. https://doi.org/10.1002/app.28819.

[12] Supaphol P, Lin JS. Crystalline memory effect in isothermal crystallization of syndiotactic polypropylenes: effect of fusion temperature on crystallization and melting behavior. Polymer. 2001;42(23):9617-9626. https://doi.org/10.1016/S0032-3861(01)00507-9.

[13] Ishida K, Han SI, Im SS, Inoue Y. Effects of fusion temperature and metal ion variation on crystallization of lightly ionized poly(butylene succinate). Macromolecular Chemistry and Physics. 2007;208(2):146-154. https://doi.org/10.1002/macp.200600417.

[14] Avrami M. Kinetics of Phase Change. I General Theory. The Journal of Chemical Physics. 1939;7:1103. https://doi.org/10.1063/1.1750380.

[15] Ozawa T. Kinetics of Non-Isothermal Crystallization. Polymer. 1971;12(3):150-&. https://doi.org/10.1016/0032-3861(71)90041-3.

[16] Alfonso GC, Ziabicki A. Memory Effects in Isothermal Crystallization .2. Isotactic Polypropylene. Colloid and Polymer Science. 1995;273(4):317-323. https://doi.org/10.1007/Bf00652344.
[17] Nakamura K, Katayama K, Amano T. Some Aspects of Nonisothermal Crystallization of Polymers .2. Consideration of Isokinetic Condition. Journal of Applied Polymer Science. 1973;17(4):1031-1041. https://doi.org/10.1002/app.1973.070170404.
[18] Arostegui A, Nazábal J. Stiffer and super-tough poly(butylene terephthalate) based blends by modification with phenoxy and maleated poly(ethylene-octene) copolymers. Polymer. 2003;44:239-249. https://doi.org/10.1016/S0032-3861(02)00496-2.
[19] Hage Jr E, Hale W, Keskkula H, Paul DR. Impact modification of poly(butylene terephthalate) by ABS materials. Polymer. 1997;38:3237-3250. https://doi.org/10.1016/S0032-3861(96)00879-8.
[20] Muthukumar M. Communication: Theory of melt-memory in polymer crystallization. The Journal of Chemical Physics. 2016;145(3). https://doi.org/10.1063/1.4959583.
[21] Liu B, Wu W. Nonisothermal crystallization kinetics of poly(butylene terephthalate)/epoxidized ethylene propylene diene rubber/glass fiber composites. Polymer Engineering and Science. 2019;59(2):330-343. https://doi.org/10.1002/pen.24909.
[22] Zhang ZH, Feng L, Li YD, Wang YT, Yan CM. Nonisothermal Crystallization Kinetics of Poly(Butylene Terephthalate)/Poly(Ethylene Terephthalate)/Glass Fiber Composites. Polymer Composites. 2015;36(3):510-516. https://doi.org/10.1002/pc.22966.
[23] Lee YC, Porter RS. Effects of Thermal History on Crystallization of Poly(Ether Ether Ketone) (Peek). Macromolecules. 1988;21(9):2770-2776. https://doi.org/10.1021/ma00187a022.
[24] Tariq M, Thurn-Albrecht T, Dolynchuk O. Heterogeneous Crystal Nucleation from the Melt in Polyethylene Oxide Droplets on Graphite: Kinetics and Microscopic Structure. 2021;11(8):924. https://doi.org/10.3390/cryst11080924.
[25] Erdemir D, Lee AY, Myerson AS. Crystal Nucleation. In: Lee AY, Myerson AS, Erdemir D, editors. Handbook of Industrial Crystallization. 3 ed. Cambridge: Cambridge University Press; 2019. p. 76-114.
[26] Kratochvil J, Kelnar I. A simple method of evaluating non-isothermal crystallization kinetics in multicomponent polymer systems. Polymer Testing. 2015;47:79-86. https://doi.org/10.1016/j.polymertesting.2015.07.010.
[27] Fillon B, Wittmann JC, Lotz B, Thierry A. Self-nucleation and recrystallization of isotactic polypropylene (α phase) investigated by differential scanning calorimetry. 1993;31(10):1383-1393. https://doi.org/https://doi.org/10.1002/polb.1993.090311013.
[28] Xu G, Shi WF, Hu P, Mo SP. Crystallization kinetics of polypropylene with hyperbranched polyurethane acrylate being used as a toughening agent. European Polymer Journal. 2005;41(8):1828-1837. https://doi.org/10.1016/j.eurpolymj.2005.02.037.
[29] Seo Y, Kim J, Kim KU, Kim YC. Study of the crystallization behaviors of polypropylene and maleic anhydride grafted polypropylene. Polymer. 2000;41(7):2639-2646. https://doi.org/10.1016/S0032-3861(99)00425-5.
[30] Huang JW, Wen YL, Kang CC, Tseng WJ, Yeh MY. Nonisothermal crystallization of high density polyethylene and nanoscale calcium carbonate composites. Polymer Engineering and Science. 2008;48(7):1268-1278. https://doi.org/10.1002/pen.21087.
[31] Uthaipan N, Jarnthong M, Peng Z, Junhasavasdikul B, Nakason C, Thitithammawong A. Effects of cooling rates on crystallization behavior and melting characteristics of isotactic polypropylene as neat and in the TPVs EPDM/PP and EOC/PP. Polymer Testing. 2015;44:101-111. https://doi.org/10.1016/j.polymertesting.2015.04.002.

[32] Toda A, Furushima Y, Schick C. Vitrification of the Entire Amorphous Phase during Crystallization of Poly(butylene terephthalate) near the Glass-Transition Temperature. Macromolecules. 2023;56(8):3110-3118. https://doi.org/10.1021/acs.macromol.3c00137.
[33] Svoboda P, Dvorackova M, Svobodova D. Influence of biodegradation on crystallization of poly (butylene adipate-co-terephthalate). Polymers for Advanced Technologies. 2019;30(3):552-562. https://doi.org/10.1002/pat.4491.
[34] Hoffman JD, Weeks JJJJoRotNBoSSAP, Chemistry. Melting process and the equilibrium melting temperature of polychlorotrifluoroethylene. 1962:13. https://doi.org/10.6028/jres.066a.003.
[35] Runt J, Miley DM, Zhang X, Gallagher KP, Mcfeaters K, Fishburn J. Crystallization of Poly(Butylene Terephthalate) and Its Blends with Polyarylate. Macromolecules. 1992;25(7):1929-1934. https://doi.org/10.1021/ma00033a015.
[36] Okamoto M, Inoue T. Crystallization Kinetics in Poly(Butylene Terephthalate)/Copolycarbonate Blend. Polymer. 1995;36(14):2739-2744. https://doi.org/10.1016/0032-3861(95)93651-2.
[37] Pillin I, Pimbert S, Feller JF, Levesque G. Crystallization kinetics of poly(butylene terephthalate) (PBT): Influence of additives and free carboxylic acid chain ends. Polymer Engineering and Science. 2001;41(2):178-191. https://doi.org/10.1002/pen.10720.
[38] Papageorgiou GZ, Achilias DS, Bikiaris DN. Crystallization Kinetics of Biodegradable Poly(butylene succinate) under Isothermal and Non-Isothermal Conditions. 2007;208(12):1250-1264. https://doi.org/https://doi.org/10.1002/macp.200700084.

PAPER III

Influence of Fusion Temperature on Nonisothermal Crystallization Kinetics of Polyamide 6

Ahmed Nasr * and Petr Svoboda

Department of Polymer Engineering, Faculty of Technology, Tomas Bata University in Zlin, Vavreckova 5669, 760 01 Zlin, Czech Republic

ABSTRACT

The effect of fusion temperature and duration on the nonisothermal crystallization kinetics of polyamide 6 (PA6) was investigated using differential scanning calorimetry (DSC) and a polarized optical microscope (OM). The rapid cooling method involved heating the polymer above its melting point, holding it at this temperature to ensure complete melting, and then rapidly cooling it to the crystallization temperature. By monitoring the heat flow during cooling, the crystallization kinetics of PA6 were characterized, including the degree of crystallinity, crystallization temperature, and crystallization rate. The study found that changing the fusion temperature and duration significantly impacted the crystallization kinetics of PA6. Increasing the fusion temperature decreased the degree of crystallinity, with smaller nucleation centers requiring a higher degree of supercooling for crystallization. The crystallization temperature shifted towards lower temperatures, and the crystallization kinetics slowed down. The study also found that lengthening the fusion time raised the relative crystallinity, but any further increase did not result in a significant change. The study showed that an increase in fusion temperature led to a longer time needed to reach a given level of crystallinity, reducing the crystallization rate. This can be explained by the thermodynamics of the crystallization process, where higher temperatures promote molecular mobility and crystal growth. Moreover, the study revealed that decreasing a polymer's fusion temperature can lead to a greater degree of nucleation and faster growth of the crystalline phase, which can significantly impact the values of the Avrami parameters used to characterize the crystallization kinetics.

KEYWORDS

polyamide 6; DSC; optical microscope; nonisothermal crystallization; fusion temperature; cooling function

1. INTRODUCTION

Polyamide 6 (PA6) is a semi-crystalline thermoplastic material with high strength, toughness, and stiffness, making it an attractive material for various applications [1,2]. During the processing of PA6, the fusion temperature plays a crucial role in controlling the crystallization behavior of the polymer [3,4]. The crystallization behavior of polyamide 6 is influenced by various factors such as temperature, cooling rate, and molecular weight [5]. Most polyamides (nylons) are characterized by a linear structure with repeating amide units. These amide groups enable hydrogen bonding within the polymer chain, which plays a critical role in the physical and chemical properties of the material [2,6]. The formation of hydrogen bonds within PA6 results in a strong, rigid, and crystalline structure that contributes to the material's high strength, stiffness, and thermal stability. This unique arrangement of chemical bonds also imparts excellent chemical resistance and low moisture absorption to PAs, making them ideal for various applications in industries such as textiles, automotive, and electronics.

Polymer crystallization involves the partial alignment of molecular chains, forming ordered regions called lamellae [7]. These folded chains combine to form larger spheroidal structures known as spherulites. This is a significant phenomenon in polymers as it influences the physical and mechanical properties of the material, such as its stiffness, strength, and resistance to deformation [8]. The way in which a polymer crystallizes, including its crystallinity and crystallization kinetics, is extremely important when designing and optimizing the technological process. This is because the crystallization behavior of a polymer has a significant impact on the end-use properties of products that are created through injection molding [9]. The crystallization process in polymers begins when the polymer is cooled after melting, stretched mechanically, or evaporated using solvents. The crystallization process impacts several properties of the polymer, including its optical, mechanical, thermal, and chemical properties [10]. The degree of crystallinity, which various analytical methods can determine, usually falls between 10% and 80%, and polymers with such a range are referred to as "semi-crystalline". In semi-crystalline polymers, the degree of crystallinity is not the only factor determining the material's properties, as the size and orientation of the molecular chains also play a significant role [11].

The effect of fusion temperature on the nonisothermal crystallization of semi-crystalline polymers has been studied extensively, with several research papers reporting on its impact on the degree of crystallinity and the crystalline structure

of the material during nonisothermal crystallization [3,4,12,13]. Ziabicki and Alfonso [12] explain the kinetics of polymer crystallization by breaking down the process into three stages: nucleation, growth, and termination. According to this theory, the crystal growth rate is directly proportional to the diffusion rate of polymer chains into the crystal lattice. Alfonso and Ziabicki [3] researched how the fusion temperature and time affect polypropylene's isothermal crystallization kinetics. The authors found that increasing the fusion temperature leads to slower overall crystallization but a higher final degree of crystallinity due to changes in the morphology and molecular ordering of the polymer crystals.

On the other hand, increasing the duration of fusion leads to faster nucleation and crystal growth. The researchers attributed these effects to changes in the polypropylene's molecular structure due to the melting and cooling process. Specifically, they suggested that the high temperatures used during fusion caused some of the crystalline regions of the material to break down, leading to a decrease in the overall degree of crystallinity. Meanwhile, longer fusion times allowed for more time for the remaining crystalline regions to reform and grow, increasing the degree of crystallinity. To our best knowledge, this study has not been conducted for polyamide 6. Overall, these studies indicate that the fusion temperature of semi-crystalline polymers can significantly impact the nonisothermal crystallization behavior of the material. The degree of crystallinity, crystalline structure, and spherulite morphology of the material can be influenced by the fusion temperature, cooling rate, and other factors. Understanding these effects can aid in developing new materials with desired properties.

A new phenomenon has been reported, which involves a memory effect in the crystallization rate of PA6 from the molten state that is influenced by its processing history [14]. Differential scanning calorimetry (DSC) and optical microscopy are the main techniques used to show that processing variables can control the melt crystallization behavior of PA6. As the process of crystallization progresses, the surface area increases, and the kinetics of growth can become more favorable. If a constant cooling rate is applied to the crystallization process, there can be initial supersaturation buildup where no surface area is available for growth. This buildup can result in fast and unpredictable crystallization kinetics, with nucleation often becoming the dominant factor.

Some authors have investigated the crystallization behavior of PA6 [5,15,16,17]. However, less attention has been paid to studying the influence of fusion temperature on the crystallization kinetics of PA6 since it affects not only the morphology of semi-crystalline polymers and the crystalline structure but also the final physical properties end-use properties of the polymers. This article

examined the impact of fusion temperature on the nonisothermal crystallization kinetics of PA6 using differential scanning calorimetry (DSC). The researchers used various models, including Avrami, Nakamura, and Ozawa models, to analyze the crystallization kinetics of PA6. The goal was to better understand the factors influencing the crystallization behavior of PA6, which is a crucial aspect in designing and processing this polymer material [18,19,20]. The results showed that the fusion temperature significantly impacts the crystallization rate and the degree of crystallinity of PA6.

Overall, this work aimed to study the effect of the fusion temperature on the nonisothermal crystallization process of PA6 by understanding the overall crystallization kinetics, growth rate, and spherulitic morphology in a wide range of crystallization temperatures by applying different cooling rates.

2. Experimental Section

Polyamide 6 was supplied by DSM Company (Genk, Belgium) with a trading name Akulon®F232-D, PA6. Figure 1 shows the molecular structure of PA6, and the main characteristics of the material are listed in Table 1. PA6 granules were used directly for the measurement itself. However, drying the granules due to moisture was necessary and took place at 80 °C for 12 h. The samples were then prepared as a thin film, melting the PA6 granules at 200 °C, and then pressed between two slides. After cooling, a thin film with a thickness of about 120 μm was formed. Different specimens were used in each experiment.

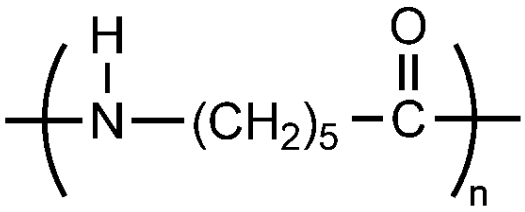

Figure 1. Molecular structure of PA6.

Table 1. Properties of pure materials.

Property	Polyamide 6 F232-D
Melt temperature (10 °C/min)	220 °C (ISO 11357)
Tensile modulus	3300 MPa (ISO 527)
Charpy notched impact strength	6 kJ/m2 at 23 °C (ISO 179)
Density	1130 kg/m3 (ISO 1183)
Viscosity	214 cm3/g (ISO 307)

A polarizing optical microscope determined nonisothermal crystallization (BHA-P Olympus, Olympus Global, Tokyo, Japan) attached to a temperature controller (Line LK 600-PM, Linkam Scientific Instruments, London, UK). The PA6 samples were melted at 200 °C for 2 min. They were then cooled at different cooling rates (15, 20, and 25 °C/min) and spherulites grew.

The behavior of the PA6 heat flow was determined using differential scanning calorimetry (DSC) on Mettler Toledo's DSC instrument, Greifensee, Switzerland. About 20 mg of the prepared samples were prepared for the measurement which was carried out with nitrogen access (30 mL/min) to avoid significant thermal degradation. The samples were melted at various fusion temperatures from 225 °C to 245 °C for 2 min and then cooled to 60 °C. The effect of cooling rates (15, 20 and 25 °C/min) was also monitored.

To prevent PA6 degradation, we utilized a maximum temperature of 245 °C throughout our experimentation, as degradation of PA6 typically begins at temperatures exceeding 300 °C [71].

3. Theoretical Background

3.1. Avrami Analysis

The Avrami model is a mathematical model commonly used to study polymers' isothermal crystallization kinetics. The model proposes that the crystallization rate in a polymer system is proportional to the amount of amorphous material remaining at any given time. The model equation includes the fraction of crystalline material formed at a given time, the isothermal crystallization temperature, a rate constant that depends on the polymer and crystallization conditions, and an Avrami exponent that describes the mechanism of

crystallization. The equation representing the model is as follows, Equation (1) [15]:

$$1 - X_t = exp(-kt^n) \quad (1)$$

where *n* is the Avrami exponent, and *k* is the Avrami rate constant. Both *n* and *k* depend on the rate of growth mechanisms and nucleation of the spherulites.

The nonisothermal crystallization parameters obtained from the DSC are used to calculate the crystallinity X_t from the area of the exothermic peak within the crystallization time t, then divided by the total area under the peak:

$$X_t = \frac{\int_0^t \left(\frac{dH}{dt}\right) dt}{\int_0^\infty \left(\frac{dH}{dt}\right) dt} \quad (2)$$

where the numerator represents the heat generated at time t and the denominator means the total heat generated up to complete crystallization.

Avrami constants can be evaluated by the linear regression, as described in Equation (1), then applying double logarithmic form as follows:

$$ln[-ln(1 - X_t)] = ln\, k + n\, ln\, t \quad (3)$$

The n and k values are obtained using Equation (3) from the slope and intercept of the linear regression line. Several authors have employed the Avrami equation to assess the rate of polymer crystallization in nonisothermal conditions.

3.2. Nakamura Model

The Nakamura model, introduced in 1973 [24], is a well-established model for characterizing the nonisothermal crystallization of polymers. This model considers both temperature and the extent of crystallization in the polymer and the kinetics of crystallization described by the Avrami equation. The crystallization rate is determined by the temperature-dependent rate constant and the Avrami exponent, which characterizes the three-dimensional growth of the crystal. The rate of crystallization can be expressed using the following equation, Equation (4):

$$X_t = 1 - \exp\left[-\left(\int_0^t K(T)dt\right)^n\right] \quad (4)$$

where K(T) is related to k(T) in equation (1) and can be calculated by the following equation, Equation (5) [72]:

$$K(T) = k(T)^{1/n} \quad (5)$$

Additionally, the Nakamura model accounts for the effect of temperature on the crystallization process through the nonisothermal term, which reflects the sensitivity of the crystallization rate to changes in temperature.

3.3. Ozawa Model

The Ozawa model is an extension of the Avrami model, which accounts for the effects of crystallite size distribution on the kinetics of nonisothermal crystallization of polymers [48]. The equation is given by:

$$X = 1 - e^{\left(\frac{K}{\Phi^m}\right)} \quad (6)$$

where X represents crystallinity, K is Ozawa's rate constant of crystallization, m is the Ozawa parameter representing the growth and nucleation of crystals, and Φ denotes the cooling rate. After two logarithms of Equation (1), Ozawa's equation takes the following form:

$$log[-ln\,(1 - X)] = log\,K - m\,log\,\Phi \quad (7)$$

4. Results and Discussion

The nonisothermal crystallization kinetics of polyamide 6 (PA6) was investigated through a rapid cooling method using differential scanning calorimetry (DSC). This technique involves heating the polymer above its melting point, holding it at this temperature to ensure complete melting, and then rapidly cooling it to the crystallization temperature. By monitoring the heat flow during cooling using DSC, the crystallization kinetics of PA6 can be characterized, including the degree of crystallinity, crystallization temperature, and crystallization rate. This approach is commonly used in materials science research to study the thermal behavior of polymers and has been proven effective in characterizing the crystallization kinetics of various types of polymers, including PA6.

Figure 2 illustrates the impact of different fusion temperatures on the heat flow [73], in which PA6 samples were heated at various fusion temperatures from 225 °C to 245 °C for 2 min and then were cooled at a cooling rate of 25 °C/min. The graph demonstrates that with increasing fusion temperature, the exothermic trace becomes narrower and shifts toward lower temperatures, then it becomes wider but still moves toward lower temperatures. At lower fusion temperatures, some

crystals remain unmelted, which act as nucleation centers. As the fusion temperature increases, more crystals melt, leading to smaller nucleation centers. Consequently, crystallization becomes more challenging, requiring a higher degree of supercooling. Therefore, the crystallization temperature shifts towards lower temperatures. This change is most noticeable in the temperature range of 225–242 °C, and then the peak remains at approximately the same temperature as the fusion temperature increases.

The presence of shoulder on some of the heat flow curves suggests the presence of "transcrystallinity" described by Freire et al. [74] meaning differences in crystallization kinetics on the surface (in contact with aluminum pan) and inside the pellet. Thickness of the sample seems to be very important. For our polarized optical microscopy measurement, it was necessary to use thicker sample (more than 100 μm) in order to be able to observe spherulites.

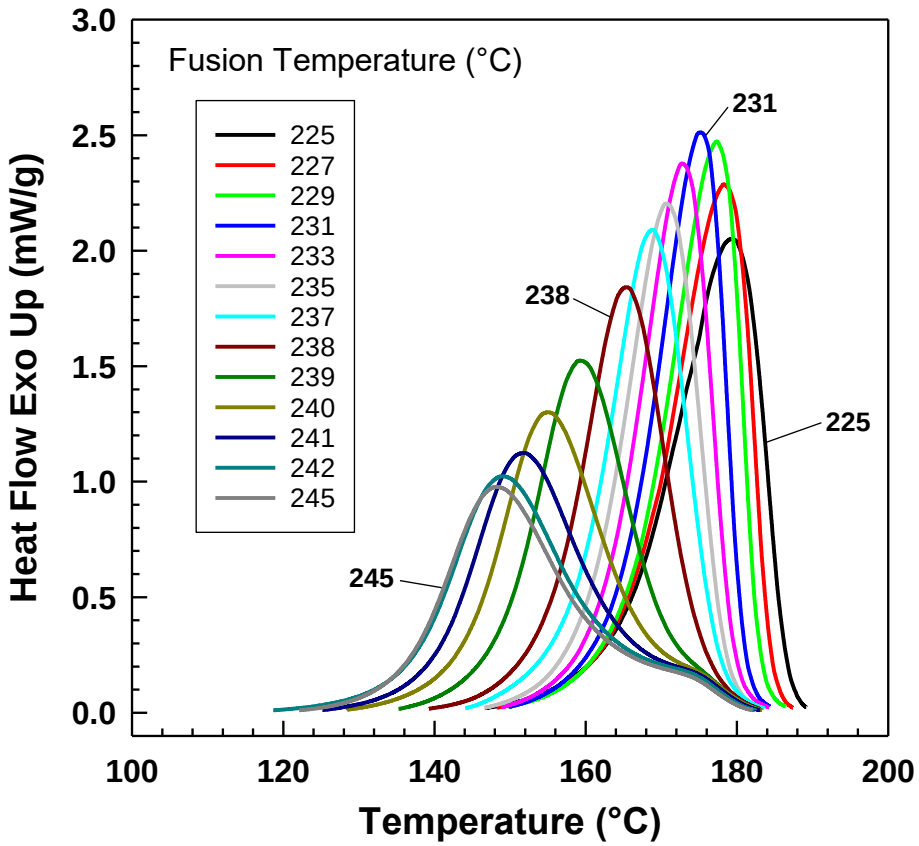

Figure 2. Exothermic heat flow of PA6 from DSC after various fusion temperatures at a cooling rate of 25 °C/min.

However, in terms of crystallization kinetics, the inverse value of crystallization is preferable. Conversely, this value decreases with increasing fusion temperature, indicating that crystallization kinetics are slowing.

The degree of crystallinity is affected by changing the fusion temperatures and time of fusion [75-78]. Relative crystallinity can be calculated by the following equation (Equation (2)), [79]. Figure 3 illustrates how the nonisothermal crystallization kinetics of PA6 is influenced by varying the fusion temperature and duration. When the fusion temperature is increased, the temperature at which relative crystallinity is achieved decreases (Figure 3a). Meanwhile, lengthening the fusion time from 2 to 7 min raises the relative crystallinity and causes the curve to shift toward higher temperatures (Figure 3b). However, any further increase in the fusion time does not result in a significant change in the relative crystallinity. It seems that 2 min fusion time is not sufficient to erase previous processing history. In the literature [80, 81], 5 min fusion time is usually used prior to crystallization.

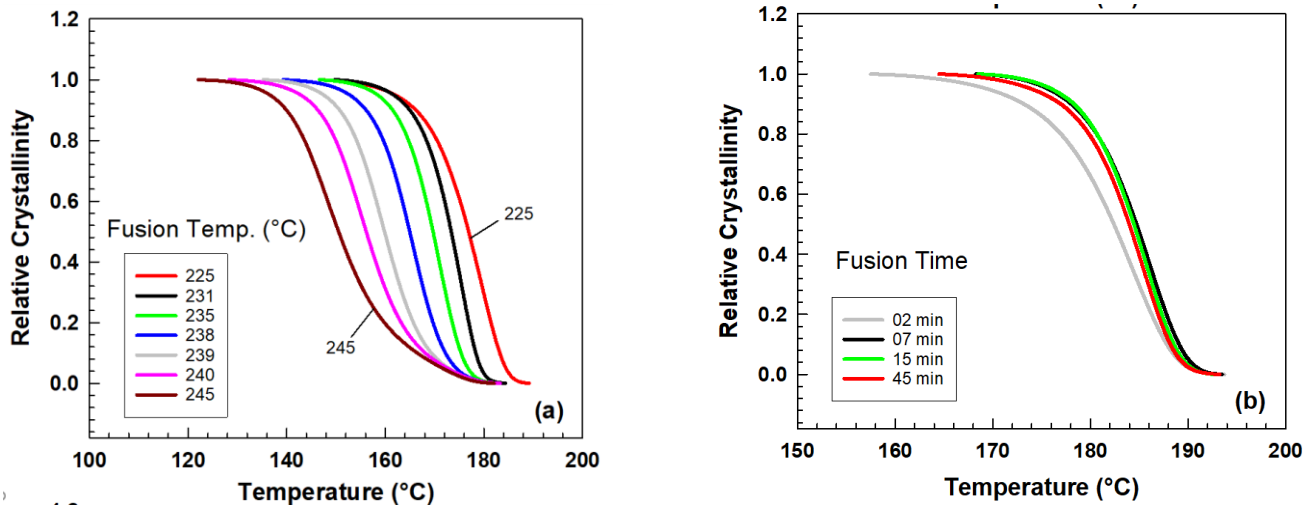

(a) (b)

Figure 3. Relative degree of crystallinity as a function of temperature for PA6 (a) fusion temperature from 225 °C to 245 °C at 25 °C/min (b) fusion time 2, 7, 15, and 45 min at constant T_f = 239 °C.

Equation (2) can be modified into crystallization time t and t0 instead of the crystallization temperature T and T_0, respectively. The relationship between the crystallization temperature and the crystallization time can be summarized in the following equation (Equation (8)) [82].

$$t = \frac{T_0 - T}{C} \tag{8}$$

where C is the cooling rate applied to the nonisothermal crystallization kinetics of PA6.

The experiment assessed the crystallinity of a material through nonisothermal crystallization and computed the corresponding half-life of crystallization. By plotting the relative crystallinity against time for various fusion temperatures, it was observed that there is a positive correlation between the fusion temperature and the crystallization half-life [46, 76, 83]. Figure 4a depicts a positive relationship between the fusion temperature (range 231–242 °C) for a fixed time of 2 min and the crystallization half-time. The results suggest that an increase in fusion temperature increases the time needed to reach the ultimate crystallinity, i.e., a reduction of the crystallization rate. This can be explained by the thermodynamics of the crystallization process, where higher temperatures promote molecular mobility and crystal growth, leading to a longer time needed to reach a given level of crystallinity. The findings are consistent with previous studies on polymer crystallization kinetics and have significant implications for the processing and properties of polymer materials [46, 49, 76]. Moreover, the study also investigated the impact of fusion time on the material's relative crystallinity, as illustrated in Figure 4b.

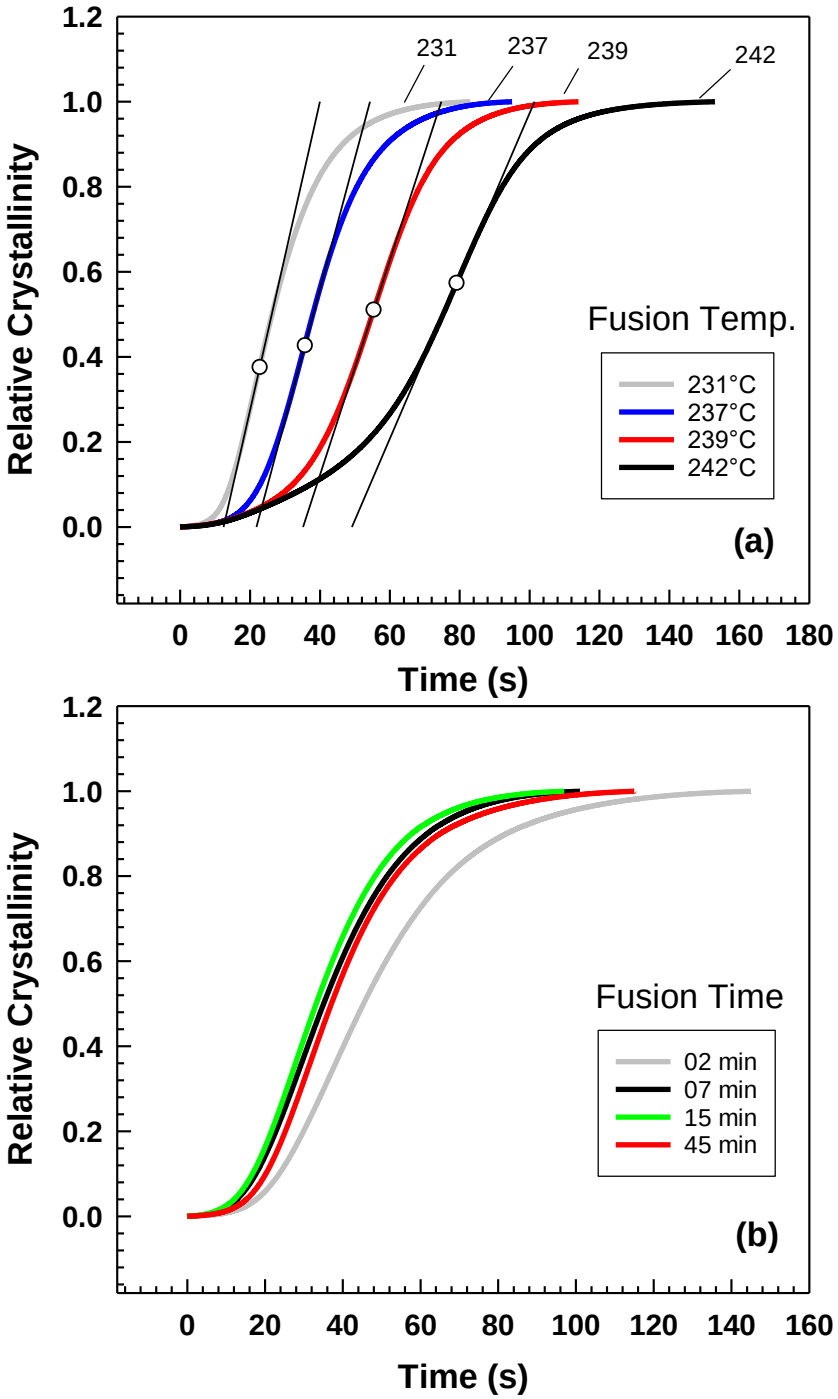

Figure 4. Crystallization kinetics from DSC relative crystallinity vs. time at different (a) fusion temperatures (b) fusion times.

As described before, the Avrami model [15] is used to study the isothermal crystallization kinetics in polymers. However, using the Avrami model for non-isothermal crystallization has been used by many authors [63, 84, 85]. Figure 5 shows the Avrami plot of ln[−ln (1 − X(t))] versus ln(t) for PA6 at different fusion temperatures. The Avrami plot shows a linear relationship where $R2 > 0.999$. As can be seen, the Avrami plots exhibit a high degree of parallelism and their temporal positions shift towards lower times as the previous fusion temperature increases [32, 55]. The Avrami model has been shown to be highly effective in predicting the nonisothermal crystallization behavior of PA6. This is because the range of temperatures in which crystallization takes place is relatively narrow, meaning that the conditions are not too different from those of an isothermal process. Notably, decreasing a polymer's fusion temperature can lead to a greater degree of nucleation and faster growth of the crystalline phase [86]. This effect can significantly impact the values of the Avrami parameters, namely n and k. Table 2 represents the Avrami parameters n and k used to characterize the crystallization kinetics. It is evident from the table that both the exponent n and the parameter k exhibit an upward trend with an increase in the fusion temperature up to 229 °C, following which they display a decline, i.e., limitations of the Avrami model by the fusion temperature of 231 °C because of the presence of shoulder on the heat flow curves after exposure to higher fusion temperatures.

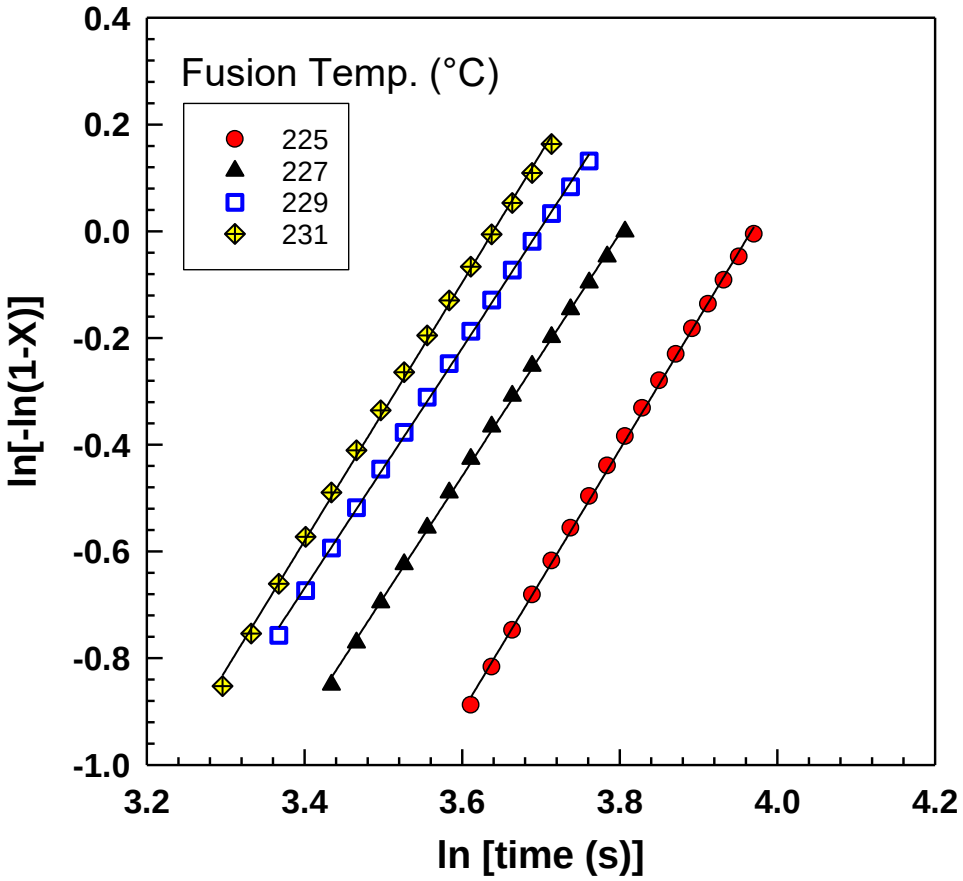

Figure 5. Avrami plot of ln [−ln(1 − X(t))] versus ln(t) at different fusion temperatures.

Table 2. Avrami parameters of nonisothermal crystallization of PA6 at different fusion temperatures.

Fusion Temp. (°C)	**Avrami Parameters**			
	R^2	**Slope**	**n**	**k (s^{-1})**
225	0.9992	0.02014	2.45	0.59E−04
227	0.9993	0.02313	2.27	1.76E−04
229	0.9993	0.02714	2.28	2.29E−04
231	0.9990	0.02912	2.48	1.22E−04

However, the Nakamura model [24], proposed in 1973, is a useful way of describing how polymers crystallize when heated. The rate of crystallization is affected by changes in temperature, and a term in the model considers this called the nonisothermal effect. This model has successfully predicted the behavior of many different polymers and has been adapted to account for other factors affecting crystallization. Table 3 displays the Nakamura K parameter, demonstrating an inverse fusion temperature correlation. As the fusion temperature increases, the K parameter decreases. Higher values of K indicate a greater nucleation rate and faster crystallization kinetics [87, 88]. This trend is commonly observed in the study of polymer crystallization and has important implications for the processing and properties of polymer materials. The crystallization kinetics of PA6 is highly influenced by changing the fusion temperature [32, 46]. Figure 6 and Table 3 show the effect of fusion temperature on (a) Nakamura K parameter, (b) inversed crystallization half-time [$t_{1/2}^{-1}$], and (c) slope at the inflection point. These kinetics parameters are dramatically decreased by increasing the fusion temperature to 242 °C, while higher fusion temperatures (T_f > 242 °C) do not affect the crystallization kinetics of PA6.

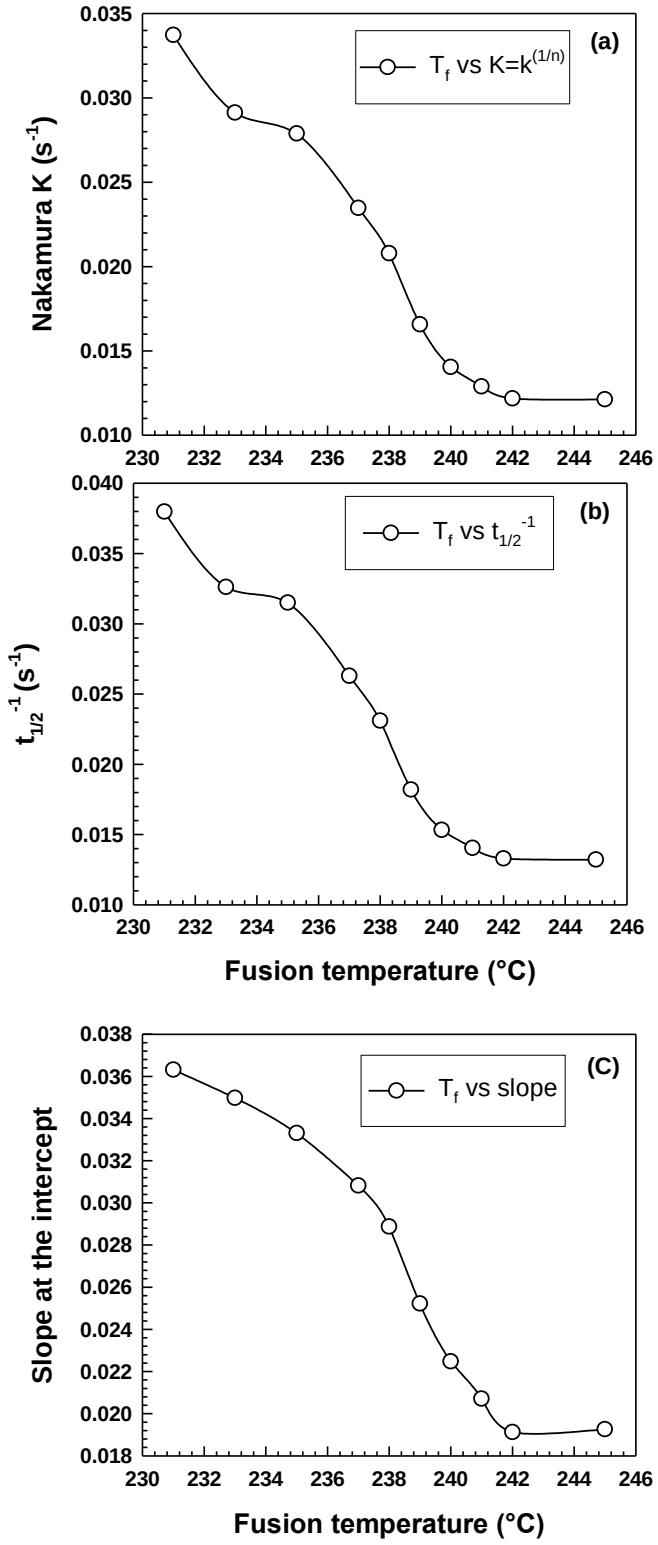

Figure 6. *Influence of fusion temperature on the kinetics parameters (**a**) Nakamura K, (**b**) $t_{1/2}^{-1}$, (**c**) slope at the intercept.*

Table 3. Kinetics parameters at different fusion temperatures.

Fusion Temp. (°C)	**Nakamura K = $k^{(1/n)}$ (s^{-1})**	**$t_{1/2}^{-1}$(s^{-1})**	**Slope**
231	0.0337	0.0380	0.0363
233	0.0291	0.0326	0.0350
235	0.0279	0.0315	0.0333
237	0.0235	0.0263	0.0308
238	0.0208	0.0231	0.0289
239	0.0166	0.0182	0.0252
240	0.0140	0.0153	0.0225
241	0.0129	0.0140	0.0207
242	0.0122	0.0133	0.0191
245	0.0121	0.0132	0.0193

The influence of the fusion temperature on the overall crystallinity of PA6 at various fusion times is depicted in Figure 7. It is worth noting that this follows the same pattern as the other kinetics parameters that have been previously discussed. The impact of the fusion temperature on the PA6 crystallization behavior is evident. The information used to construct the figure is also presented in Table 4.

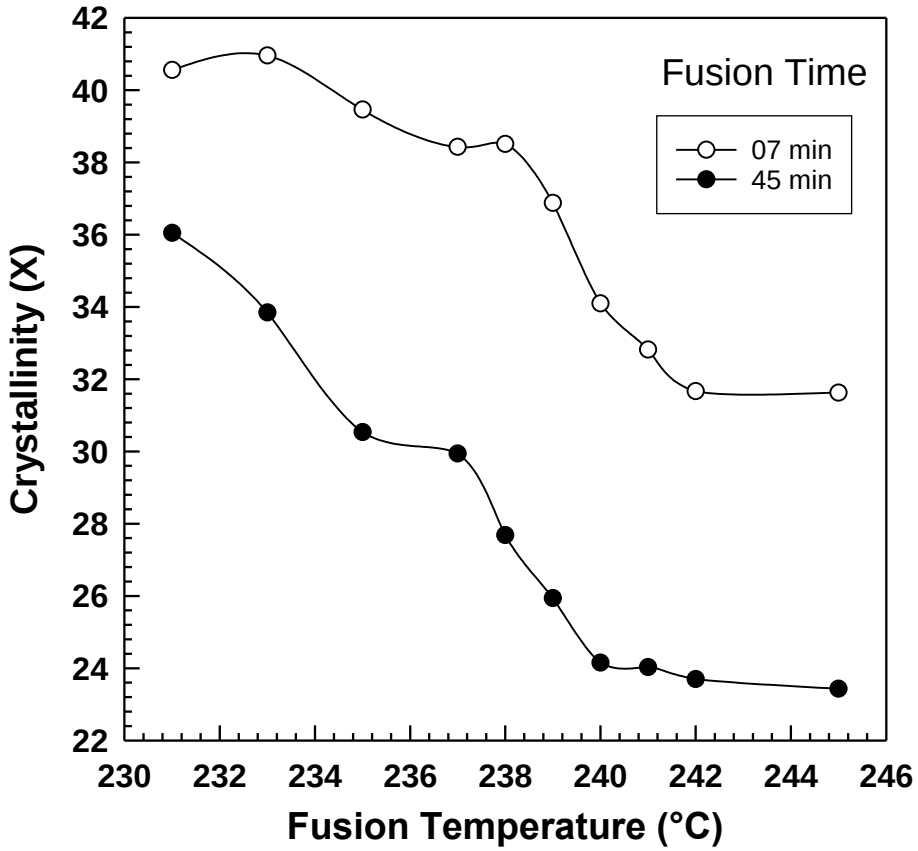

Figure 7. PA6 crystallinity vs. fusion temperature at different fusion times.

Table 4. Crystallinity of PA6 at different fusion times.

Fusion Temperature (°C)	**Crystallinity**	
	7 min	**45 min**
231	40.56	36.05
233	40.96	33.85
235	39.46	30.53
237	38.43	29.94
238	38.51	27.68
239	36.88	25.94
240	34.1	24.15
241	32.82	24.03
242	31.67	23.70
245	31.63	23.43

The crystallinity of PA6 samples was obtained from DSC at a fixed fusion temperature of 239 °C and different cooling rates of 15, 20, and 25 °C/min. Figure 8 shows a linear relationship between log(-ln [1-X]) and log Φ, and the Ozawa model seems appropriate to describe the nonisothermal crystallization of PA6 [48, 89]. This linear relationship was obtained due to the narrow range of cooling rates that were used in the experiment. However, other works that used a wider range did not obtain this linearity [76, 90]. After constructing the graph (Figure 8) of the dependence of log [-ln(1-X)] on log Φ, it was possible to obtain the parameters K and m from the directive of the line or section by linear regression.

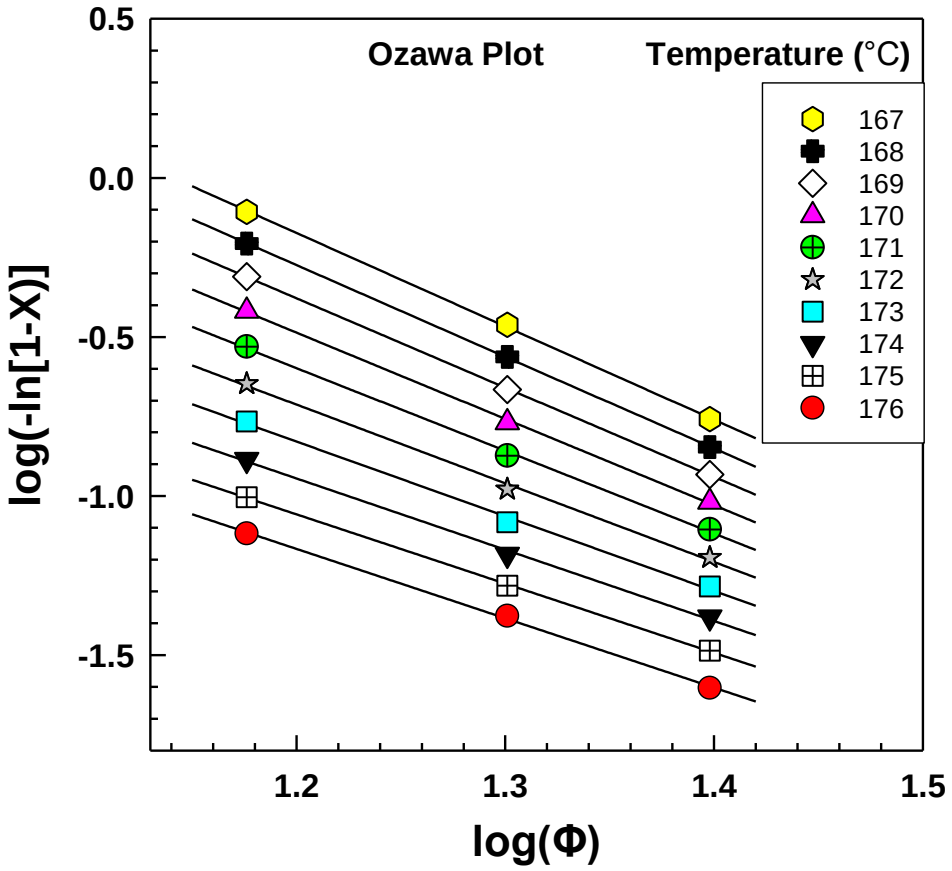

Figure 8. DSC results from the Ozawa plot for PA6.

Table 5 presents the results of an analysis of the cooling function K(T) and Ozawa exponent (m) based on the data obtained from Figure 8. The logarithmic cooling function log K(T) and the Ozawa exponent were determined from the slope and intercept of the graph and were found to range from 1.449 to 3.349 and 2.2 to 2.9, respectively, with R^2 values higher than 0.99. The Ozawa cooling functions were calculated at various fusion temperatures ranging from 235 °C to 245 °C. These findings are important for characterizing the nonisothermal crystallization kinetics of the material and provide valuable insight into the thermal behavior of the polymer. Such analyses are commonly used in materials science research to better understand the processing and properties of polymers, and the results can inform the development of new materials with tailored properties.

Table 5. Ozawa exponents and cooling functions of PA6.

Temperature (°C)	**Slope**	**Intercept**	**RSQ**
	m	**log[K(T)]**	**R^2**
176	2.2	1.449	0.9988
175	2.2	1.552	0.9997
174	2.2	1.741	0.9979
173	2.3	1.986	0.9970
172	2.5	2.255	0.9974
171	2.6	2.521	0.9985
170	2.7	2.770	0.9994
169	2.8	2.993	0.9999
168	2.9	3.186	0.9999
167	2.9	3.349	0.9995

Figure 9 illustrates the relationship between the fusion temperature and the Ozawa cooling function K(T). The graph demonstrates that the cooling function K(T) decreases and shifts towards the left side as the fusion temperature increases. It is worth noting that the cooling function K(T) is a function of both nucleation and growth rate [48]. The graph in Figure 6 illustrates that, for the PA6 polymer, the cooling function K(T) increases exponentially as the temperature decreases. This is because as the crystallization temperature decreases, the thermodynamic driving force for crystallization becomes stronger. However, when the temperature becomes low enough, the viscosity of the polymer significantly increases, making it difficult for polymer

chains to reach the growth point. This observation is a natural consequence of the PA6 polymer.

Similar K(T) dependencies to the crystallization temperature were detected for different fusion temperatures (235 °C to 245 °C). In comparison, the K(T) increases while decreasing the fusion temperature. The Ozawa cooling functions of PA6 might result from the number of spherulites generated at different fusion temperatures. A polarized optical microscope analyzed PA6 samples; the samples were heated at different fusion temperatures (235–246 °C) for 2 min and then were cooled down at a cooling rate of 20 °C/min.

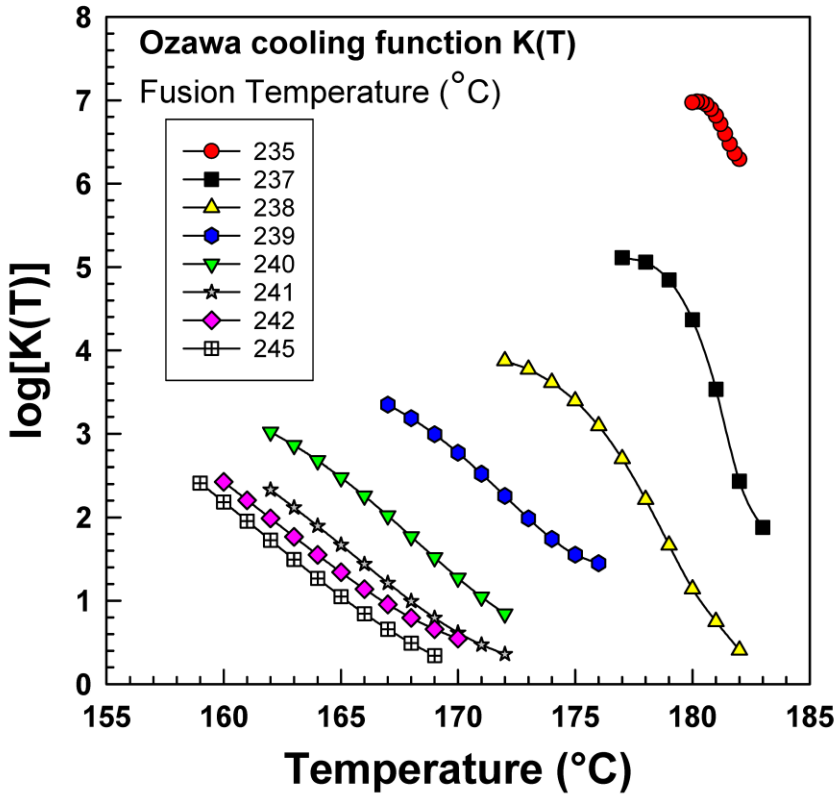

Figure 9. *Ozawa cooling function.*

As shown in Figure 9, the average number of spherulites decreases with increasing temperature. Raising the temperature from 235 °C to 239 °C reduces the number of spherulites by half. This reduction in the number of spherulites occurs due to the destructive effect of high temperature that reduces the nucleation cores' production [46].

Polarized optical microscopy (OM) is used to observe the morphology of PA6 spherulites formed during nonisothermal crystallization. These spherulites are spherical and exhibit highly ordered Maltese cross pattern structures [91, 92]. Understanding the details of the spherulite morphology and growth rate is crucial for controlling the final product's physical properties. Figure 10 presents OM images of PA6 that have undergone a cooling process from 200 °C to 100 °C at a rate of 20 °C/min. During this cooling process, the sample begins to crystallize. The results indicate that spherulites are present during the cooling process. These spherulites have a circular cross-section and exhibit a Maltese cross-pattern system, which suggests that they are oriented along or perpendicular to the crystalline molecular axis concerning the spherulitic radius [76]. The size of the crystallites is highly dependent on the crystallization temperature and time. Figure 11 illustrates the impact of temperature on the rate of spherulite formation during the crystallization process. These spherulite structures are formed due to the presence of many nucleation sites and the rapid cooling of the molten polymer, which impedes normal crystal growth.

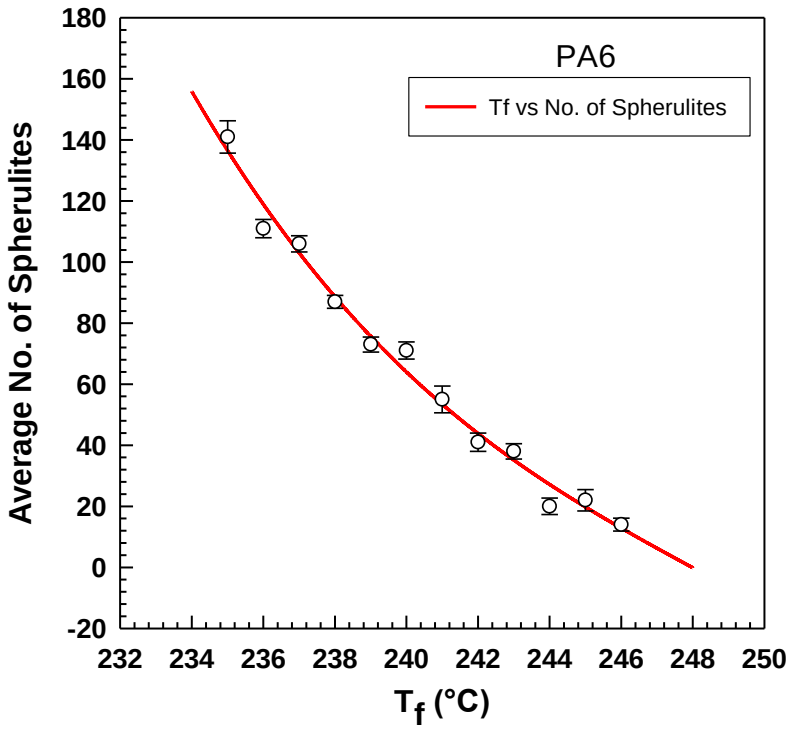

Figure 10. *Effect of the fusion temperature on the number of spherulites of PA6 crystallization.*

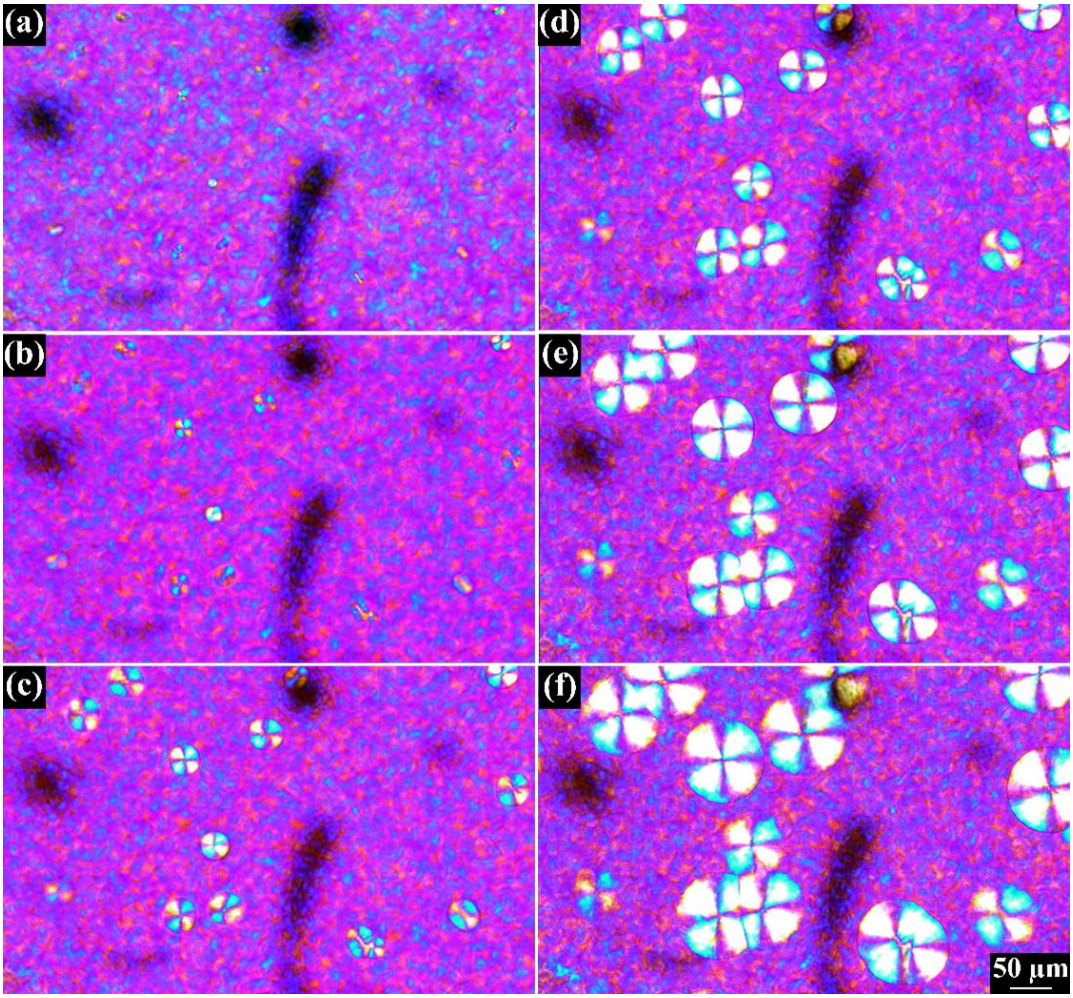

Figure 11. *Nonisothermal crystallization by polarized optical microscope at 20 °C/min cooling rate at different temperatures (**a**) 186.3 °C, (**b**) 183 °C, (**c**) 179.6 °C, (**d**) 176.3 °C, (**e**) 173.8 °C, (**f**) 169.8 °C.*

Figure 12 shows the analysis of melting temperature as a function of crystallization temperature that was performed according to the Hoffman–Weeks theory. Where the extrapolated line crosses the Tm = Tc line, there one can find an equilibrium melting point T_m^0. Our T_m^0 was found to be at 242 °C that is very close to Wang et al. who reported equilibrium melting point for pure PA6 to be about 243 °C [93].

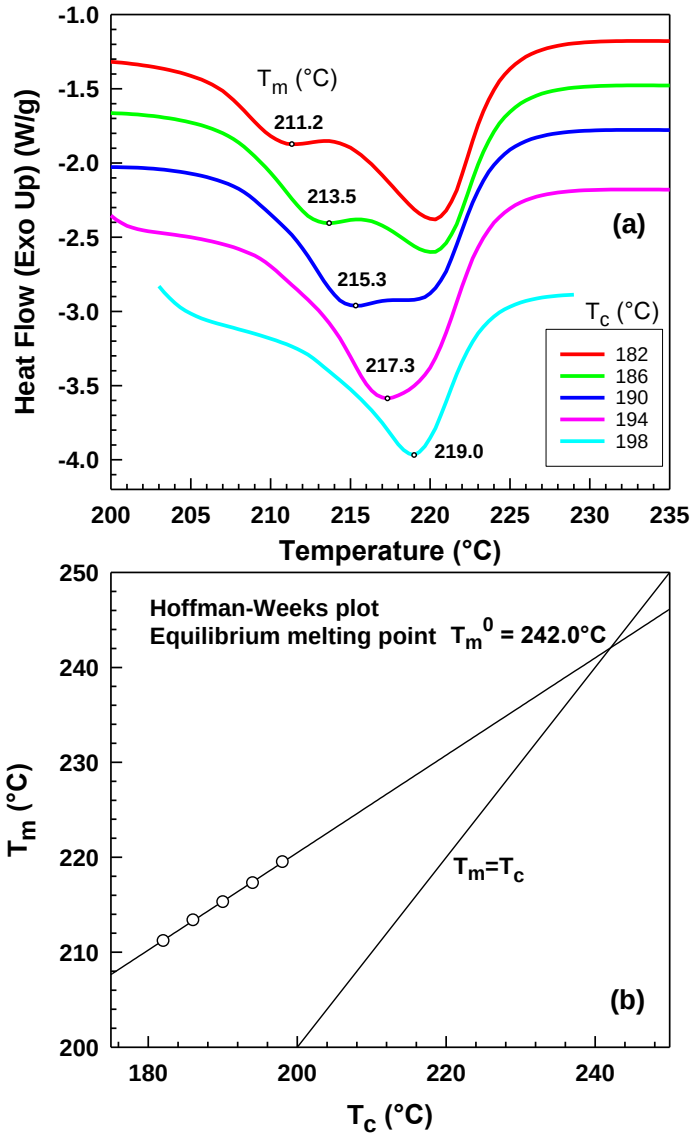

Figure 12. *(**a**) Determination of melting temperature after isothermal crystallization at various temperatures, (**b**) Hoffman–Weeks plot for equilibrium melting point determination, melting point of peak I vs. crystallization temperature.*

5. CONCLUSION

In conclusion, the manuscript studied the influence of fusion temperature and duration on the nonisothermal crystallization kinetics of polyamide 6 (PA6) using differential scanning calorimetry (DSC) and polarized optical microscope (OM). It was found that increasing the fusion temperature led to narrower and lower exothermic traces, resulting in smaller nucleation centers, a shift in crystallization temperature, and a decrease in crystallization kinetics. Additionally, a correlation between the fusion temperature and the crystallization half-time was also observed, indicating that higher temperatures result in longer times needed to reach a given level of crystallinity due to increased molecular mobility and crystal growth. The Ziabicki, Ozawa, and Nakamura models were used to study the crystallization kinetics and found that changing the fusion temperature greatly affected the degree of nucleation and growth of the crystalline phase. The study has implications for the processing and properties of polymer materials.

ACKNOWLEDGMENTS

The authors thank Tomas Bata University in Zlin for supporting this research through its Internal Grant Agency (IGA/FT/2023/008).

REFERENCES

1. Kausar, A. Physical properties of hybrid polymer/clay composites. In *Hybrid Polymer Composite Materials: Properties and Characterisation*; Elsevier: Amsterdam, The Netherlands, 2017; pp. 115–132. https://doi.org/10.1016/B978-0-08-100787-7.00005-6.
2. R. J. Gaymans, Polyamides, Synthetic Methods in Step-Growth Polymers (Eds.: M. E. Rogers, T. E. Long), Wiley, New York, 2003, pp. 135– 195. For the ring-opening aminolysis-condensation (ROAC) of diamines and dilactones, see refs. [5e, g]. https://doi.org/10.1002/0471220523.ch3.
3. Alfonso, G.C.; Ziabicki, A. Memory effects in isothermal crystallization II. Isotactic polypropylene. *Colloid Polym. Sci.* **1995**, *273*, 317–323. https://doi.org/10.1007/bf00652344.
4. Supaphol, P.; Lin, J.-S. Crystalline memory effect in isothermal crystallization of syndiotactic polypropylenes: effect of fusion temperature on crystallization and melting behavior. *Polymer* **2001**, *42*, 9617–9626. https://doi.org/10.1016/s0032-3861(01)00507-9.
5. Millot, C.; Fillot, L.-A.; Lame, O.; Sotta, P.; Seguela, R. Assessment of polyamide-6 crystallinity by DSC. *J. Therm. Anal. Calorim.* **2015**, *122*, 307–314. https://doi.org/10.1007/s10973-015-4670-5.
6. Rudin, A. (Ed.) Chapter 1—Introductory Concepts and Definitions. In *The Elements of Polymer Science and Engineering*; Academic Press: San Diego, CA, USA; 1982; p. 1–40.
7. Payal, R.; Sommer, J.-U. Crystallization of Polymers under the Influence of an External Force Field. *Polymers* **2021**, *13*, 2078. https://doi.org/10.3390/polym13132078.
8. Hoffman, J.D.; Lauritzen, J.I. Crystallization of bulk polymers with chain folding: theory of growth of lamellar spherulites. *J. Res. Natl. Bur. Stand. Sect. A: Phys. Chem.* **1961**, *65A*, 297–336. https://doi.org/10.6028/jres.065a.035.
9. Kratochvíl, J.; Kelnar, I. A simple method of evaluating non-isothermal crystallization kinetics in multicomponent polymer systems. *Polym. Test.* **2015**, *47*, 79–86. https://doi.org/10.1016/j.polymertesting.2015.07.010.
10. Mathew, A.P.; Oksman, K.; Sain, M. The effect of morphology and chemical characteristics of cellulose reinforcements on the crystallinity of polylactic acid. *J. Appl. Polym. Sci.* **2006**, *101*, 300–310. https://doi.org/10.1002/app.23346.
11. Ramanujam, B.T.S.; Annamalai, P.K. Conducting polymer-graphite binary and hybrid composites: Structure, properties, and applications. In *Hybrid Polymer Composite Materials: Applications*; Elsevier: Amsterdam, The Netherlands, 2017; pp. 1–34. https://doi.org/10.1016/B978-0-08-100785-3.00001-2.
12. Ziabicki, A.; Alfonso, G.C. Memory effects in isothermal crystallization. I. Theory. *Colloid Polym. Sci.* **1994**, *272*, 1027–1042. https://doi.org/10.1007/bf00652372.
13. Ishida, K.; Han, S.-I.; Im, S.-S.; Inoue, Y. Effects of Fusion Temperature and Metal Ion Variation on Crystallization of Lightly Ionized Poly(butylene succinate). *Macromol. Chem. Phys.* **2007**, *208*, 146–154. https://doi.org/10.1002/macp.200600417.
14. Khanna, Y.P.; Kuhn, W.P. Measurement of crystalline index in nylons by DSC: Complexities and recommendations. *J. Polym. Sci. Part B-Polym. Phys.* **1997**, *35*, 2219–2231. https://doi.org/10.1002/(SICI)1099-0488(199710)35:14%3C2219::AID-POLB3%3E3.0.CO;2-R.
15. Seguela, R. Overview and critical survey of polyamide6 structural habits: Misconceptions and controversies. *J. Polym. Sci.* **2020**, *58*, 2971–3003. https://doi.org/10.1002/pol.20200454.
16. Mondal, A.; Sohel, A.; Arif, P.M.; Thomas, S.; SenGupta, A. Effect of ABS on non-isothermal crystallization kinetics of polyamide 6. *J. Therm. Anal. Calorim.* **2021**, *146*, 2489–2501. https://doi.org/10.1007/s10973-020-10443-1.

17. Wu, B.; Gong, Y.; Yang, G. Non-isothermal crystallization of polyamide 6 matrix in all-polyamide composites: crystallization kinetic, melting behavior, and crystal morphology. *J. Mater. Sci.* **2011**, *46*, 5184–5191. https://doi.org/10.1007/s10853-011-5452-5.
18. Avrami, M. Kinetics of Phase Change. I General Theory. *J. Chem. Phys.* **1939**, *7*, 1103. https://doi.org/10.1063/1.1750380.
19. Ozawa, T. Kinetics of non-isothermal crystallization. *Polymer* **1971**, *12*, 150–158. https://doi.org/10.1016/0032-3861(71)90041-3.
20. Nakamura, K.; Katayama, K.; Amano, T. Some aspects of nonisothermal crystallization of polymers. II. Consideration of the isokinetic condition. *J. Appl. Polym. Sci.* **1973**, *17*, 1031–1041. https://doi.org/10.1002/app.1973.070170404.
21. Tang, G.; Wang, X.; Jiang, S.; Zhou, K.; Bai, Z.; Wang, B.; Tai, Q.; Song, L.; Hu, Y. Thermal degradation and combustion behaviors of flame retarded glass fiber reinforced polyamide 6 composites based on cerium hypophosphite. *Polym. Compos.* **2016**, *37*, 3073–3082. https://doi.org/10.1002/pc.23505.
22. Di Lorenzo, M.; Silvestre, C. Non-isothermal crystallization of polymers. *Prog. Polym. Sci.* **1999**, *24*, 917–950. https://doi.org/10.1016/s0079-6700(99)00019-2.
23. Cebe, P.; Thomas, D.; Merfeld, J.; Partlow, B.P.; Kaplan, D.L.; Alamo, R.G.; Wurm, A.; Zhuravlev, E.; Schick, C. Heat of fusion of polymer crystals by fast scanning calorimetry. *Polymer* **2017**, *126*, 240–247. https://doi.org/10.1016/j.polymer.2017.08.042.
24. Freire, L.; Combeaud, C.; Monge, G.; Billon, N.; Haudin, J. Transcrystallinity versus spherulitic crystallization in polyamide 66: An experimental study. *Polym. Cryst.* **2019**, *2*. https://doi.org/10.1002/pcr2.10028.
25. He, C.; Cao, X.; Huo, G.; Luo, S.; He, X. Non-Isothermal Crystallization Behaviour and Kinetics of LLDPE/REDMUD Blends. *Polym. Polym. Compos.* **2015**, *23*, 483–494. https://doi.org/10.1177/096739111502300707.
26. Wang, H.-L.; Shi, T.-J.; Yang, S.-Z.; Hang, G.-P. Crystallization behavior of PA6/SiO2 organic–inorganic hybrid material. *Mater. Res. Bull.* **2006**, *41*, 298–306. https://doi.org/10.1016/j.materresbull.2005.08.023.
27. Shi, J.; Yang, X.; Wang, X.; Lu, L. Non-isothermal crystallization kinetics of nylon 6/attapulgite nanocomposites. *Polym. Test.* **2010**, *29*, 596–602. https://doi.org/10.1016/j.polymertesting.2010.03.007.
28. Wang, Y.; Liu, W.; Zhang, H. The morphology and non-isothermal crystallization characteristics of poly(trimethylene terephthalate)/BaSO4 nanocomposites prepared by in situ polycondensation. *Polym. Test.* **2009**, *28*, 402–411. https://doi.org/10.1016/j.polymertesting.2009.02.004.
29. Poisson, C.; Colaers, M.; Van Puyvelde, P.; Goderis, B. Memory Effects in the Quiescent Crystallization of Polyamide 12: Self-Seeding, Post-Condensation, Disentangling, and Self-Nucleation beyond the Equilibrium Melting Temperature. *Macromolecules* **2023**, *56*, 2747–2760. https://doi.org/10.1021/acs.macromol.2c02102.
30. Yu, Y.; Zeng, F.; Chen, J.; Kang, J.; Yang, F.; Cao, Y.; Xiang, M. Regulating polycrystalline behavior of the β-nucleated isotactic polypropylene/graphene oxide composites by melt memory effect. *Polym. Compos.* **2019**, *40* (Suppl. S1), E440–E448. https://doi.org/10.1002/pc.24745.
31. Jeziorny, A. Parameters characterizing the kinetics of the non-isothermal crystallization of poly(ethylene terephthalate) determined by d.s.c. *Polymer* **1978**, *19*, 1142–1144. https://doi.org/10.1016/0032-3861(78)90060-5.
32. Pourali, M.; Peterson, A.M. A tale of two polyamides: Comparing the crystallization kinetics of a hot-melt adhesive and a PA 6/66 copolymer. *Thermochim. Acta* **2022**, *710*. https://doi.org/10.1016/j.tca.2022.179176.
33. Papageorgiou, D.G.; Papageorgiou, G.Z.; Bikiaris, D.N.; Chrissafis, K. Crystallization and melting of propylene–ethylene random copolymers. Homogeneous nucleation and β-nucleating agents. *Eur. Polym. J.* **2013**, *49*, 1577–1590. https://doi.org/10.1016/j.eurpolymj.2013.02.002.

34. Papageorgiou, G.Z.; Tsanaktsis, V.; Papageorgiou, D.G.; Chrissafis, K.; Exarhopoulos, S.; Bikiaris, D.N. Furan-based polyesters from renewable resources: Crystallization and thermal degradation behavior of poly(hexamethylene 2,5-furan-dicarboxylate). *Eur. Polym. J.* **2015**, *67*, 383–396. https://doi.org/10.1016/j.eurpolymj.2014.08.031.
35. Uthaipan, N.; Jarnthong, M.; Peng, Z.; Junhasavasdikul, B.; Nakason, C.; Thitithammawong, A. Effects of cooling rates on crystallization behavior and melting characteristics of isotactic polypropylene as neat and in the TPVs EPDM/PP and EOC/PP. *Polym. Test.* **2015**, *44*, 101–111. https://doi.org/10.1016/j.polymertesting.2015.04.002.
36. Lee, Y.; Porter, R.S. Effects of thermal history on crystallization of poly(ether ether ketone) (PEEK). *Macromolecules* **1988**, *21*, 2770–2776. https://doi.org/10.1021/ma00187a022.
37. Svoboda, P.; Trivedi, K.; Stoklasa, K.; Svobodova, D.; Ougizawa, T. Study of crystallization behaviour of electron beam irradiated polypropylene and high-density polyethylene. *R. Soc. Open Sci.* **2021**, *8*. https://doi.org/10.1098/rsos.202250.
38. Androsch, R.; Schick, C. Crystal Nucleation of Polymers at High Supercooling of the Melt. *Polym. Cryst. I Chain. Microstruct. Process.* **2017**, *276*, 257–288. https://doi.org/10.1007/12_2015_325.
39. Levy, A. Robust Numerical Resolution of Nakamura Crystallization Kinetics. *Int. J. Theor. Appl. Math.* **2017**, *3*, 143. https://doi.org/10.11648/j.ijtam.20170304.13.
40. Seo, J.; Zhang, X.; Schaake, R.P.; Rhoades, A.M.; Colby, R.H. Dual Nakamura model for primary and secondary crystallization applied to nonisothermal crystallization of poly(ether ether ketone). *Polym. Eng. Sci.* **2021**, *61*, 2416–2426. https://doi.org/10.1002/pen.25767.
41. Lee, S.; Ree, M.; Park, C.; Jung, Y.; Jin, Y.; Bae, D. Synthesis and non-isothermal crystallization behaviors of poly(ethylene isophthalate-co-terephthalate)s. *Polymer* **1999**, *40*, 7137–7146. https://doi.org/10.1016/s0032-3861(99)00119-6.
42. Wang, Z.-Q.; Zhao, Y.-K.; Wu, X.-F. Non-Isothermal Crystallization Kinetics of Graphene Oxide-Carbon Nanotubes Hybrids/Polyamide 6 Composites. *J. Chem. Soc. Pak.* **2019**, *41*, 394. https://doi.org/10.52568/000760%2Fjcsp%2F41.03.2019.
43. Bassett, D.C. Polymer Spherulites: A Modern Assessment. *J. Macromol. Sci. Part B* **2007**, *42*, 227–256. https://doi.org/10.1081/mb-120017116.
44. Wang, B.; Wang, W.; Wang, H.; Hu, G. Isothermal crystallization kinetics and melting behavior of in situ compatibilized polyamide 6/Polyethylene-octene blends. *J. Polym. Res.* **2010**, *17*, 429–437. https://doi.org/10.1007/s10965-009-9329-0.

PAPER IV

Elastic Electrically Conductive Composites Based on Vapor-Grown Carbon Fibers for Use in Sensors

Ahmed Nasr *, Ondřej Mrhálek and Petr Svoboda

Department of Polymer Engineering, Faculty of Technology, Tomas Bata University in Zlin, Vavreckova 5669, 760 01 Zlin, Czech Republic

ABSTRACT

Elastic electrically conductive composites with an ethylene octene copolymer matrix (EOC) and vapor-grown carbon fibers (VGCF) were prepared by ultrasonication in a toluene solution, and their morphology, mechanical and electrical properties were also evaluated. EOC/CF composites were estimated for their mechanical and viscoelastic properties. The morphology of the composites was analyzed using scanning electron microscopy (SEM), and stress–strain curves were generated to measure the stress and tensile modulus of the composites. The experimental results were compared with various theoretical models, including the Burgers model, which separates viscoelastic behavior into several components. A dynamic mechanical analysis was also used to measure the composites' storage modulus, loss modulus, and damping factor at different frequencies. The composites' complex viscosity and storage modulus were increased with higher wt.% of CF, which enhances the elastic response. Electrical resistivity measurements were conducted on the composites and it was found that the resistivity decreased as the sample was loaded and increased as it was unloaded. Overall, the study provides insights into the mechanical and viscoelastic properties of EOC/CF composites, which could be helpful in developing sensors such as pressure/strain sensors.

KEYWORDS

carbon fibres; ethylene-octene copolymer; electrical properties; mechanical properties.

1. INTRODUCTION

Nanotechnology has recently become an increasingly popular area of research, with a particular interest in using nanofillers in composite materials. One area of focus for researchers has been the development of conductive polymer composites (CPCs) for use in various electronic applications, including pressure–strain sensors, organic vapor detectors, actuators and temperature sensors [1-4]. Carbon fibers (CFs) have long been considered an excellent conductive filler for these composites, with research into their use dating back to 1960. In particular, vapor-grown carbon fibers (VGCFs), which were first developed in 1980, have gained popularity as a reinforcement material for composite materials due to their high strength and modulus [5, 6].

Percolation theory can be used to explain the mechanism of electrical conductivity in CPCs, where the filler creates a continuous conductive pathway. The percolation threshold refers to the minimum volume fraction of the filler required to make this pathway. Elastic composites may experience a significant decrease in electrical conductivity when stretched due to the disruption of the conductive pathways [2, 7]. The polymer matrix in these composites can be various [8, 9]. Nevertheless, thermoplastic elastomers have grown in recent years due to their unique properties, which combine processability as thermoplastics and rubbery properties as elastomers. They are a particular class of polymers that generally consist of hard and soft phases [10]. Lozano-Perez et al. conducted a study to examine the impact of the rigid segment on electromechanical behavior. The findings demonstrated that an increased content of rigid segments increases the tensile modulus, mechanical hysteresis, and electrical response [11].

Several researchers have investigated the mechanical properties of CPCs [12]. Zhang et al. studied the strain–sensing behavior of elastomeric composites under mechanical cyclic loading [13]. The electrical resistance of the elastomeric composites shows perfect recoverability after cyclic loading. The conductivity and electrical resistance depend on the shape of the filler particles. A comparative study with various carbon fillers was investigated by Theravalappil et al. They found that the longer carbon fibers create conductive paths at lower concentrations than multi-walled carbon nanotubes [14]. Even though using thermoplastic elastomers as a matrix for CPCs has already been investigated, little attention has been paid to copolymers of polyethylene/poly(α-olefin), e.g., ethylene-octene copolymer (EOC).

This study focused on the preparation of elastic CPCs using EOC and CF and the subsequent evaluation of their mechanical and electrical properties. The

resulting EOC/CF composites demonstrated exceptional elasticity, making them highly suitable for use in pressure and strain sensors.

2. EXPERIMENTAL

2.1. Materials

The Dow Chemical Company supplied the ethylene-octene copolymer Engage 8842 used in this study. The octene content was 45 wt.%, the density 0.857 g/cm^3 and the melt flow index 1.0 g/10 min (190 °C/2.16 kg). Carbon fibers were provided by Showa Denko, Japan, under the trade name VGCF (vapor-grown carbon fibers). The properties of VGCF are represented in Table 1.

Table 1. Properties of CF.

Average diameter	150 nm
Average length	15 μm
Aspect ratio	10–500
Density	2.0 g/cm3

2.2. Sample Preparation and Morphology

An EOC matrix with 10, 15, 20, 25, 30 and 35 wt.% of fillers was blended by ultrasonication method. First, the calculated amount of filler was added to the EOC/toluene solution.The sonication process was then applied at 80 °C (Dr. Hielscher GmbH apparatus; amplitude 88 μm, power density 300 W/cm2, and frequency 24 kHz) for one hour. The composite was precipitated with acetone and dried at 50 °C for 12 h. Finally, the samples were prepared by compression molding at 100 °C in the hydraulic press and cut into a rectangular shape (50 × 10 × 0.5 mm). The morphology and dispersion of CF in the polymer matrix were analyzed by scanning electron microscopy (SEM) on a Vega LMU Tescan with a voltage of 10 kV. Before analysis, samples were put into liquid nitrogen and were broken after 1 min.

2.3. Mechanical Properties

Tensile stress-strain measurement, creep behavior and frequency sweep were carried out using a Mettler Toledo DMA1 at room temperature. The stress–strain experiment was set up from 0 to 5 N with the force changing at a rate of 0.5 N/min.

From the beginning of the stress–strain curves, the tensile modulus was evaluated. Creep behavior was tested at standard tensile mode with various loads for 5 min. Force 0.2, 0.5, 1, 2, 3, 4 and 5 N was applied to connect mechanical with electrical properties. At the frequency sweep measurement, frequencies were set up from 0.1 to 100 Hz. Storage modulus (E′) and Tan δ were evaluated.

2.4. Electrical Properties

The samples were put between the clamps of a multimeter UNI-T UT71C and electrical resistance was measured. Various calibrated weights (20, 50, 100, 200, 300, 400 and 500 g) were then placed on the lower clamp holding the sample and the electrical resistance was measured again after stretching. First, the sample was loaded with the weight for 5 min; then, it was unloaded for 5 min. This process was repeated. The test was continuous, and the electrical resistance was recorded every 1 s by software UNI-T UT71ABC. The measurements were performed at room temperature (25 °C).

3. RESULTS AND DISCUSSION

3.1. Sample Morphology

The morphology of EOC/CF composites was obtained using scanning electron microscopy (SEM). Figure 1 shows the morphology of the composite with 30 wt.% CF. As can be seen, filler particles are uniformly dispersed, proving the efficiency of ultrasonication mixing. The conductivity path exists in a place where the fibers are crossed. In fact, there are more contacts in the sample volume (invisible on SEM). The picture shows only the sample’s surface after the fracture break at low temperatures.

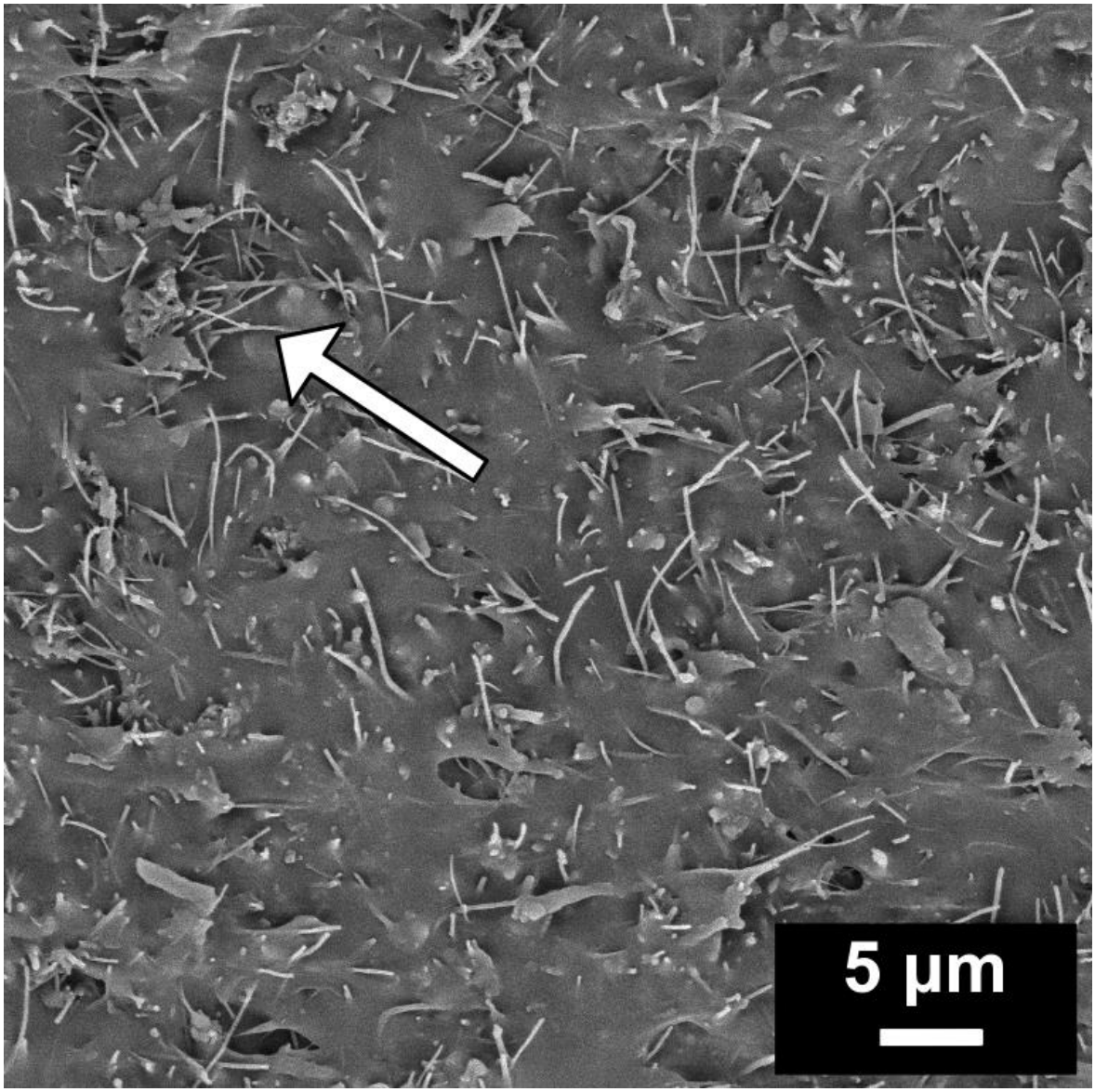

Figure 1. SEM image of EOC/CF composite with 30 wt.% of CF.

3.2. Mechanical Properties

Stress–strain curves are illustrated in Figure 2. Stress increases with a higher content of the filler for the same strain, implying a higher modulus. The reinforcing effect of the CF filler in the EOC matrix causes this. Even though the stress and tensile modulus are higher, EOC/CF composites remained elastic.

Several theoretical models have been described in the literature to elucidate the mechanical properties of composites containing different types of fillers. Among these models, the hydrodynamic theory proposed by Einstein [15] is considered the earliest one for spherical filler particles, which explains the viscosity of colloidal suspensions [15].

$$\eta = \eta_0 (1 + 2.5 \phi) \quad (9)$$

where η is the viscosity of the suspension, η_0 is the viscosity of the incompressible fluid and ϕ is the volume fraction of the spherical particles.

This model predicts an increase in viscosity due to the presence of the filler. Einstein's theory also assumes that spherical particles are uniformly dispersed in the polymer matrix and perfectly bonded with the matrix. Guth and Gold generalize Einstein's equation to predict the tensile modulus of filled composites instead of the viscosity. Furthermore, this model includes and explains the interaction between the matrix and fillers at a higher content of filler [15-18]. The Guth–Gold model is shown in Equation (2):

$$\frac{E_c}{E_0} = (1 + 2.5 \phi + 14.1 \phi^2) \quad (10)$$

where E_c is the tensile modulus of the composite, E_0 is the unfilled polymer matrix's tensile modulus and ϕ is the filler's volume fraction. Equation (2) describes the increase in the tensile modulus of the composite with spherical particles as a function of the filler content. Nevertheless, it was found that in the case of non-spherical particles, the tensile modulus could increase more than is predicted by Equation (2) [15, 17]. Considering the shape of the fillers, Guth and Smallwood presented the shape factor f for non-spherical particles in Equation (3) [19]:

$$\frac{E_c}{E_0} = (1 + 0.67 f\phi + 1.62 f^2 \phi^2) \quad (11)$$

The results presented in Figure 3 compare the experimental tensile modulus of EOC/CF composites with the Guth–Gold model for spherical particles and the Guth–Smallwood model for non-spherical particles, with varying shape factors.

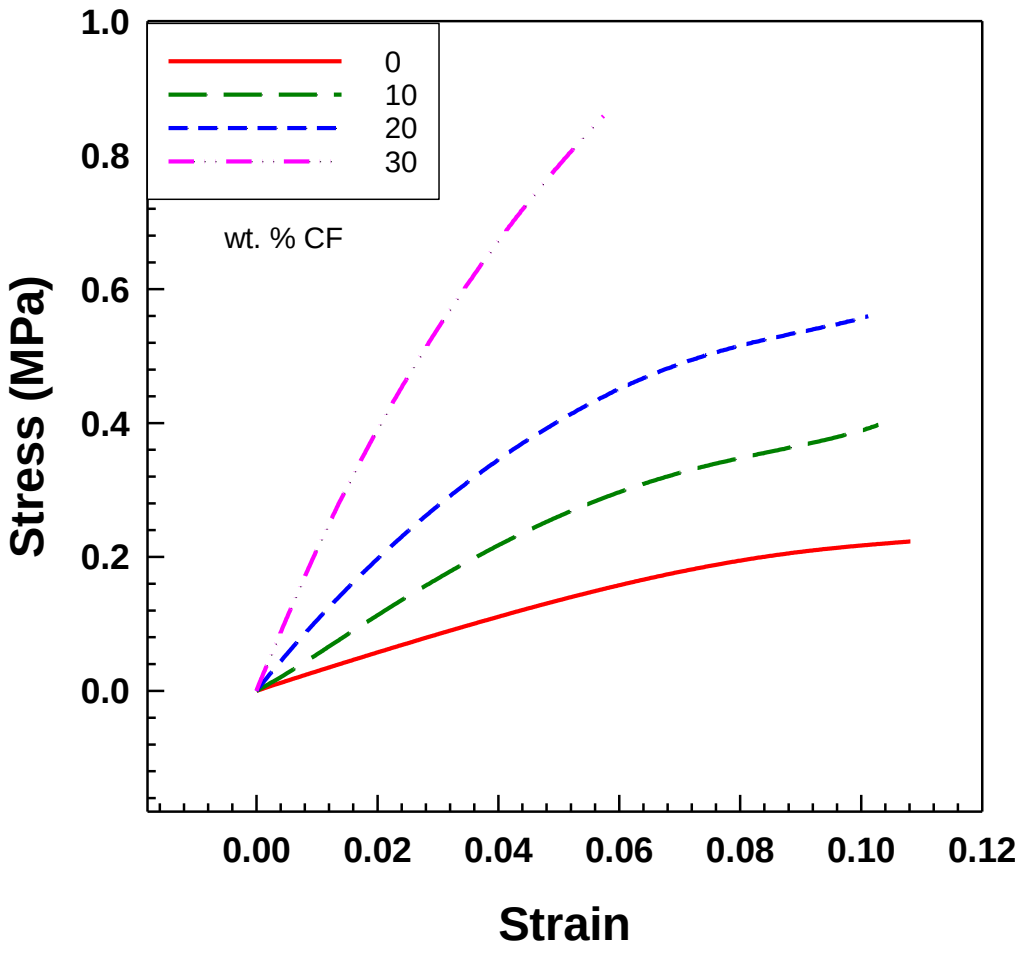

Figure 2. Tensile stress–strain curves of EOC/CF composites measured by DMA at room temperature.

As the weight percentage of CF increases from 0% to 30%, the tensile modulus of the composites significantly increases from 4 MPa to 28 MPa, respectively. The obtained experimental data agree with the Guth–Smallwood model for non-spherical particles, which suggests that the carbon fibers have a non-spherical shape with a shape factor of 0.5 [20].

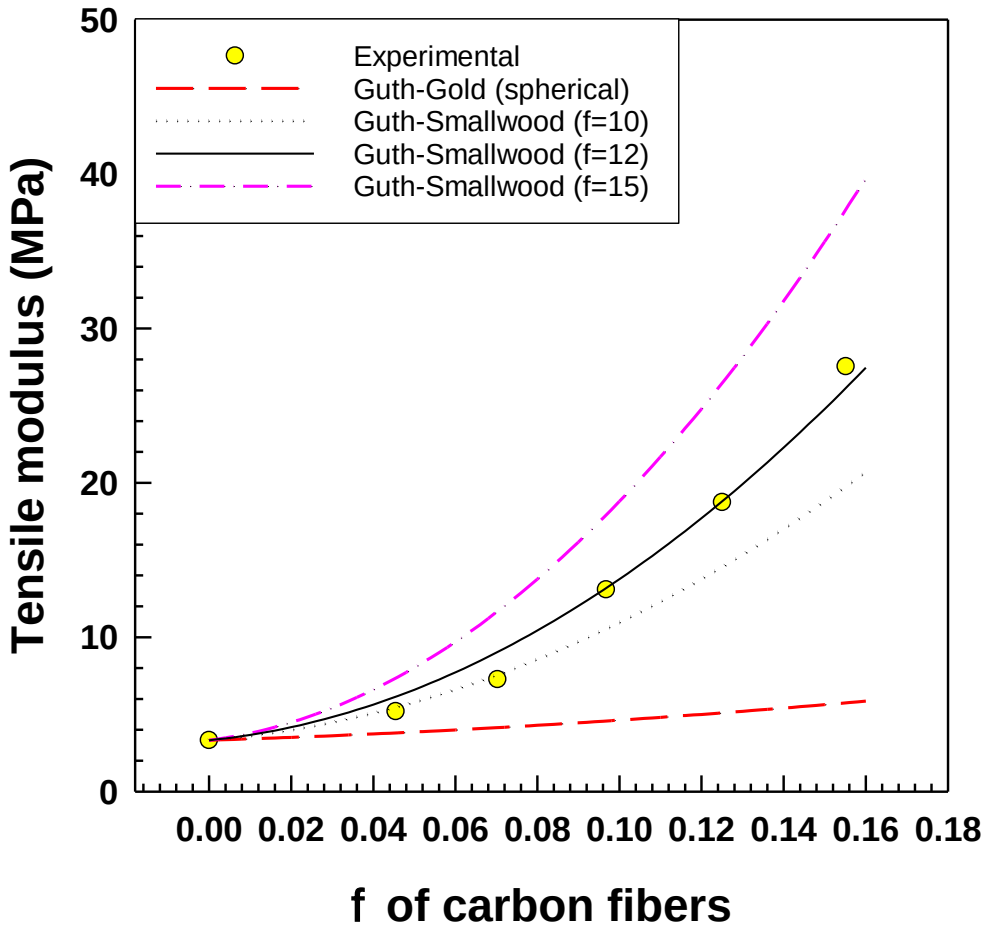

Figure 3. Experimental tensile modulus vs. prediction of tensile modulus by Guth-Gold model for spherical and Guth–Smallwood model for non-spherical particles.

Several models describe and evaluate the creep behavior of polymer materials, exhibiting both elastic and viscous responses when a force is applied. Viscoelastic parameters from these models can be used to predict polymer creep deformation mechanisms. One of these models is the four-parameter model, known as the Burgers model, which can separate viscoelastic behavior into several components: an instantaneous elastic response, a retarded elastic response and a viscous response (Figure 4) [21-23].

The Burgers model consists of the Maxwell and Kelvin models connected in series. The following equations determine the overall creep strain of the Burgers model:

$$\varepsilon = \varepsilon_1 + \varepsilon_2 + \varepsilon_3 \quad (12)$$

$$\varepsilon = \frac{\sigma_0}{E_M} + \frac{\sigma_0}{E_K}\left(1 - e^{\frac{-E_K t}{\eta_K}}\right) + \frac{\sigma_0}{\eta_M} t \quad (13)$$

where ε_1 is the strain of the Maxwell spring, ε_2 is the strain of the Kelvin unit and ε_3 is the strain of the Maxwell dashpot. E_M and η_M are the modulus and viscosity of the Maxwell spring and dashpot. E_K and η_K are the modulus and viscosity of the Kelvin spring and dashpot. In addition, σ0 and t are the applied stress and creep test time, respectively.

Furthermore, for another evaluation of creep behavior, we can define creep compliance J(t) as a ratio of the strain per unit of the applied stress according to the following equations [24-26].

$$J(t) = \frac{\varepsilon(t)}{\sigma_0} \quad (14)$$

$$J(t) = \frac{1}{E_M} + \frac{1}{E_K}\left(1 - e^{\frac{-E_K t}{\eta_K}}\right) + \frac{t}{\eta_M} \quad (15)$$

Nevertheless, this study also uses the six-parameter model, which combines the Maxwell model and two Kelvin models connected in series (Figure 4) [22]. These equations can define the total creep strain and respective creep compliance:

$$\varepsilon = \frac{\sigma_0}{E_0} + \frac{\sigma_0}{E_1}\left(1 - e^{\frac{-E_1 t}{\eta_1}}\right) + \frac{\sigma_0}{E_2}\left(1 - e^{\frac{-E_2 t}{\eta_2}}\right) + \frac{\sigma_0}{\eta_0} t \quad (16)$$

$$J(t) = \frac{1}{E_0} + \frac{1}{E_1}\left(1 - e^{\frac{-E_1 t}{\eta_1}}\right) + \frac{1}{E_2}\left(1 - e^{\frac{-E_2 t}{\eta_2}}\right) + \frac{t}{\eta_0} \quad (17)$$

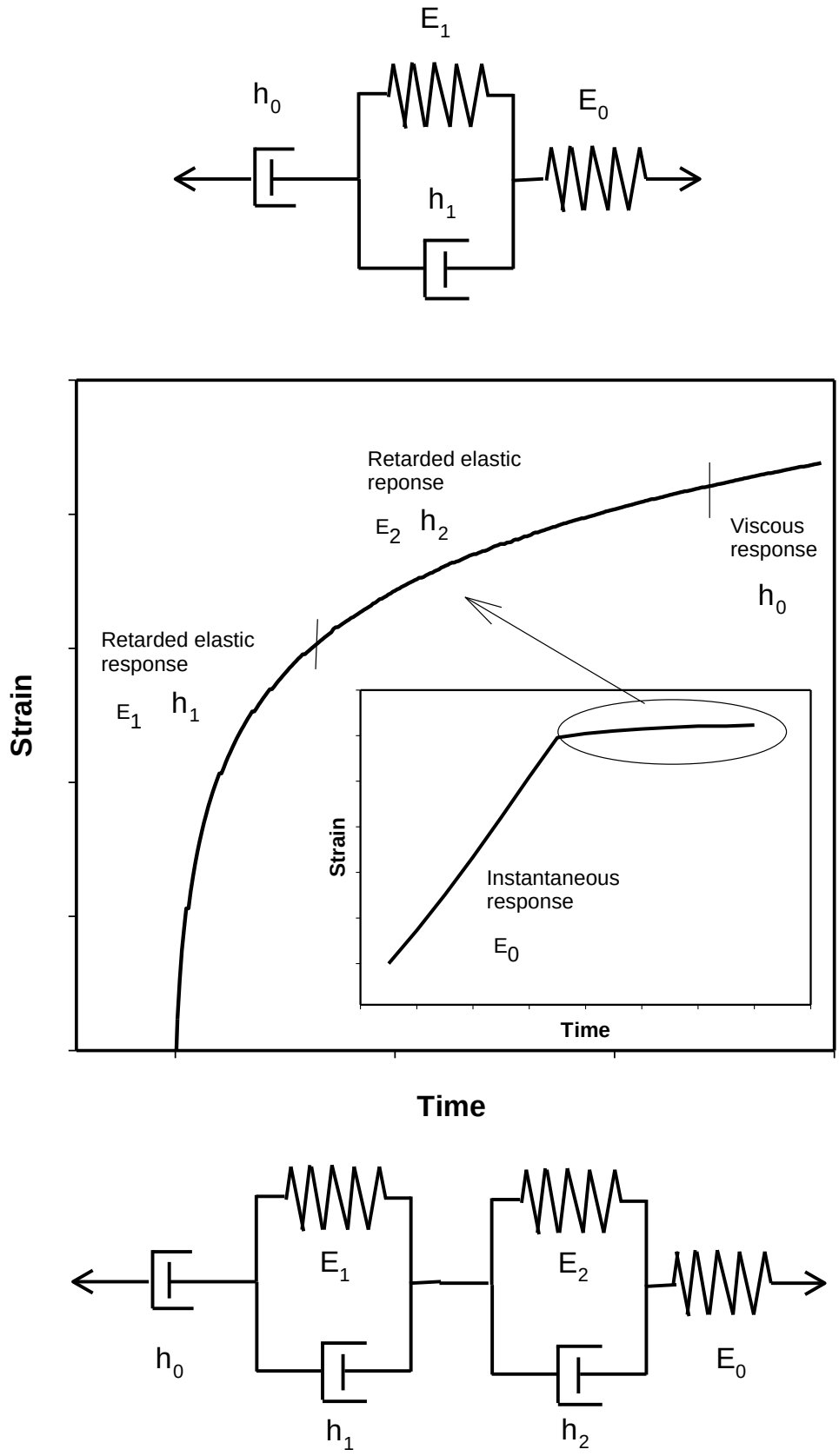

Figure 4. Scheme of Burgers model (four-parameter) and six-parameter model.

According to Figure 5, the six-parameter model fitted the experimental data better than the four-parameter model. The parameter values of both models are included in Tables 2 and 3.

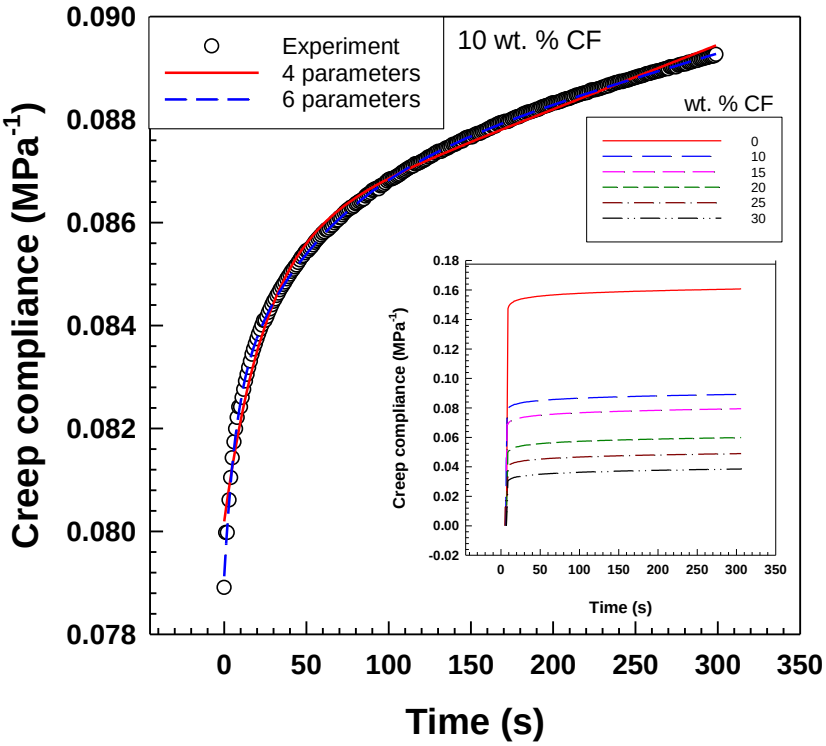

Figure 5. Creep compliance curves measured by DMA at room temperature. Experimental data vs. Burgers model and six-parameter model.

In Figure 6, the creep compliance J(t) is depicted, which is a measure of the ability of a material to deform over time under constant stress. After 300 s from the start, the graph illustrates that the creep compliance decreases by increasing the weight percentage of CF in EOC composites. This indicates that EOC/CF composites with a higher weight percentage of CF exhibit less deformation over time under constant stress.

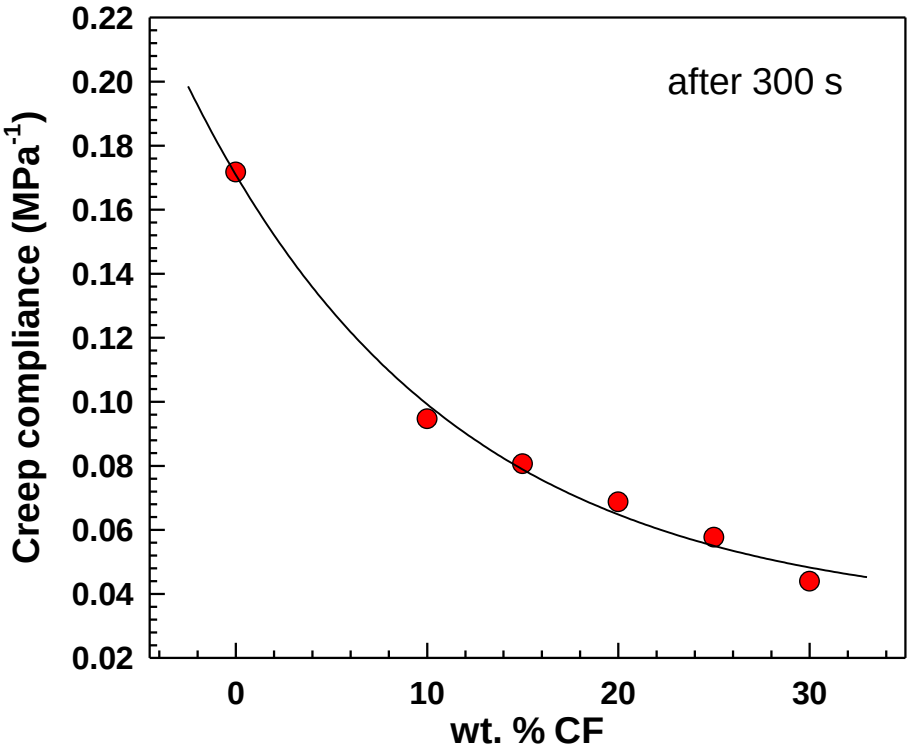

Figure 6. Creep compliance vs. CF content. Evaluated after 300 s from start of the measurement.

Figure 7a shows parameter J0 which represents 1/E0 from the six-parameter model. J0 decreases with a higher content of CF from 0.15 MPa−1 to 0.03 MPa−1. This indicates that the stiffness of the composite decreases as the amount of CF increases. This behavior is attributed to the fact that carbon fibers are more rigid than the polymer matrix and the decrease in stiffness is due to the reduction in the composite's polymer amount.

Figure 7b shows the parameter EM from the Burgers model, which EM increases with an increasing wt.% of CF from 6.7 MPa to 31.7 MPa. The increase in EM with the increasing filler content is attributed to the forming of a percolated particle network structure, improving the composites' mechanical and electrical properties [27].

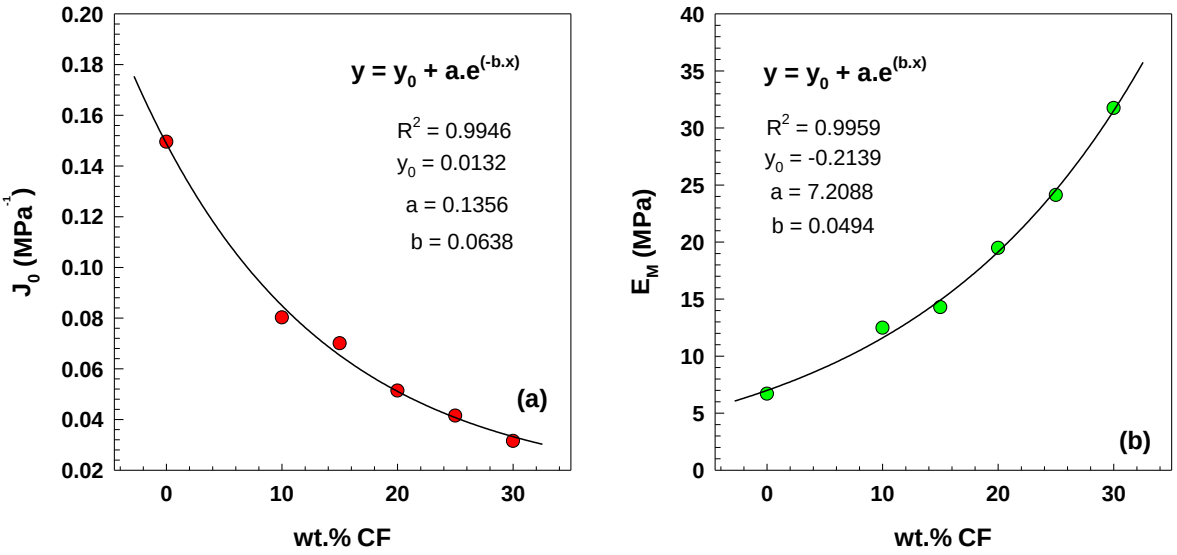

Figure 7. (a) Parameter J0 vs. CF content; (b) parameter EM vs. CF content.

The viscoelastic behavior of the samples was studied using dynamic mechanical analysis. This technique allowed for the measurement of crucial dynamic parameters such as storage modulus (E′), loss modulus (E″), and damping factor (Tan δ) as a function of frequency. Typically, at a specific temperature, the storage modulus increases with a higher frequency [28, 29].

As shown in Figure 8a, the storage modulus of EOC/CF composites increases with increasing frequency. The growth of the exponential slope is observed due to the various CF contents, ranging from 0.68 to 3.8 with an increasing wt.% CF. The equations and parameters that describe this relationship are included in Figure 8b. The increase in storage modulus with increasing frequency and filler content is a crucial factor in determining the stiffness and elastic response of the composites. This behavior is attributed to the forming of a percolated particle network structure, which improves the composites' mechanical and electrical properties.

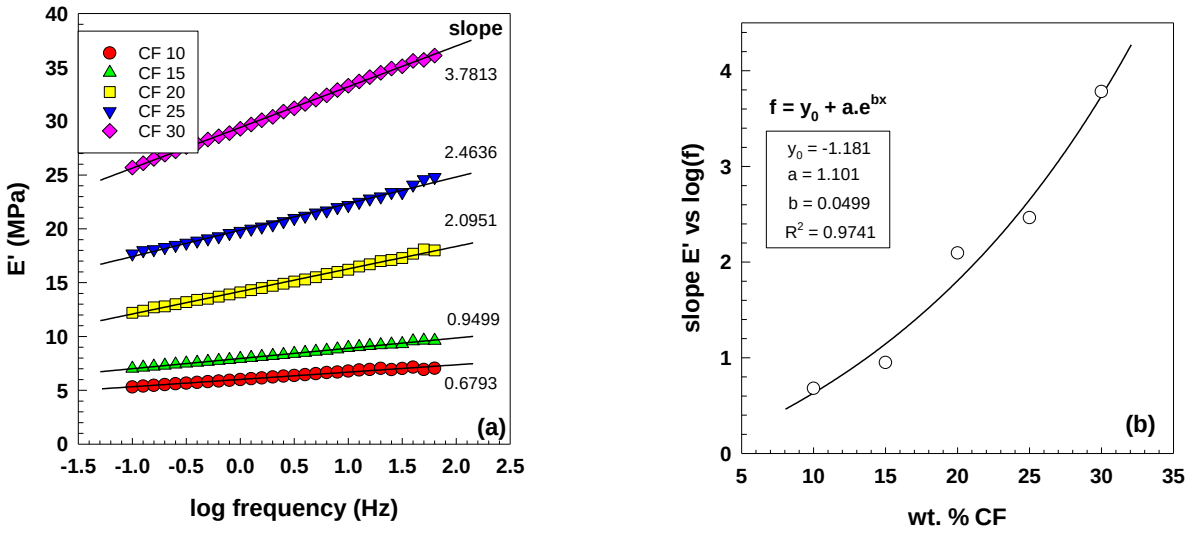

Figure 8. (a) Storage modulus as a function of frequency for EOC/CF composites measured by DMA at room temperature; (b) dependence of slope E' vs. log(f) on CF content.

In elastic electrically conductive composites, an increase in the storage modulus with increasing filler content leads to an increase in complex viscosity, improving the elastic response. This is because the storage modulus is closely related to the material's elasticity. It has been observed that as the filler content increases, there is a significant increase in the storage modulus of polymer composites, which leads to the formation of a percolated particle network structure [30, 31]. In their study, Fernandez et al. noted that the frequency dependence of the storage modulus was reduced as the carbon fiber content increased, resulting in less viscoelastic behavior in the composites [32]. This observation highlights the filler content's importance in determining the composites' mechanical behavior. In Equation (10), Tan δ is defined as a ratio of the loss modulus and storage modulus:

$$Tan(\delta) = \frac{E''}{E'} \qquad (10)$$

Viscoelastic liquids behavior is generally observed when Tan δ decreases with the frequency. On the other hand, the positive slope of Tan δ curves indicates elastic behavior [33]. Conversely, materials displaying an increase in Tan δ with frequency demonstrate their elastic behavior. Figure 9a shows the Tan δ behavior of elastic electrically conductive composites (EOC) with varying CF content, measured at room temperature. At lower CF content, Tan δ increases with increasing frequency, while no significant increase is observed for samples with

25 and 30 wt.% CF. Figure 9b illustrates the dependence of Tan δ on the CF content at a frequency of 0.1 Hz and includes an equation and parameters to describe the dependence.

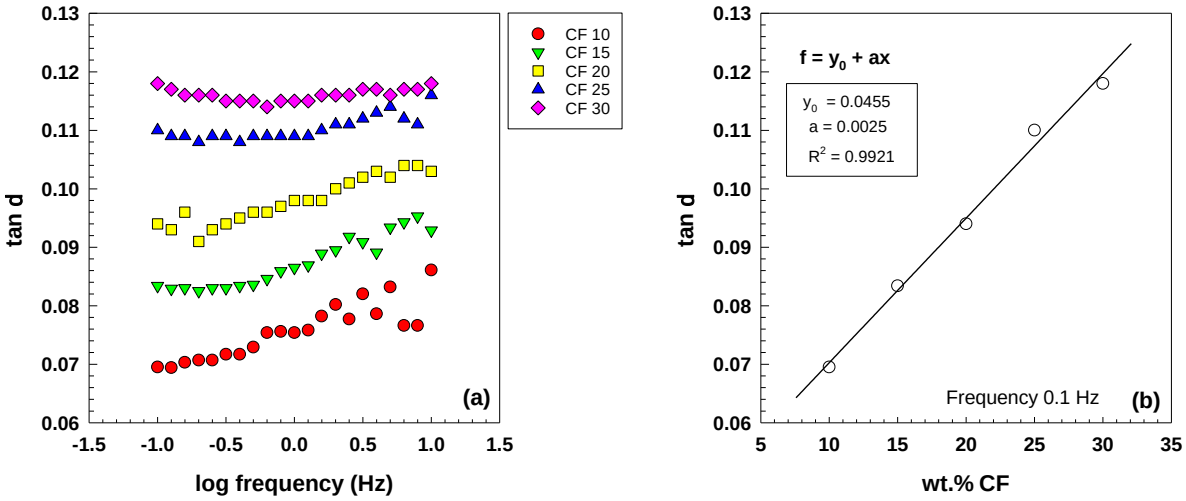

Figure 9. (a) Tan δ as a function of frequency for EOC/CF composites measured by DMA at room temperature; (b) dependence of Tan δ on CF content for frequency 0.1 Hz.

Table 2. Values of the four-parameter model.

Sample	Four-Parameter Model				
	E_m (MPa)	E_k (MPa)	η_m (MPa·s)	η_k (MPa·s)	R^2
EOC	6.7	142.6	67,114.7	3099.2	0.991
EOC/10 wt% CF	12.5	181.6	79,980.1	4501.2	0.993
EOC/15 wt% CF	14.3	175.1	76,050.2	4321.9	0.993
EOC/20 wt% CF	19.5	193.3	83,418.2	5017.1	0.992
EOC/25 wt% CF	24.1	222.2	92,440.7	6160.3	0.994
EOC/30 wt% CF	31.7	240.1	97,204.5	6803.7	0.994

Table 3. Values of the six-parameter model.

Sample	Six-Parameter Model						
	E_0 (MPa)	η_0 (MPa·s)	E_1 (MPa)	η_1 (MPa.s)	E_2 (MPa)	η_2 (MPa·s)	R^2
EOC	6.8	86,936.1	220.2	978.6	194.9	8612.1	0.9995
EOC/10 wt% CF	12.6	109,715.6	298.2	1964.3	244.6	13,323.8	0.9996
EOC/15 wt% CF	14.5	102,613.3	286.7	1684.1	231.4	12,130.8	0.9995
EOC/20 wt% CF	20.1	108,270.9	327.2	1480.5	239.9	11,713.2	0.9996
EOC/25 wt% CF	24.7	120,924.9	403.9	2206.1	271.9	14,217.2	0.9997
EOC/30 wt% CF	32.8	123,687.4	437.8	2034.5	286.3	14,497.8	0.9996

3.3. Electrical properties

Previous research by Theravalappil et al. has shown that elastic electrically conductive composites reinforced with carbon fibers (EOC/CF) have a percolation threshold at 10 wt.% CF. This result is lower than that observed for multi-walled carbon nanotube (MWCNT) composites due to the longer length of the carbon fibers, which allows for the formation of a conductive path at a lower concentration [14]. Generally, composites with filler concentrations close to the percolation threshold exhibit a high electrical resistance and gauge factor [9], making it difficult to measure their electrical properties accurately.

This study used EOC/CF composites with concentrations of 15, 20, and 25 wt.% CF was used, which is above the percolation threshold, allowing for the observation and analysis of their electrical behavior under strain. In our previous paper, we focused on AC conductivity [14] while this work is focused on DC conductivity change with stretching. The two loading and unloading cycles for the EOC composite with 25 wt.% CF and calibrated weight 50 g are presented in Figure 10. One cycle starts by loading the sample and electrical resistivity was measured every 1 s for 5 min. Measurement continues for 5 min with the unloading sample and the cycle ends. The sample loading process corresponds with the stress increase (Figure 10a) and decrease of the electrical resistivity and resistance change, respectively (Figure 10b,c). Furthermore, the unloading sample causes an increase in the electrical resistivity and resistance change.

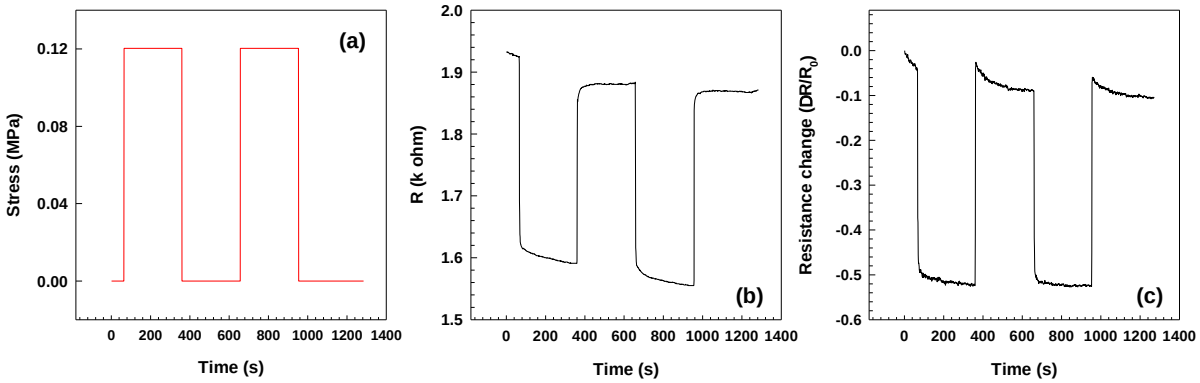

Figure 10. Loading/unloading cycles for (a) stress, (b) resistivity and (c) resistance change for EOC composite with 25 wt.% CF.

In general, positive piezoresistivity, when the applied strain changes the electrical resistivity, is more usual than negative piezoresistivity. Many researchers reported results with positive piezoresistivity when the electrical resistance was increased with an applied tensile strain [34-37]. Nevertheless, Figure 10b shows that the electrical resistivity decreases with applied strain, which the realignment of carbon fibers could explain during the loading process. The schema of this process is illustrated in Figure 11. While loading, the sample is stretched and the length of the sample increases. The distance between two fibers also increases (a2> a1), increasing the electrical resistivity. For the electrons, it is not very easy to find the conductive path. On the other hand, the width and thickness are reduced during sample loading, which causes a decrease in the distance between two fibers (b2< b1) and creates new conductive paths. This effect supports the tunneling, which requires a small distance (order in Angstroms) of the adjacent fibers. The tunneling effect leads to a decrease in the electrical resistance. The overall behavior results from the competition between these effects [9, 35, 38].

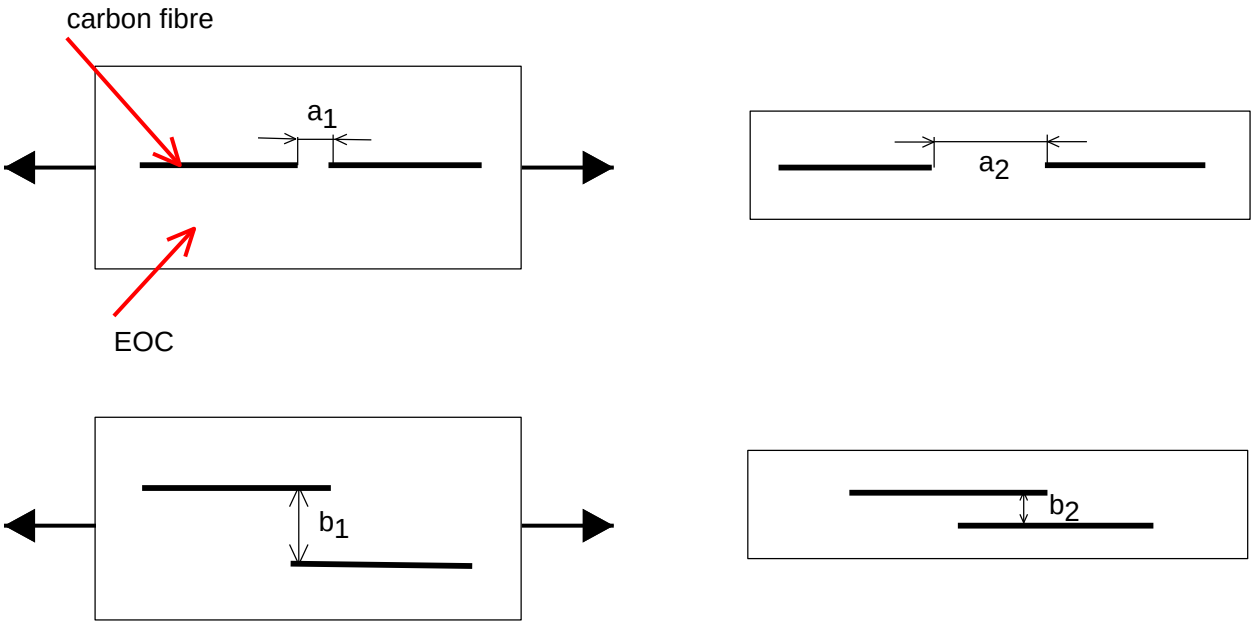

Figure 11. Schema of conductivity path explaining negative resistance change and gauge factor.

The previous explanation can be applied to the negative resistance change (Figure 12) and negative gauge factor (Figure 13), which are defined in Equation (11):

$$GF = \frac{\Delta R/R_0}{\Delta l/l_0} \quad (18)$$

where $\Delta R/R_0$ is the relative resistance change, Δl is the change of the length during loading and l_0 is the length of the sample before loading.

Generally, most materials exhibit a positive gauge factor; their electrical resistance increases under tensile strain. However, some materials display a negative gauge factor, such as nickel (−12), n-type silicon (−135), and Si nanowires (−285). It is worth noting that negative gauge factors are relatively rare and not well understood. In contrast, polymer composites filled with semiconducting particles typically exhibit a positive gauge factor, indicating that the electrical resistance increases with tensile strain [39]. These observations are essential because they provide insights into the behavior of various materials under strain and can inform the selection and development of materials for sensor applications. Further work is needed to understand the underlying mechanisms responsible for the negative gauge factor behavior and to identify ways to mitigate it.

The strain dependence of resistance change for elastic electrically conductive (EOC) composites with varying weight percentages of CF (15, 20, and 25 wt.%) is depicted in Figure 12 and Table 4. The graph depicts the relationship between the strain, tensile stress, and calibrated weights ranging from 20 to 500 g. Unexpectedly, the resistance change decreases to negative values. This observation is significant as it suggests that the composite material exhibits non-linear behavior under stress, and its electrical properties may not be suitable for specific sensor applications.

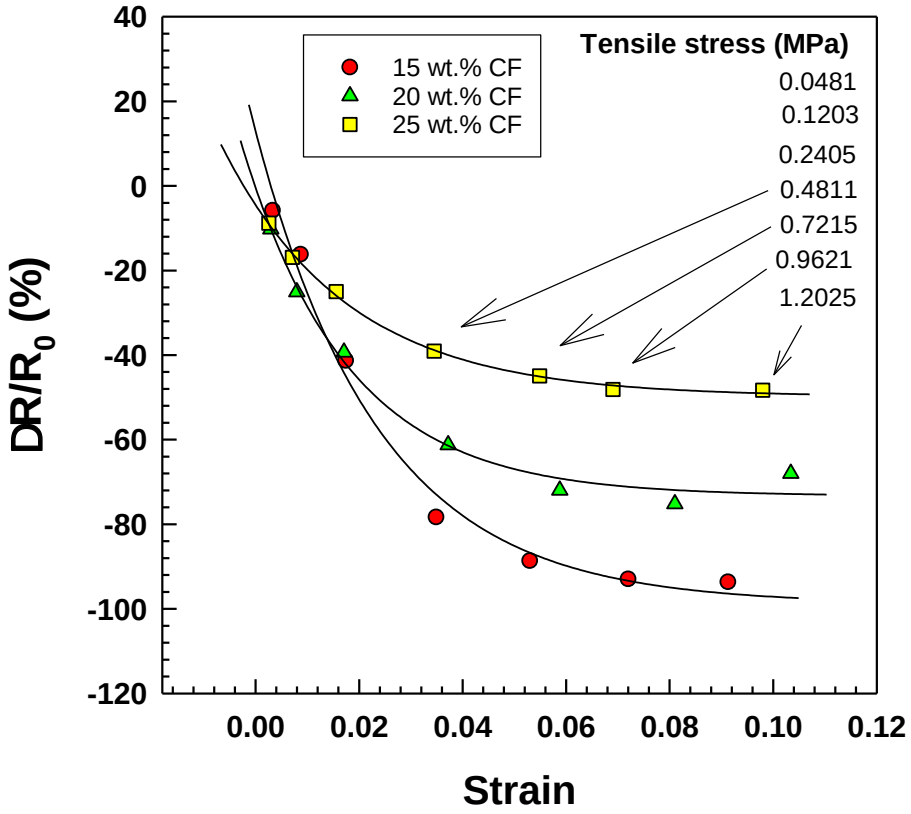

Figure 12. Strain dependence of resistance change for EOC/CF composites with various tensile stresses.

Additionally, Figure 13 and Table 5 illustrate the fact that the gauge factor, which is a measure of a material's sensitivity to strain, reaches negative values. The data presented in Table 5 show the linear regression parameters (y0, a, b, and R2) for each weight percentage of carbon fiber. Interestingly, the gauge factor for the 25 wt.% of composite is significantly lower than the gauge factors for the 15 wt.% and 20 wt.% composites and it also exhibits a negative y-intercept. These

results suggest that the composite material's electrical conductivity and strain sensitivity are strongly influenced by the weight percentage of carbon fiber [40, 41]. The negative gauge factor values observed in this study are worrying as they indicate that the material's electrical resistance decreases under tensile strain, which could lead to inaccurate sensor readings. Further investigation is needed to understand the underlying causes of this behavior and to develop strategies to improve the stability and reliability of EOC composites for use in sensor applications.

Table 4. Values of negative resistance change.

wt.% CF	**y_0**	**a**	**b**	**R^2**
15	−98.82	111.8	41.96	0.9886
20	−73.32	72.92	48.76	0.9876
25	−49.85	45.36	41.06	0.9978

Table 5. Values of negative gauge factor.

wt.% CF	**y_0**	**a**	**b**	**R^2**
15	−15.52	13.81	7.619	0.9824
20	−14.09	13.13	7.902	0.9841
25	−7.252	6.008	9.577	0.9881

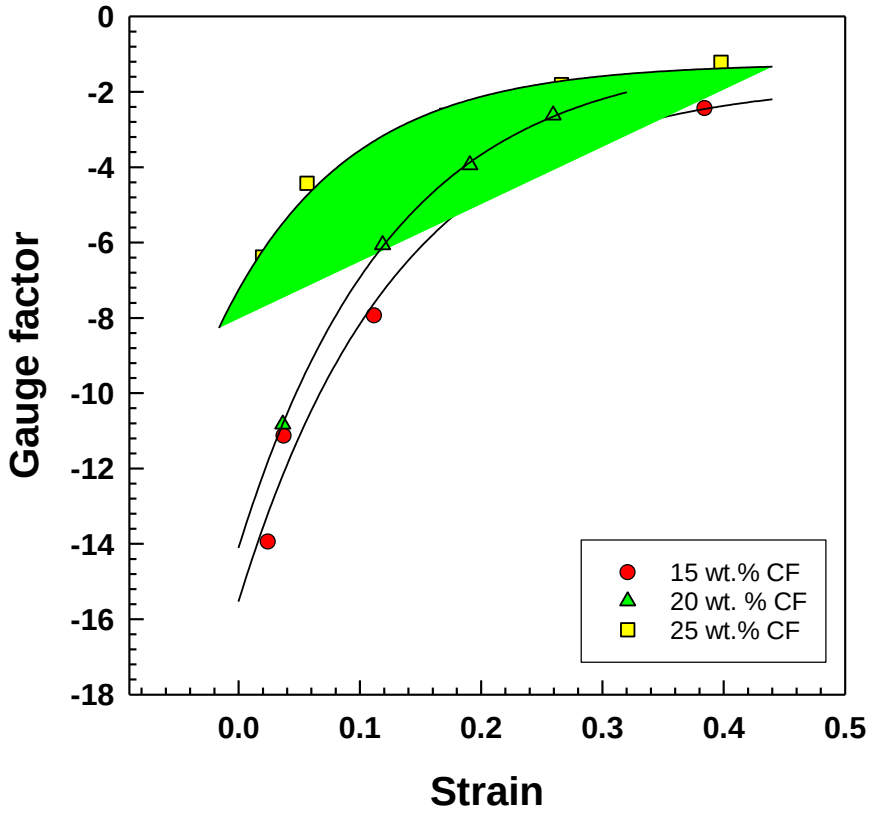

Figure 13. Strain dependence of gauge factor for EOC/CF composites.

As can be seen in Figure 14, resistivity variations were observed during multiple loading and unloading cycles at a tensile stress of 1.202 MPa. The results indicate that the loading/unloading process is consistent across two cycles and a prolonged period, with no substantial changes in resistivity. Furthermore, the resistivity levels oscillate between two values, indicating the stability of the material. These findings highlight the importance of repeatability in pressure and strain sensors, as it ensures consistency in measurement accuracy over time [42]. Therefore, the ability of a material to maintain stable resistivity values during loading/unloading cycles is a critical factor to consider when selecting materials for use in pressure and strain sensors. The findings of this study suggest that carbon fiber-based composites may be suitable for use in these applications due to their ability to maintain stable resistivity values over prolonged periods.

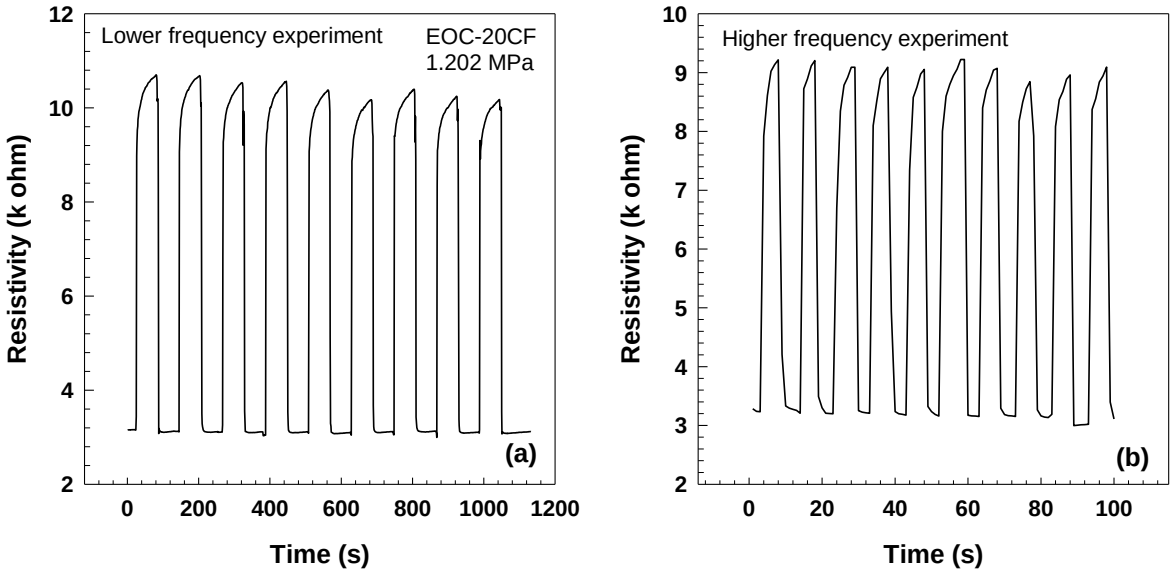

Figure 14. Resistivity vs. time for loading/unloading cycles after (a) 1 min and (b) 5 s of EOC composite with 20 wt.% CF and tensile stress 1.202 MPa.

4. CONCLUSIONS

In conclusion, the study followed the effect of carbon fibers in an elastic polymer matrix on the mechanical properties and morphology of EOC/CF composites, which were investigated using numerous analytical techniques. The SEM images confirmed the efficient dispersion of the CF filler in the EOC matrix, and the stress−strain curves showed that the addition of CF improved the tensile modulus and stress of the composites without sacrificing their elasticity. The mechanical behavior of the composites was also evaluated using theoretical models such as the Guth−Gold and Guth−Smallwood models, which were used to estimate the tensile modulus of the composites with different filler shapes. The viscoelastic behavior of the composites was evaluated using the Burgers model, and the dynamic mechanical analysis revealed that the storage modulus increased with frequency, and the Tan δ curves indicated elastic behavior. The electrical properties of the composites were also investigated, and the results showed that the EOC/CF composites exhibited a percolation threshold at 10 wt.% CF. Overall, this investigation points to unique combinations of thermoplastic elastomers and carbon fibers, which have implications for developing advanced composites with improved properties and can be used in electronics engineering, especially the pressure/strain sensors.

ACKNOWLEDGMENTS

The authors thank Tomas Bata University in Zlin for supporting this research through the Internal Grant Agency, ref. No: IGA/FT/2023/008.

REFERENCES

[1] Ding SQ, Han BG, Dong XF, Yu X, Ni YQ, Zheng QF, Ou JP. Pressure-sensitive behaviors, mechanisms and model of field assisted quantum tunneling composites. Polymer. 2017;113:105-118. https://doi.org/10.1016/j.polymer.2017.02.058.

[2] Lv W, Jiang N, Ding JN, Liu ZF, Yuan NY, Ovalle-Robles R, Inoue K, Lepro X, Fang SL. Three-Dimensional Conducting Elastomeric Composites Based on Buckling Carbon Nanotube Sheets for Interconnects and Temperature Sensor. Journal of Nanoscience and Nanotechnology. 2017;17(3):1934-1941. https://doi.org/10.1166/jnn.2017.12861.

[3] Njuguna MK, Yan C, Hu N, Bell JM, Yarlagadda PKDV. Sandwiched carbon nanotube film as strain sensor. Composites Part B-Engineering. 2012;43(6):2711-2717. https://doi.org/10.1016/j.compositesb.2012.04.022.

[4] Slobodian P, Riha P, Lengalova A, Svoboda P, Saha P. Multi-wall carbon nanotube networks as potential resistive gas sensors for organic vapor detection. Carbon. 2011;49(7):2499-2507. https://doi.org/10.1016/j.carbon.2011.02.020.

[5] Chae HG, Choi YH, Minus ML, Kumar S. Carbon nanotube reinforced small diameter polyacrylonitrile based carbon fiber. Composites Science and Technology. 2009;69(3-4):406-413. https://doi.org/10.1016/j.compscitech.2008.11.008.

[6] Chae HG, Sreekumar TV, Uchida T, Kumar S. A comparison of reinforcement efficiency of various types of carbon nanotubes in poly acrylonitrile fiber. Polymer. 2005;46(24):10925-10935. https://doi.org/10.1016/j.polymer.2005.08.092.

[7] Gong S, Zhu ZH, Meguid SA. Carbon nanotube agglomeration effect on piezoresistivity of polymer nanocomposites. Polymer. 2014;55(21):5488-5499. https://doi.org/10.1016/j.polymer.2014.08.054.

[8] Christ JF, Hohimer CJ, Aliheidari N, Ameli A, Mo CK, Potschke P. 3d Printing of Highly Elastic Strain Sensors Using Polyurethane/Multiwall Carbon Nanotube Composites. Sensors and Smart Structures Technologies for Civil, Mechanical, and Aerospace Systems 2017. 2017;10168. https://doi.org/10.1117/12.2259820.

[9] Yan Y, Sencadas V, Zhang JS, Zu GQ, Wei DB, Jiang ZY. Processing, characterisation and electromechanical behaviour of elastomeric multiwall carbon nanotubes-poly (glycerol sebacate) nanocomposites for piezoresistive sensors applications. Composites Science and Technology. 2017;142:163-170. https://doi.org/10.1016/j.compscitech.2017.02.007.

[10] Drobny JG. Handbook of Thermoplastic Elastomers, 2nd Edition. Handbook of Thermoplastic Elastomers, 2nd Edition. 2014:1-441.

[11] Lozano-Perez C, Cauich-Rodriguez JV, Aviles F. Influence of rigid segment and carbon nanotube concentration on the cyclic piezoresistive and hysteretic behavior of multiwall carbon nanotube/segmented polyurethane composites. Composites Science and Technology. 2016;128:25-32. https://doi.org/10.1016/j.compscitech.2016.03.010.

[12] Zhou SB, Xiao AG, Huang XB, Chen YD, Zhuang YB, Chen ZA. Mechanical Properties of Elastomeric Terpolymer Composites Containing Carbon Nanotubes. Polymer-Plastics Technology and Engineering. 2013;52(1):66-69. https://doi.org/10.1080/03602559.2012.720333.

[13] Zhang R, Deng H, Valenca R, Jin JH, Fu Q, Bilotti E, Peijs T. Strain sensing behaviour of elastomeric composite films containing carbon nanotubes under cyclic loading. Composites Science and Technology. 2013;74:1-5. https://doi.org/10.1016/j.compscitech.2012.09.016.

[14] Theravalappil R, Svoboda P, Vilcakova J, Poongavalappil S, Slobodian P, Svobodova D. A comparative study on the electrical, thermal and mechanical properties of ethylene–octene copolymer based composites with carbon fillers. Materials & Design. 2014;60:458-467. https://doi.org/10.1016/j.matdes.2014.04.029.

[15] Jha V, Hon AA, Thomas AG, Busfield JJC. Modeling of the effect of rigid fillers on the stiffness of rubbers. Journal of Applied Polymer Science. 2008;107(4):2572-2577. https://doi.org/10.1002/app.27324.
[16] Mandal S, Alam S. Studies on the mechanical, thermal, and morphological properties of poly(ether ether ketone)/poly(ether sulfone)/barium titanate nanocomposites: Correlation of experimental results with theoretical predictive models. Journal of Applied Polymer Science. 2012;126(2):724-733. https://doi.org/10.1002/app.36735.
[17] Rezende CA, Braganca FC, Doi TR, Lee LT, Galembeck F, Boue F. Natural rubber-clay nanocomposites: Mechanical and structural properties. Polymer. 2010;51(16):3644-3652. https://doi.org/10.1016/j.polymer.2010.06.026.
[18] Wu YP, Jia QX, Yu DS, Zhang LQ. Modeling Young's modulus of rubber-clay nanocomposites using composite theories. Polymer Testing. 2004;23(8):903-909. https://doi.org/10.1016/j.polymertesting.2004.05.004.
[19] Dewey JM. Theory of Filler Reinforcement. Journal of Applied Physics. 1945;16(1):55-55. https://doi.org/10.1063/1.1707501.
[20] Hamid Y, Svoboda P, Svobodova D. Influence of Electron Beam Irradiation on High-Temperature Mechanical Properties of Ethylene Vinyl Acetate/Carbon Fibers Composites. 2020;26(3):325-335. https://doi.org/https://doi.org/10.1002/vnl.21747.
[21] Dai ZH, Gao Y, Liu LQ, Potschke P, Yang JL, Zhang Z. Creep-resistant behavior of MWCNT-polycarbonate melt spun nanocomposite fibers at elevated temperature. Polymer. 2013;54(14):3723-3729. https://doi.org/10.1016/j.polymer.2013.05.013.
[22] Hernandez-Estrada ZJ, Figueroa JDC, Rayas-Duarte P, Pena RJ. Viscoelastic characterization of glutenins in wheat kernels measured by creep tests. Journal of Food Engineering. 2012;113(1):19-26. https://doi.org/10.1016/j.jfoodeng.2012.05.033.
[23] Papanicolaou GC, Lagas GP, Zaoutsos SP. Viscoelastic Behavior of Hybrid Building Materials. Journal of Applied Polymer Science. 2015;132(6). https://doi.org/10.1002/App.41429.
[24] Goodarzi V, Kokabi M, Kashani MR, Bahramian AR. Prediction of Long-Term Mechanical Properties of PVDF/BaTiO3 Nanocomposite. Journal of Applied Polymer Science. 2014;131(16). https://doi.org/10.1002/App.40596.
[25] Wang HC, Thompson DG, Schoonover JR, Aubuchon SR, Palmer RA. DMA-FTIR creep-recovery study of a poly(ester urethane) elastomer with molecular-level viscoelastic modeling. Macromolecules. 2001;34(20):7084-7090. https://doi.org/10.1021/ma001783b.
[26] Yang JL, Zhang Z, Schlarb AK, Friedrich K. On the characterization of tensile creep resistance of polyamide 66 nanocomposites. Part II: Modeling and prediction of long-term performance. Polymer. 2006;47(19):6745-6758. https://doi.org/10.1016/j.polymer.2006.07.060.
[27] Wang Y, Cheng Y, Chen J, Wu D, Qiu Y, Yao X, Zhou Y, Chen C. Percolation networks and transient rheology of polylactide composites containing graphite nanosheets with various thicknesses. Polymer. 2015;67:216-226. https://doi.org/https://doi.org/10.1016/j.polymer.2015.04.076.
[28] Al Ahsan M, Tareq MSH, Hosur M, Tcherbi-Narteh A. Thermo-mechanical analysis of seawater-conditioned carbon/polymer composites reinforced with nanoclay/graphene nanoparticles. Mrs Advances. 2021;6(14):369-377. https://doi.org/10.1557/s43580-021-00015-2.
[29] Anwer MAS, Naguib HE. Study on the morphological, dynamic mechanical and thermal properties of PLA carbon nanofibre composites. Composites Part B-Engineering. 2016;91:631-639. https://doi.org/10.1016/j.compositesb.2016.01.039.

[30] McNally T, Potschke P, Halley P, Murphy M, Martin D, Bell SEJ, Brennan GP, Bein D, Lemoine P, Quinn JP. Polyethylene multiwalled carbon nanotube composites. Polymer. 2005;46(19):8222-8232. https://doi.org/10.1016/j.polymer.2005.06.094.
[31] Zeng RT, Hu W, Wang M, Zhang SD, Zeng JB. Morphology, rheological and crystallization behavior in non-covalently functionalized carbon nanotube reinforced poly(butylene succinate) nanocomposites with low percolation threshold. Polymer Testing. 2016;50:182-190. https://doi.org/10.1016/j.polymertesting.2016.01.003.
[32] Fernandes RR, Tamijani AY, Al-Haik M. Mechanical characterization of additively manufactured fiber-reinforced composites. Aerospace Science and Technology. 2021;113. https://doi.org/10.1016/J.Ast.2021.106653.
[33] Durmus A, Woo M, Kasgoz A, Macosko CW, Tsapatsis M. Intercalated linear low density polyethylene (LLDPE)/clay nanocomposites prepared with oxidized polyethylene as a new type compatibilizer: Structural, mechanical and barrier properties. European Polymer Journal. 2007;43(9):3737-3749. https://doi.org/10.1016/j.eurpolymj.2007.06.019.
[34] Wang SK, Chung DDL. Piezoresistivity in continuous carbon fiber polymer-matrix composite. Polymer Composites. 2000;21(1):13-19. https://doi.org/10.1002/pc.10160.
[35] Todoroki A, Yoshida J. Electrical resistance change of unidirectional CFRP due to applied load. Jsme International Journal Series a-Solid Mechanics and Material Engineering. 2004;47(3):357-364. https://doi.org/10.1299/jsmea.47.357.
[36] Yan X, Bowen CR, Yuan C, Hao Z, Pan M. Carbon fibre based flexible piezoresistive composites to empower inherent sensing capabilities for soft actuators. Soft Matter. 2019;15(40):8001-8011. https://doi.org/10.1039/C9SM01046G.
[37] Pan M, Yuan CG, Anpalagan H, Plummer A, Zou J, Zhang JH, Bowen C. Soft Controllable Carbon Fibre-based Piezoresistive Self-Sensing Actuators. Actuators. 2020;9(3). https://doi.org/10.3390/act9030079.
[38] Wang DJ, Chung DDL. Through-thickness piezoresistivity in a carbon fiber polymer-matrix structural composite for electrical-resistance-based through-thickness strain sensing. Carbon. 2013;60:129-138. https://doi.org/10.1016/j.carbon.2013.04.005.
[39] Biccai S, Boland CS, O'Driscoll DP, Harvey A, Gabbett C, O'Suilleabhain DR, Griffin AJ, Li ZL, Young RJ, Coleman JN. Negative Gauge Factor Piezoresistive Composites Based on Polymers Filled with MoS2 Nanosheets. Acs Nano. 2019;13(6):6845-6855. https://doi.org/10.1021/acsnano.9b01613.
[40] Alarifi IM. Investigation the conductivity of carbon fiber composites focusing on measurement techniques under dynamic and static loads. Journal of Materials Research and Technology. 2019;8(5):4863-4893. https://doi.org/https://doi.org/10.1016/j.jmrt.2019.08.019.
[41] Birgin HB, D'Alessandro A, Corradini A, Laflamme S, Ubertini F. Self-sensing asphalt composite with carbon microfibers for smart weigh-in-motion. Materials and Structures. 2022;55(5):138. https://doi.org/10.1617/s11527-022-01978-w.
[42] Slobodian P, Olejnik R, Matyas J, Babar DG. Improving sensitivity of the polyurethane/CNT laminate strain sensor by controlled mechanical preload. IOP Conference Series: Materials Science and Engineering. 2016;108(1):012022. https://doi.org/10.1088/1757-899X/108/1/012022.

Study the crystallization, electroconductivity and mechanical properties in selected engineering polymers and blends

Studium krystalizace, elektrické vodivosti a mechanických vlastností vybraných inženýrských polymerů a směsí

Doctoral Thesis Summary

Published by: Tomas Bata University in Zlín,

nám. T. G. Masaryka 5555, 760 01 Zlín.

Edition: published electronically

Typesetting by: Ahmed Nasr

This publication has not undergone any proofreading or editorial review.

Publication year: 2023